Journal of Medicinal Chemistry

Article

Novel Tetrahydropyrido[4,3-d]pyrimidines as Potent Inhibitors of Chaperone Heat Shock Protein 90

Fen Jiang, Hui-Jie Wang, Yu-Hui Jin, Qiong Zhang, Zhi-Hui Wang, Jian-Min Jia, Fang Liu, Lei Wang, Qi-Chao Bao, Dong-Dong Li, Qi-Dong You, and Xiao-Li Xu

J. Med. Chem., **Just Accepted Manuscript** • DOI: 10.1021/acs.jmedchem.6b00912 • Publication Date (Web): 09 Nov 2016

Just Accepted

ACS Publications

Journal of Medicinal Chemistry is published by the American Chemical Society. 1155 Sixteenth Street N.W., Washington, DC 20036

Novel Tetrahydropyrido[4,3-d]pyrimidines as Potent Inhibitors of Chaperone Heat Shock Protein 90

Fen Jiang[a,b], Hui-Jie Wang[a,b], Yu-Hui Jin[a,b], Qiong Zhang[a,b], Zhi-Hui Wang[a,b], Jian-Min Jia[a,b], Fang Liu[a,b], Lei Wang [a,b], Qi-Chao Bao[a,b], Dong-Dong Li[a,b], Qi-Dong You[a,b*] and Xiao-Li Xu[a,b*]

[a] State Key Laboratory of Natural Medicines, and Jiang Su Key Laboratory of Drug Design and Optimization, China Pharmaceutical University, Nanjing 210009, China

[b] Department of Medicinal Chemistry, School of Pharmacy, China Pharmaceutical University, Nanjing 210009, China

ABSTRACT

Heat-shock protein 90 (Hsp90) is a potential target for oncology therapeutics. Some inhibitors have shown anti-tumor effects in clinical trials, spurring the discovery of small-molecule Hsp90 inhibitors. Here, we describe the structural optimization studies of a hit compound, tetrahydropyrido[4,3-d]pyrimidine-based Hsp90 inhibitor **15**, which exhibits inhibitory activity against Hsp90. A series of analogues were synthesized, and their structure-activity relationships and structure-property relationships were analyzed. These explorations led to the discovery of compound **73**, which exhibited potent in vitro activities, good physicochemical properties, favorable ADME properties and potent anti-tumor effect in an HCT116 xenograft model. Furthermore, **73** exhibited no ocular toxicity in a rat retinal damage model, suggesting it is a relatively safe Hsp90 inhibitor. As a promising anti-tumor agent, **73** was progressed for further pre-clinical evaluation.

INTRODUCTION

Heat-shock protein 90 (Hsp90), which is the most abundant intracellular mammalian protein, is crucial for the correct folding, function, and stability of a wide range of proteins called clients.[1,2] More than 200 Hsp90 clients have been identified to date, including numerous receptors, kinases, and transcription

factors that are necessary for tumor development.[3] Inhibiting the function of Hsp90 can lead to the degradation of many oncogenic proteins, thereby shutting down multiple signaling transduction pathways in cancer cells and potentially resulting in wide-ranging anti-cancer effects.[4,5] Thus, Hsp90 has been widely studied in the past decade as a promising protein target for the discovery of new drugs to treat cancers.

Hsp90 is composed of three domains: a N-terminal adenosine triphosphate/adenosine diphosphate (ATP/ADP)-binding domain, a middle domain involved in client protein binding, and a C-terminal dimerization domain.[6] The chaperone activity of Hsp90 depends on the dynamic conformational changes of these domains, which are driven by nucleotide binding and hydrolysis.[7] Small molecules can be designed to occupy the ATP-binding site to inhibit the function of Hsp90. To date, over 20 distinct N-terminal Hsp90 inhibitors have entered into clinical trials, and many other synthetic inhibitors are under preclinical evaluation.[8–11] Geldanamycin analogues, such as 17-AAG (**1**)[12] and IPI504 (**2**)[13] (Figure 1), entered into clinical trials and showed some activities, providing a proof-of-concept for Hsp90 inhibition in humans.[14,15] Despite their clinical effects, the development of geldanamycin analogues was limited by formulation and toxicity issues.[16] Hence, inhibitors with improved drug-like properties are needed, and as a result, synthetic small-molecule Hsp90 inhibitors are currently in clinical development.[17] These small-molecule Hsp90 inhibitors can be divided into two major classes according to their structures (Figure 1). The purine class is designed based on the structure of ATP and includes BIIB021 (**3**)[18], PU-H71 (**4**)[19], and MPC-3100 (**5**)[20], etc. The resorcinol class is another important class of Hsp90 inhibitors and includes STA-9090 (**6**)[21], NVP-AUY922 (**7**)[22], and AT13387 (**8**)[23], etc. Some other Hsp90 inhibitors that do not belong to these two major classes have also been developed, such as SNX-5422 (**9**)[24] and NVP-HSP990 (**10**)[25]. Up to now, a number of clinical trials have been conducted to evaluate the anti-tumor effects of these inhibitors, and clinical efficacy has been observed in combined therapy. In a phase II study, **1** was proven to be effective in patients with Her-2-positive metastatic breast cancer when used in combination with trastuzumab.[26] The combination of **1** and bortezomib was also active in multiple myeloma patients.[27] In a phase I/II study, **8** showed encouraging activity in combination with crizotinib in patients with non-small cell lung cancer, and it may help overcome

crizotinib resistance.[28] Current clinical developments of Hsp90 inhibitors mainly focus on identifying which cancer types sensitive to an Hsp90 inhibitor and with which drug combination.[29]

Despite the combined therapy efficacy, limited single-agent activity was observed in clinical trials. One possible reason for the monotherapy-failure was that most inhibitors exhibited various adverse effects that limited the clinical dosages. The first-generation Hsp90 inhibitors, geldanamycin analogues, suffered from serious hepatotoxicity because of the presence of a benzoquinone moiety.[30] The second-generation synthetic inhibitors showed no hepatotoxicity, however, still suffered from some other adverse effects, such as neurological toxicities and gastrointestinal side effects.[16] This may be partially due to the pan-Hsp90 inhibition.[31] Hsp90 has four paralogs, including Hsp90α, Hsp90β, Grp94, and Trap-1. Reported results indicated that each paralog was responsible for chaperoning a distinct spectrum of client proteins.[32] Most of the Hsp90 inhibitors in clinical trials exhibited pan-Hsp90 inhibition and the lack of selectivity led to potential mechanism-based toxicities. To reduce the potential adverse effects, isoform-selective inhibitors have been developed, including the Hsp90α/β selective inhibitors (such as **11**) and Grp94 selective inhibitors (such as **12**, **13**).[33−35] These isoform-selective inhibitors showed promising anti-cancer effects and had potential for further development. Ocular toxicity was the most common adverse effect observed in the clinical trials of Hsp90 inhibitors, such as **7**, **8**, **9**.[36−38] Though the ocular disorders were often reversible through dose-limiting, the limited clinical dosage would lead to insufficient drug exposure and reduced anti-tumor efficacy. Interestingly, ocular disorders were not observed in the clinical trials of some other inhibitors, such as **1** and **6**. Recent research indicated that Hsp90 played a critical role in normal retinal function, and high drug exposure level in retina led to structural damage of the retina.[39] Thus, ocular toxicities of Hsp90 inhibitors can be avoided by reducing the drug exposure level in retina. Reduced ocular toxicity would improve the therapeutic index and benefit to the clinical development of Hsp90 inhibitors.

Different core structures would contribute to improved efficacy and safety profile, so a study aimed to identify novel potent and safe Hsp90 inhibitors was conducted. In our previous study, a Rapid Overlay of Chemical Structures (ROCS) model was constructed and applied to virtually screen the Topscience database. Compound **14**, containing the 5,6,7,8-tetrahydropyrido[4,3-d]pyrimidine core,

displayed the most potent Hsp90 inhibition (IC_{50}, 45.39 μM) in the fluorescence polarization (FP) assay. Preliminary structural modification led to compound **15**, which exhibited greater than 450-fold-improved Hsp90 inhibition activity (IC_{50}, 0.101 μM) compared to **14**.[40] Here, we report further optimization studies centered on compound **15**. Investigating the structure-activity relationships and structure-property relationships led to the identification of compound **73**, which showed potent anti-tumor efficacy in an HCT116 human colon carcinoma xenograft model and other favorable properties. No ocular toxicity in a rat retinal damage model indicated the good safety profile of **73**.

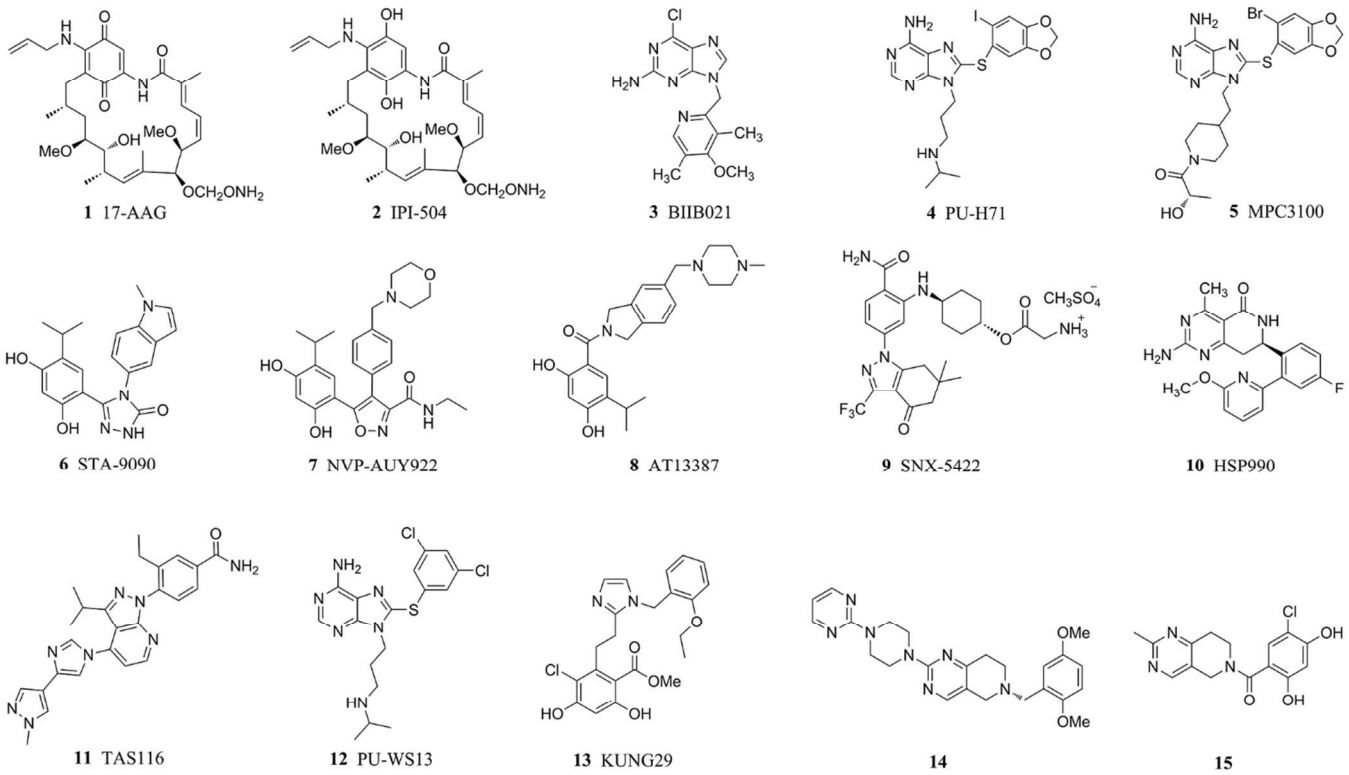

Figure 1. Some representative Hsp90 inhibitors and compounds **14** and **15**

CHEMISTRY

Derivatives **24**−**28** were synthesized using the route summarized in Scheme 1. The 5-chlorine- and 5-bromine-substituted benzoic acid intermediates **17a** and **17b** were prepared from commercial **16a** and **16b** via benzyl protection of the phenyl groups and subsequent benzyl ester hydrolysis. The intermediate **17c** was prepared according to previously reported procedures.[41] Briefly, Friedel-Crafts acylation of the commercial **18** was conducted in the presence of boron trifluoride, and subsequent protection of the

phenol groups with benzyl bromide gave **19**. Then Wittig reaction was used to obtain the olefin intermediate, and subsequent hydrolysis of the methyl ester yielded **17c**.

N-Boc-3-Pyrrolidinone (**20a**) or N-Boc-4-piperidone (**20b**) was refluxed in N,N-dimethylformamide dimethyl acetal to obtain **21a** or **21b** and then cyclized with acetamidine hydrochloride in the presence of sodium acetate in refluxed EtOH. Subsequently, the Boc group was deprotected in trifluoroacetic acid (TFA) to obtain the key intermediates **22a** or **22b**, which condensed with the substituted benzoic acid **17a**−**c** using standard 1-ethyl-3-(3-dimethylaminopropyl)carboiimide/hydroxybenzotriazole (EDCI/HOBt) coupling conditions to give **23a**−**e**. The benzyl protecting groups in **23a**−**c** were deprotected using BBr_3 to obtain the target compounds **24**−**26**. For **23d** and **23e**, Pd/C catalytic hydrogenation simultaneously removed the benzyl protecting groups and reduced the isopropenyl group to the isopropyl to give **27** and **28**.

Scheme 1. Synthetic route of compounds **24**−**28**[a]

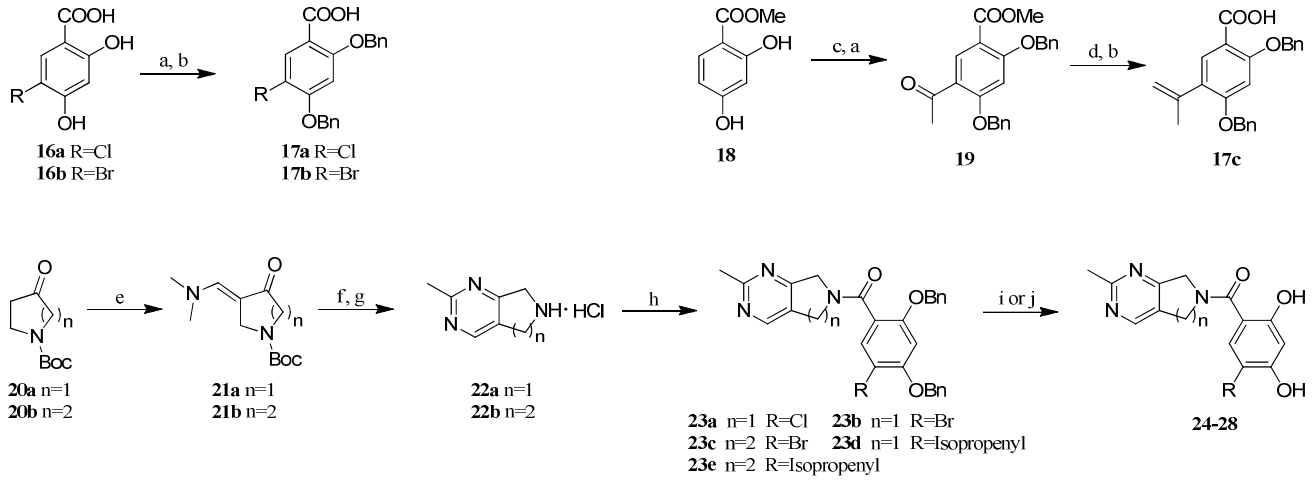

[a]Reagents and conditions: (a) BnBr, K_2CO_3, acetone, reflux, 8 h; (b) NaOH, MeOH/H_2O, 70 °C, 3 h; (c) Ac_2O, $BF_3{\cdot}OEt_2$, 75 ºC, 3 h; (d) $MePPh_3Br$, $KOC(CH_3)_3$, tetrahydrofuran (THF), room temperature (rt), 1 h; (e) N,N-dimethylformamide dimethyl acetal, reflux, 1.5 h; (f) acetamidine hydrochloride, Et_3N, EtOH, reflux, 42 h; (g) trifluoroacetic acid (TFA), 0 °C to rt, 1 h; (h) substituted benzoic acid (**17a**, **17b**, and **17c**), EDCI, HOBt, Et_3N, dichloromethane (DCM), rt, 24 h; (i) BBr_3, DCM, 0 ºC, 3 h; (j) 10% Pd/C, H_2, MeOH, rt, 4 h.

Derivatives **35**−**65** were synthesized using the route described in Scheme 2. Cyclization of **29** with urea in the presence of sodium methanolate gave intermediate **30**. Subsequent chlorination using phosphorus oxychloride provided **31**. Removal of the 4-chloro atom on the pyrimidine ring using

activated zinc powder produced **32**. The benzyl was removed using 1-chloroethyl chloroformate (ACE-Cl) to give **33** and then coupled with **17c** in the presence of EDCI/HOBt to form the key intermediate **34**. Substitution of the 2-chloro group with different amines or alcohols and subsequent hydrogenation afforded the target compounds.

Scheme 2. Synthetic route of compounds **35**−**65**[a]

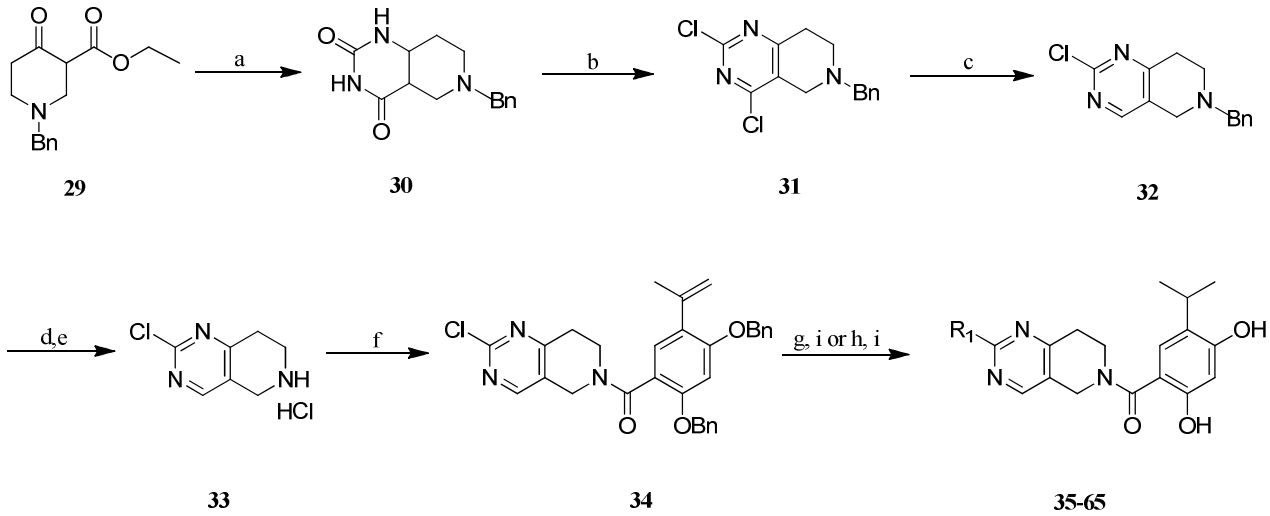

[a]Reagents and conditions: (a) urea, MeONa, EtOH, reflux, 24 h; (b) $POCl_3$, N_2, 3 h; (c) activated zinc powder, NH_4OH, EtOH, reflux, 12 h; (d) ACE-Cl, DCM, 0 °C to rt, then reflux, 10 h; (e) MeOH, reflux, 1 h; (f) **17c**, EDCI, HOBt, Et_3N, DCM, rt, 24 h; (g) different amines, K_2CO_3, dioxane, 85 ºC, 24 h; (h) different alcohols, NaH, THF, rt, 10 h; (i) 10% Pd/C, H_2, MeOH, rt, 4 h.

Derivatives **68**−**78** were synthesized using the route described in Scheme 3. The 4-chloro atom on the pyrimidine ring of intermediate **31** was substituted with different alcohols and amines, and subsequent substitution of the 2-chloro atom of the pyrimidine ring with 2-methoxyethoxy gave the key intermediates **66a**−**k**. The benzyl group was removed using $Pd(OH)_2$ under a hydrogen atmosphere, and the resulting amines were converted into the amide intermediates **67a**−**k** via EDCI/HOBt-mediated coupling with the intermediate **17c**. Hydrogenation in the presence of 10% Pd/C yielded the desired compounds **68**−**78**.

Scheme 3. Synthetic route of compounds **68**−**78**[a]

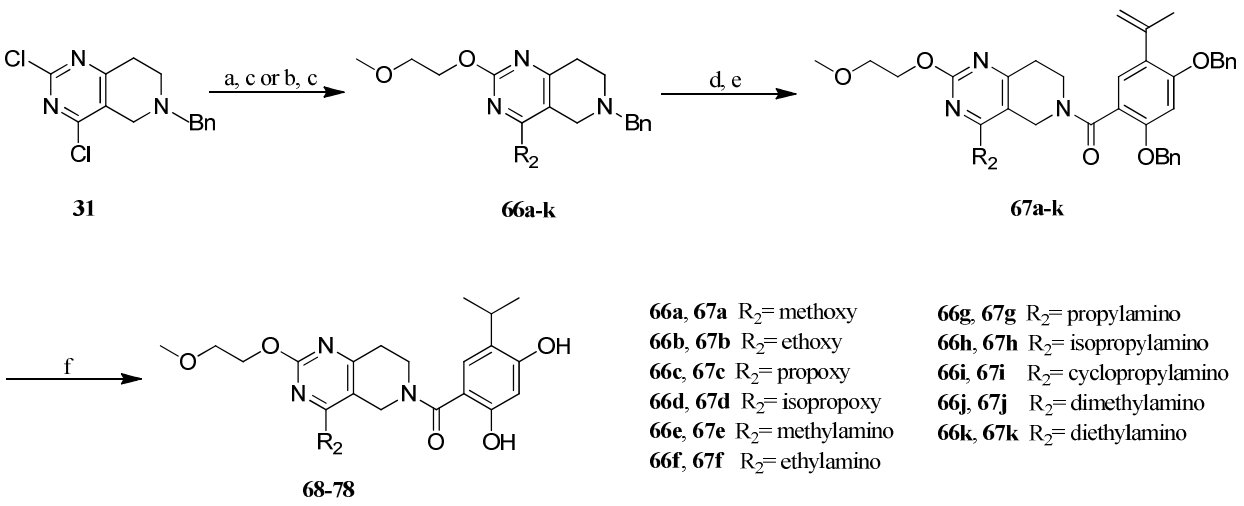

[a]Reagents and conditions: (a) different alcohols, NaH, THF, rt to 0 ºC, 0.5 h; (b) different amines, N, N-diisopropylethylamine (DIPEA), THF, reflux, 24 h; (c) 2-methoxyethanol, NaH, THF, reflux, 1 h; (d) $Pd(OH)_2$, H_2, MeOH, rt, 6 h; (e) **17c**, EDCI, HOBt, Et_3N, DCM, rt, 24 h; (f) 10% Pd/C, H_2, MeOH, rt, 4 h.

RESULTS AND DISCUSSION

Preliminary SAR study lead to compound 50 with potent activities

In our previous study, compound **15** was identified to be a potent Hsp90 inhibitor (FP IC_{50}, 0.101 μM).[40] Docking analysis showed that compound **15** inserted deep into the ATP binding pocket of Hsp90 (Figure 2). The resorcinol moiety and carbonyl group formed tight network of hydrogen bonds with residues Asp93, Thr184 and conserved water molecules, which anchored the compound into the ATP pocket. The 5'-chlorine atom on the resorcinol moiety incompletely occupied a hydrophobic sub-pocket consisting of Leu107, Phe138, Val150 and Val186, and with potential for further optimization. Relatively hydrophobic groups could occupy the pocket more snugly and improve the affinity to Hsp90. SAR study at 5'-position of resorcinol family Hsp90 inhibitors has been well established in previous study. For instance, during the discovery process of **7** and **8**, isopropyl was demonstrated to be the most suitable substituent at this position.[22,23] The isopropyl occupied the hydrophobic pocket snugly and resulted in significant improved Hsp90 inhibition and anti-proliferative activities. As reference, to improve the activities of **15**, our SAR study firstly focused on the 5'-position of the resorcinol. Derivatives of compound **15** were designed in which the chlorine atom was replaced by bromine atom or isopropyl group. Inspired by the isoindoline core of **8**, the tetrahydropyrido[4,3-d]pyrimidine core was

converted into 6,7-dihydro-*5H*-pyrrolo[3,4-d]pyrimidine to investigate the influence of the ring size on activities.[23] These investigations resulted in target compounds **24**–**28**.

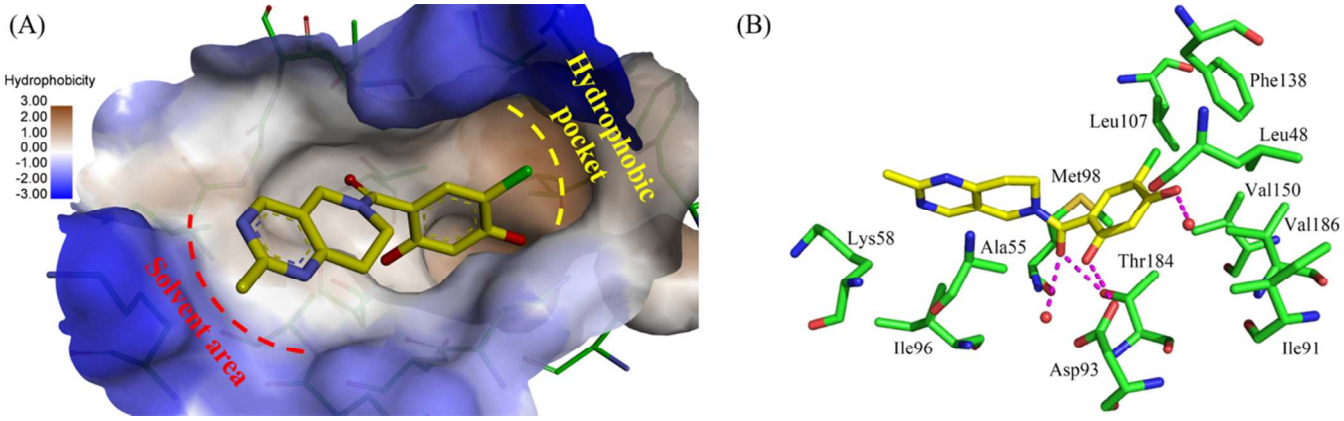

Figure 2. Docking analysis of the binding mode between Hsp90 and compound **15** (protein structure from PDB 2XJX).[23] (A) Compound **15** inserts into the active site of Hsp90 with a surface colored in terms of the hydrophobic state. (B) The detailed interaction between Hsp90 and compound **15**. The carbon atoms of compound **15** and the residues in the Hsp90's active site are shown in yellow and green, respectively. Conserved water molecules are presented as red spheres, and hydrogen bonds are indicated by magenta dashed lines.

The Hsp90-inhibition activities of the synthesized derivatives were determined using FP assay. Anti-proliferative effects were also evaluated against two cancer cell lines (HCT116 human colon carcinoma cell line and MCF-7 human breast adenocarcinoma cell line). As shown in Table 1, substituting the chlorine atom on the resorcinol moiety with a bromine atom had no significant effects on the biochemical potency, whereas the isopropyl analogue **27** showed 4-fold more potent activity than compound **15** in the FP assay. The results indicated that an isopropyl group was the optimal substituent for the R_1 position, and was similar to the group at this position in clinical resorcinol family inhibitors. The analogues **24**, **26**, and **28**, in which the tetrahydropyrido[4,3-d]pyrimidine core was changed into pyrrolo[3,4-d]pyrimidine, showed decreased biochemical potencies relative to **15**, **25**, and **27**. Thus, the tetrahydropyrido[4,3-d]pyrimidine moiety was retained as the molecular core for further optimization.

In this series, compounds **27** and **28** showed comparable Hsp90 inhibition activities with the reference compound **8**, while the anti-proliferative activities were much weaker. Permeability is an important factor that can impact cellular effects of compounds. Results showed that **27** and **28** exhibited over 2-fold lower permeability (33.33×10^{-6} cm/s and 27.03×10^{-6} cm/s respectively, shown in Table S1)

than that of the reference compound **8** (74.32 × 10^{-6} cm/s). In consideration of the 2- or 3-fold lower enzyme potency, lower permeability should partially lead to the weaker cellular activities of **27** and **28**.

Table 1. SAR exploration of the R_1 position and the core

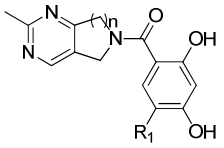

Compd	n	R_1	FP IC_{50} (μM)[a]	Anti-proliferative activities IC_{50} (μM)[a]	
				HCT116	MCF-7
15	2	Cl	0.101 ± 0.012	2.83 ± 0.92	1.91 ± 1.21
24	1	Cl	0.474 ± 0.203	10.66 ± 0.54	5.48 ± 2.36
25	2	Br	0.132 ± 0.010	1.53 ± 1.24	1.73 ± 1.03
26	1	Br	0.262 ± 0.015	1.55 ± 0.35	3.72 ± 0.64
27	2	isopropyl	0.026 ± 0.011	1.15 ± 0.03	1.48 ± 0.35
28	1	isopropyl	0.038 ± 0.014	1.63 ± 0.31	2.14 ± 0.55
8	—	—	0.013 ± 0.002	0.07 ± 0.02	0.02 ± 0.01

[a]Values shown are the mean ± SD (n = 3).

Based on the docking analysis of compound **15**, the methyl group at the 2-position of the pyrimidine ring was exposed to the solvent area, and substitution at this position would be tolerated. Thus, various substituents were investigated to elucidate the SARs of this position, leading to target compounds **35**−**58.**

Various amines and alcohols were introduced to give derivatives **35**−**58**. Table 2 summarized the SARs of these compounds. The amine substituted compounds **35**−**48** showed decreased Hsp90-binding affinity with respect to **27**. Among the primary amine substituted analogues, **35** incorporating a

methylamine substituent possessed the best activity in FP assay. The activities were significantly reduced when bigger groups were introduced. Similar trends were observed in the analogues bearing secondary amines. Compared with the amine substituted compounds, **49**−**58** introduced alcohol substituents showed higher activities in FP assay, with IC_{50} values ranging from 0.056 μM to 0.103 μM. These results suggested that alcohol substituents were more suitable than amine substituents at this position.

Cellular effects of this series showed similar change tendency with the FP data. Most of the amine substituted compounds exhibited decreased anti-proliferative activities, except **35** and **39** which incorporating small amine substituents. Despite weaker affinity to Hsp90 compared with **27**, most of the alcohol substituted analogues showed improved or retained cellular effects. Among which, **50** with an ethoxyl group possessed the best anti-proliferative activities. Permeability determination showed that compound **50** (72.41×10^{-6} cm/s) exhibited a 2-fold increased permeability compared with that of **27** (33.33×10^{-6} cm/s). The increased permeability should contribute to the improved cellular effects.

Table 2. Preliminary exploration of the R_2 position

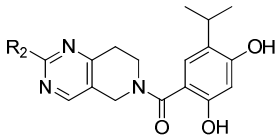

Compd	R_2	FP IC_{50} (μM)[a]	Anti-proliferative activities IC_{50} (μM)[a]	
			HCT116	MCF-7
35		0.113 ± 0.004	0.74 ± 0.07	1.25 ± 0.15
36		0.167 ± 0.008	1.56 ± 0.48	1.58 ± 0.11
37	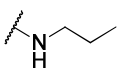	0.238 ± 0.007	2.34 ± 0.64	2.37 ± 0.13
38		0.222 ± 0.003	2.43 ± 0.38	2.68 ± 0.35
39		0.164 ± 0.009	1.02 ± 0.17	1.39 ± 0.06

40		0.201 ± 0.003	4.42 ± 1.27	2.16 ± 1.00
41	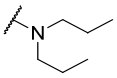	0.370 ± 0.020	5.70 ± 1.04	3.09 ± 1.83
42	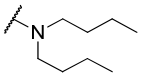	0.343 ± 0.015	1.29 ± 0.02	1.12 ± 0.14
43		0.113 ± 0.007	1.14 ± 0.28	4.55 ± 1.20
44		0.172 ± 0.003	1.55 ± 0.03	4.46 ± 1.05
45		0.110 ± 0.009	1.47 ± 0.55	1.82 ± 0.06
46	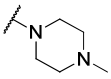	0.271 ± 0.004	1.71 ± 0.05	2.18 ± 0.57
47	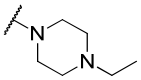	0.191 ± 0.003	1.65 ± 0.06	1.43 ± 0.66
48	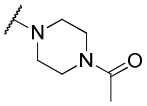	0.270 ± 0.012	1.60 ± 0.04	3.62 ± 1.33
49		0.075 ± 0.015	1.16 ± 0.17	0.63 ± 0.08
50		0.056 ± 0.002	0.76 ± 0.09	0.62 ± 0.05
51	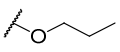	0.060 ± 0.004	1.08 ± 0.21	1.34 ± 0.16
52		0.065 ± 0.005	1.24 ± 0.05	0.96 ± 0.10
53	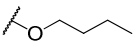	0.088 ± 0.001	1.27 ± 0.06	0.88 ± 0.24
54	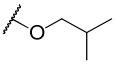	0.065 ± 0.001	1.23 ± 0.08	1.33 ± 0.04
55	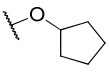	0.071 ± 0.007	1.72 ± 0.13	1.19 ± 0.11
56	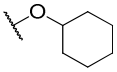	0.103 ± 0.024	2.78 ± 0.63	1.87 ± 0.45
57	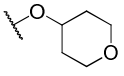	0.056 ± 0.006	0.60 ± 0.02	0.82 ± 0.05

58	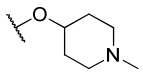	0.076 ± 0.006	1.70 ± 0.09	1.79 ± 0.34

[a]Values shown are the mean ± SD (n = 3).

To accurately analyze the binding modes of the compounds and guide further optimization, the crystal structure of **50** was obtained in complex with the Hsp90α N-terminal. As shown in Figure 3A−B, the crystal structure revealed that the resorcinol moiety bound deep into the ATP-binding pocket of Hsp90. The 2-hydroxyl and carbonyl group of the amide formed a tight network of hydrogen bonds with the Asp93 and Thr184 residues and a conserved water molecule. The 4-hydroxyl group formed a hydrogen bond with another conserved water molecule. This tight network of hydrogen bonds ensured high binding affinity between the molecule and the protein. The isopropyl moiety at the 5'-position of the resorcinol moiety was efficiently embedded within a large hydrophobic cavity, bound by the Leu48, Met98, Leu107, Phe138, Val150, and Val186 residues.

Interestingly, the tetrahydropyrido[4,3-d]pyrimidine core of the molecule bound to the protein in two different conformations (referred as conformation A/B), possibly because of the conformational flexibility of the tetrahydropyrido ring. In order to understand the different binding modes of conformations A and B better, we obtained the overlaps of Hsp90-**50** complex and Hsp90-**8** complex. As shown in Figure 3C, conformation A of compound **50** was well overlapped with **8**, and the two compounds adopt same binding modes with the protein. Both the tetrahydropyrido[4,3-d]pyrimidine core in **50** and the isoindoline core in **8** were adjacent to the H2 helix of the protein and formed hydrophobic interactions with residues Ala55, Lys58, Ile96, and Met98. The ethoxyl in **50** inserted into the solvent area and bound non-specifically, just like the methylpiperazine moiety in **8**. Correspondingly, the protein adopted an open-loop conformation which was similar to that of the 17-dimethylaminoethylamino-17-demethoxygeldanamycin (17-DMAG) bound conformation.[42] When **50** adopted conformation B, it possessed different binding modes with **8** (Figure 3D). The tetrahydropyrido[4,3-d]pyrimidine core along with the ethoxyl group induced rearrangement of the flexible sequence 104−111 in the protein and formed extended hydrophobic interactions with rearranged residues Leu107 and Ile110. Protein conformational changes were observed in the protein-compound crystal complexes of some other Hsp90 inhibitors, such as **3**.[43] In the two conformations, the ethoxyl

group at the 2-position of the pyrimidine ring exposed to the solvent surface of the protein, with potential for further optimization.

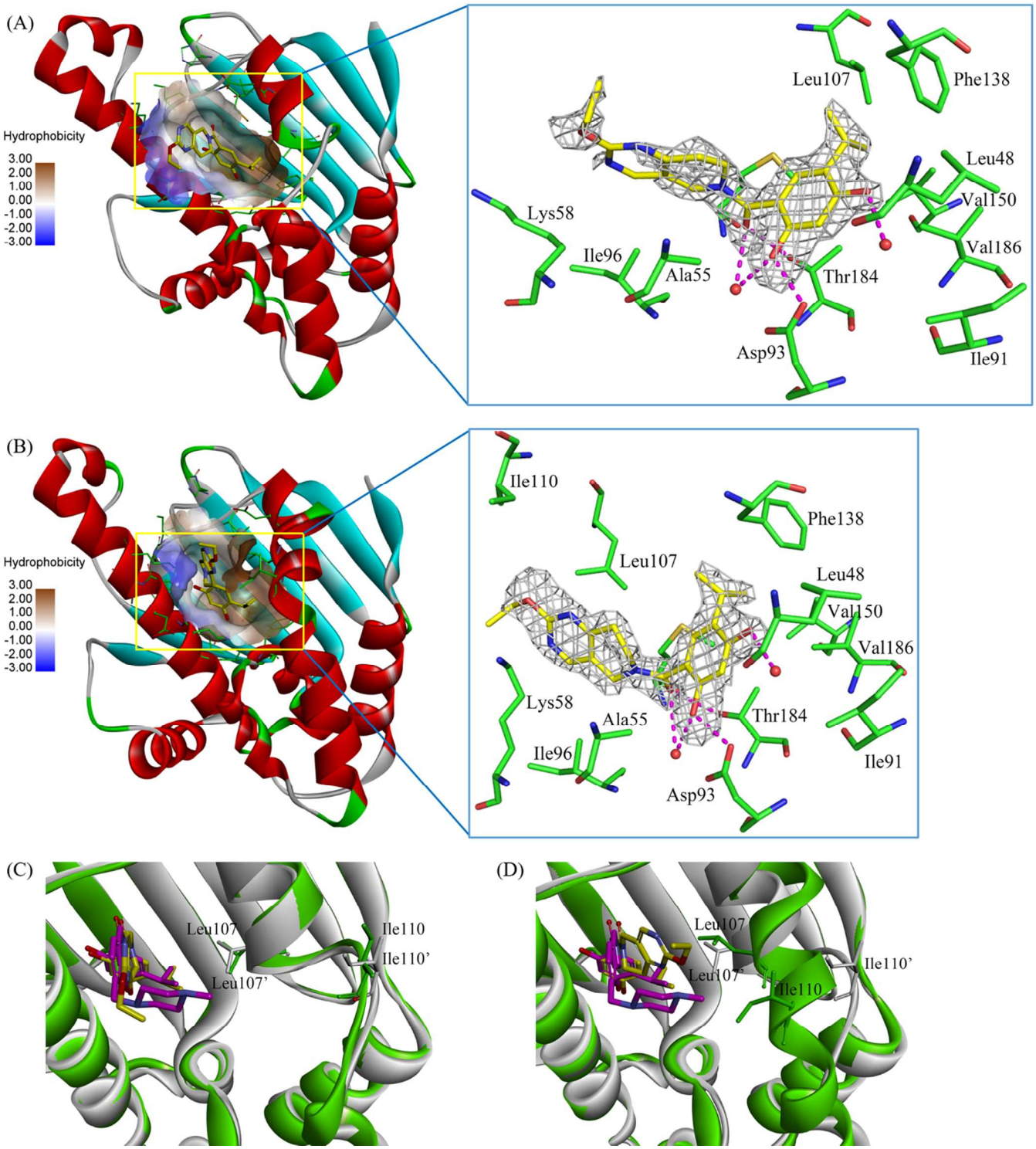

Figure 3. X-ray structure of compound **50** bound to the active site of Hsp90 (PDB: 5GGZ). (A) Compound **50** adopts

conformation A to bind with the open-loop conformation of Hsp90. (B) Compound **50** adopts conformation B to bind with the extended α-helix conformation of Hsp90. The active site of Hsp90 is surfaced according to the hydrophobic state, and detailed interaction is shown. The carbon atoms of compound **50** and the residues in the active site of Hsp90 are yellow and green, respectively. Conserved water molecules are shown as red spheres, and hydrogen bonds are indicated by magenta dashed lines. The omit $F_o - F_c$ electron density for **50** is shown at the 3.0 σ contour level. (C) Overlaps of Hsp90-**50** complex and Hsp90-**8** complex when **50** adopts conformation A. (D) Overlaps of Hsp90-**50** complex and Hsp90-**8** complex when **50** adopts conformation B. The protein in Hsp90-**50** complex and Hsp90-**8** complex are colored as green and grey, respectively. Compound **50** is colored yellow and compound **8** is colored magenta.

Lead optimization to improve activities and drug-like properties

Though the lead compound **50** displayed high binding affinity to Hsp90 and potent anti-proliferative activities, its biological potency was still much weaker than that of the clinical compounds, such as compounds **7** and **8**.[22,23] In addition, the solubility of **50** was relatively low (66 μg/mL). In consideration that resorcinol class Hsp90 inhibitors were intravenously administrated in clinical trials, higher solubility should be favorable. Hence, further optimization should focus on both the biological activities and physicochemical properties of these compounds. Based on the X-ray structural analysis of compound **50**, the ethoxyl group at the 2-position of the pyrimidine ring was exposed to the solvent area, indicating this position should be suitable for introducing solubilizing groups. Thus, compounds that incorporated polar and flexible moieties as solubilizing functionalities were designed and synthesized.

Various substituted alcohols were introduced to the 2-position of the pyrimidine ring afforded analogues **59**−**65**. Data concerning the biochemical activities and physicochemical properties of the analogues were summarized in Table 3. All compounds of this series exhibited FP IC_{50} values lower than 30 nM, indicating higher affinity to Hsp90 than that of **50**. Compound **59** (2-methoxyethoxy group) showed significantly improved anti-proliferative activities with respect to **50**, with IC_{50} values of 0.17 μM in HCT116 cells and 0.12 μM in MCF-7 cells. Unfortunately, the other compounds (**60**−**65**) in this series showed decreased cellular activities. The inconsistency between the FP activities and anti-proliferative activities may be attributable to the unsuitable physicochemical properties of these compounds, such as low permeability.

To explain this inconsistency, physicochemical properties of these compounds were determined. The partition coefficient (CLogP) values were calculated using ChemBioDraw software (CambridgeSoft).

Distribution coefficient (Log $D_{7.4}$) and intrinsic aqueous solubility were obtained using a Gemini Profiler instrument (Pion Inc., MA, USA) by the "gold standard" Avdeef−Bucher potentiometric titration method.[44] Permeability was determined using the double-sink parallel artificial membrane permeability assay (PAMPA) on a PAMPA Explorer instrument (Pion Inc., MA, USA). As shown in Table 3, the most potent compound (**59**) showed the most favorable Log $D_{7.4}$ (2.14) and membrane permeability (55.55 × 10^{-6} cm/s). Additionally, **59** showed 2-fold improved intrinsic solubility compared to that of the lead compound **50**. The favorable physicochemical properties of compound **59** indicated that it possessed balanced hydrophilic and hydrophobic properties. Compounds **60**−**65**, which had more polar basic substituents, exhibited improved intrinsic solubility but obviously decreased Log $D_{7.4}$ values ranging from 1.04 to 1.48 and correspondingly lower permeability ranging from 3.06 × 10^{-6} cm/s to 30.25 × 10^{-6} cm/s. The lower Log $D_{7.4}$ and membrane permeability should lead to the inconsistent activities of compounds **60**−**65** between enzymatic and cellular levels.

Table 3. Further exploration of the R_2 position

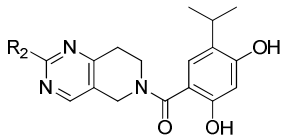

Compd	R_2	FP IC_{50} (μM)[a]	Anti-proliferative activities IC_{50} (μM)[a]		Physicochemical properties[b]			
			HCT116	MCF-7	CLogP	Log *D* pH 7.4	Solubility (μg/mL)	Pe, pH 7.4[a] (10^{-6}cm/s)
50		0.056 ± 0.002	0.76 ± 0.09	0.62 ± 0.05	2.70	2.95	66.0	72.41 ± 5.36
59	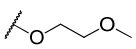	0.019 ± 0.001	0.17 ± 0.04	0.12 ± 0.01	2.06	2.14	139.8	55.55 ± 3.56
60	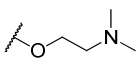	0.030 ± 0.005	2.38 ± 0.19	1.58 ± 0.05	2.27	1.04	148.2	3.25 ± 0.17
61	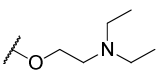	0.032 ± 0.004	0.89 ± 0.09	2.90 ± 0.83	3.32	1.17	151.4	25.70 ± 2.71

62	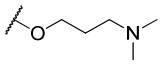	0.036 ± 0.004	0.92 ± 0.17	2.37 ± 0.05	2.62	1.09	155.6	4.15 ± 0.12
63	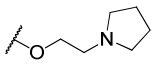	0.029 ± 0.004	0.98 ± 0.19	1.93± 0.08	2.94	1.12	145.5	3.06 ± 0.11
64	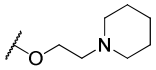	0.030 ± 0.002	0.78 ± 0.09	2.33 ± 0.82	3.50	1.21	174.6	20.46 ± 2.20
65	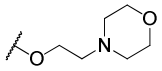	0.028 ± 0.006	1.06 ± 0.10	1.23 ± 0.14	2.29	1.48	139.9	30.25 ± 3.53

[a]Values shown are the mean ± SD (n = 3). [b]The partition coefficient (CLogP) values were calculated using ChemBioDraw software (CambridgeSoft). The distribution coefficient (Log $D_{7.4}$) and intrinsic aqueous solubility were obtained using a Gemini Profiler instrument (Pion Inc., MA, USA) by the "gold standard" Avdeef−Bucher potentiometric titration method. Permeability was determined using the double-sink parallel artificial membrane permeability assay (PAMPA) on a PAMPA Explorer instrument (Pion Inc., MA, USA).

According to the X-ray structural analysis of compound **50**, the 4-position of the pyrimidine ring is surrounded by the hydrophobic side chains of the Lys58, Ile96 and Met98 residues, and hydrophobic substituents at this position may facilitate improved activities. Thus, a series of compounds with substituents introduced at the 4-position of the pyrimidine ring were investigated. Table 4 summarized the activities and physicochemical properties of compounds **68**−**78**. Alkoxyl groups were introduced to yield compounds **68**−**71**. Compounds **68**−**70** bearing small hydrophobic residues (methoxyl, ethyoxyl, and n-propoxyl group) retained the Hsp90 affinity and cellular activities. Compound **70** (n-propoxyl group) showed better cellular activities than compound **59**, possibly because of its higher permeability (87.71×10^{-6} cm/s). Compound **71** (isopropoxyl group) showed slightly decreased activities in the FP and anti-proliferative assays relative to those of **68**−**70**. Alkylamino moieties were introduced to yield **72**−**78**. Compounds **72**−**77** retained their activities at enzymatic and cellular levels, among which **73** exhibited the best activities with IC_{50} values of 0.14 μM in HCT116 cells and 0.10 μM in MCF-7 cells. Compound **78** (IC_{50}, 0.102 μM) with a diethylamino substitution exhibited markedly decreased potency with respect to the dimethylamino analogue **77** (IC_{50}, 0.016 μM) in the FP assay. Indeed, the diethylamino group was too big for the hydrophobic pocket around the 4-position of the pyrimidine ring. Correspondingly, the cellular effects of **78** were dramatically decreased.

Physicochemical properties determination of this series revealed that compounds **68**−**77** possessed acceptable CLogP values ranging from 2.99 to 4.05, Log $D_{7.4}$ values ranging from 2.21 to 3.84, and

permeability ranging from 56.35 × 10^{-6} cm/s to 87.71 × 10^{-6} cm/s.[45] Alkoxyl substituted compounds **68**–**71** possessed decreased solubility compared with **59**. Most of the alkylamino bearing compounds showed improved or retained solubility, except for **74**. In this series, compound **73** exhibited the most favorable physicochemical properties.

Table 4. R_3 expansion

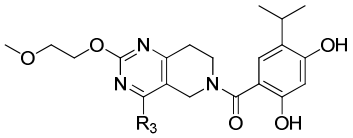

Compd	R_3	FP IC_{50} (μM)[a]	Anti-proliferative activities IC_{50} (μM)[a]		Physicochemical properties[b]			
			HCT116	MCF-7	CLogP	Log *D* pH 7.4	Solubility (μg/mL)	Pe, pH 7.4[a] (10^{-6}cm/s)
59	H	0.019 ± 0.001	0.17 ± 0.04	0.12 ± 0.01	2.06	2.14	139.8	55.55 ± 3.56
68		0.030 ± 0.001	0.25 ± 0.05	0.14 ± 0.03	2.99	2.56	93.5	75.75 ± 3.17
69		0.026 ± 0.002	0.32 ± 0.06	0.18 ± 0.02	3.52	2.74	86.1	77.26 ± 4.69
70	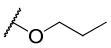	0.036 ± 0.011	0.12 ± 0.03	0.04 ± 0.01	4.05	3.59	73.6	87.71 ± 5.45
71		0.058 ± 0.008	0.74 ± 0.07	0.25 ± 0.04	3.83	3.84	40.2	79.43 ± 3.37
72		0.017 ± 0.001	0.27 ± 0.01	0.29 ± 0.03	2.88	2.21	177.7	57.50 ± 6.86
73		0.028 ± 0.002	0.14 ± 0.02	0.10 ± 0.01	3.40	2.32	192.3	71.47 ± 1.68
74	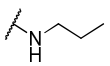	0.032 ± 0.002	0.40 ± 0.06	0.35 ± 0.11	3.93	2.92	114.3	78.67 ± 12.10
75		0.030 ± 0.003	0.79 ± 0.05	0.25 ± 0.03	3.71	2.98	137.4	62.44 ± 2.86
76	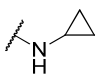	0.019 ± 0.002	0.23 ± 0.02	0.16 ± 0.01	3.46	2.45	157.0	56.35 ± 7.13

77		0.016 ± 0.001	0.26 ± 0.02	0.33 ± 0.12	2.96	2.35	152.7	82.96 ± 7.07
78		0.102 ± 0.003	3.57 ± 0.04	2.89 ± 0.35	4.02	3.08	95.9	107.14 ± 9.65

[a]Values shown are the mean ± SD (n = 3). [b]The partition coefficient (CLogP) values were calculated using ChemBioDraw software (CambridgeSoft). The distribution coefficient (Log $D_{7.4}$) and intrinsic aqueous solubility were obtained using a Gemini Profiler instrument (Pion Inc., MA, USA) by the "gold standard" Avdeef−Bucher potentiometric titration method. Permeability was determined using the double-sink parallel artificial membrane permeability assay (PAMPA) on a PAMPA Explorer instrument (Pion Inc., MA, USA).

Hsp90α selectivity versus Grp94 of selected compounds

Reported results indicated that flexible sequence 104−111 on Hsp90α/β could adopt a compound-induced rearrangement and form an extended α-helix conformation. The equivalent sequence in Grp94 and Trap-1 were disordered and unable to accommodate the extended α-helix conformation. This unique conformation rearrangement was chemotype-dependent and believed to contribute to the Hsp90α/β selective inhibition.[43] The clinical compounds, including **3** and **9**, induced conformation rearrangement of sequence 104−111 on Hsp90α/β and exhibited moderate selectivity versus Grp94 and Trap-1. However, compound **7** which adopted similar bound conformation with the four isoforms, showed no isoform selectivity. The crystal structure of **50** with Hsp90α revealed that the tetrahydropyrido ring in the molecule could adopt two different conformations (conformation A/B) to bind to the protein. When the tetrahydropyrido ring adopt conformation B, the flexible sequence 104−111 on Hsp90α was induced to form the extended α-helix conformation, indicating the compound might show some Hsp90α selectivity. Thus, the Hsp90α selectivity versus Grp94 of some selected compounds were determined. The results were shown in Table 5.

Compound **27** with a tetrahydropyrido[4,3-d]pyrimidine core, showed a 10-fold selectivity. Correspondingly, compound **28** with a reduced ring-size core showed no selectivity, indicating that the conformation flexibility of the tetrahydropyrido[4,3-d]pyrimidine core contributed to the Hsp90α selective inhibition. Substitution at R_2 position were tolerated for the Hsp90α selectivity, compounds **49**−**54** and **59**−**61** showed maintained selectivity (6.6-fold to 10.9-fold). The influence of substituents at R_3 position on selectivity was also investigated. Results showed that analogues **69**−**71** and **73**−**75** bearing relatively big substituents possessed improved selectivity (over 20-fold), suggesting that

hydrophobic substituents at R_3 position were favorable for the compound adopting conformation B.

Table 5. Hsp90α selectivity versus Grp94

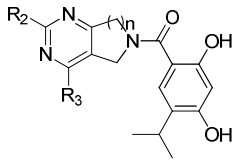

Compd	n	R_2	R_3	Hsp90α FP IC_{50} (μM)[a]	Grp94 FP IC_{50} (μM)[a]	Fold Grp94/ Hsp90α
27	2	CH_3	H	0.026 ± 0.011	0.245 ± 0.016	9.4
28	1	CH_3	H	0.038 ± 0.014	0.050 ± 0.003	1.3
49	2		H	0.075 ± 0.015	0.498 ± 0.007	6.6
50	2		H	0.056 ± 0.002	0.561 ± 0.016	10.0
51	2	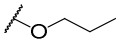	H	0.060 ± 0.004	0.498 ± 0.009	8.3
52	2		H	0.065 ± 0.005	0.518 ± 0.015	8.0
53	2	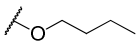	H	0.088 ± 0.001	0.670 ± 0.017	7.6
54	2	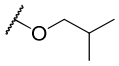	H	0.065 ± 0.001	0.706 ± 0.005	10.9
59	2	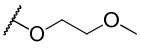	H	0.019 ± 0.001	0.198 ± 0.005	10.4
60	2	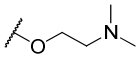	H	0.030 ± 0.005	0.290 ± 0.013	9.7
61	2	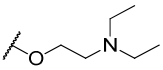	H	0.032 ± 0.004	0.217 ± 0.004	6.8
68	2	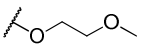		0.030 ± 0.001	0.232 ± 0.006	7.7
69	2	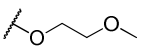		0.026 ± 0.002	0.608 ± 0.015	23.4

70	2	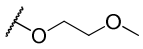	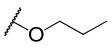	0.036 ± 0.011	0.929 ± 0.009	25.8
71	2	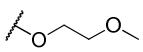		0.058 ± 0.008	1.316 ± 0.018	22.7
72	2	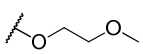		0.017 ± 0.001	0.196 ± 0.006	11.5
73	2	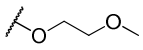		0.028 ± 0.002	0.729 ± 0.018	26.0
74	2	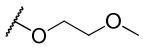	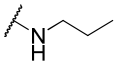	0.032 ± 0.002	0.796 ± 0.009	24.9
75	2	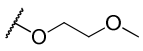		0.030 ± 0.003	0.787 ± 0.008	26.2
76	2	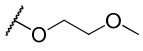		0.019 ± 0.002	0.216 ± 0.003	11.4
77	2	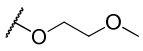		0.016 ± 0.001	0.195 ± 0.006	12.2
78	2	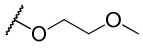		0.102 ± 0.003	1.100 ± 0.016	10.8
8	—	—	—	0.013 ± 0.002	0.022 ± 0.007	1.7

[a]Values shown are the mean ± SD (n = 3).

In vitro anti-cancer effects

The anti-proliferative activities of compounds **59**, **70** and **73** were evaluated using a panel of human cancer cell lines from diverse tissue origins. As summarized in Table 6, the three compounds exhibited broad-spectrum activities and potently inhibited cell proliferation, with IC_{50} values ranging from 0.018 to 0.434 μM. To evaluate the selective anti-proliferative effects of the compounds on cancer cells, we determined their effects on normal human liver cells (L-02). Despite the potent anti-proliferative effects against various cancer cell lines, the three compounds showed much lower cytotoxicity on L-02 cells. The compounds' good cellular selectivity supporting a potentially safer in vivo profile.

Table 6. Anti-proliferative effects of **59**, **70** and **73** in a panel of human cancer cell lines and normal human liver cells (L-02)

Cell line	Tissue	Anti-proliferative activities IC_{50} (μM)[a]

		59	70	73	8
MDA-MB-231	Breast carcinoma	0.129 ± 0.023	0.122 ± 0.015	0.119 ± 0.007	0.038 ± 0.004
MDA-MB-468	Breast carcinoma	0.172 ± 0.033	0.139 ± 0.025	0.135 ± 0.015	0.066 ± 0.009
SKBr3	Breast carcinoma	0.175 ± 0.056	0.220 ± 0.033	0.243 ± 0.025	0.071 ± 0.017
T47D	Breast carcinoma	0.183 ± 0.034	0.178 ± 0.032	0.195 ± 0.024	0.024 ± 0.004
BT474	Breast carcinoma	0.144 ± 0.016	0.118 ± 0.019	0.095 ± 0.017	0.032 ± 0.007
U2OS	Human osteosarcoma	0.107 ± 0.067	0.171 ± 0.030	0.052 ± 0.012	0.067 ± 0.010
MKN28	Human gastric carcinoma	0.325 ± 0.073	0.407 ± 0.029	0.434 ± 0.093	0.129 ± 0.009
A549	Human pulmonary carcinoma	0.168 ± 0.002	0.060 ± 0.014	0.194 ± 0.017	0.050 ± 0.006
HepG2	Hepatocellular carcinoma	0.119 ± 0.037	0.222 ± 0.024	0.153 ± 0.009	0.018 ± 0.005
K562	Chronic myeloid leukemia	0.109 ± 0.003	0.150 ± 0.009	0.119 ± 0.005	0.038 ± 0.005
MV4-11	Acute monocytic leukemia	0.031 ± 0.001	0.018 ± 0.002	0.027 ± 0.003	0.011 ± 0.003
L-02	Normal human liver cells	27.62 ± 3.02	30.94 ± 3.91	33.95 ± 7.33	11.64 ± 5.04

[a]Values shown are the mean ± SD (n = 3).

To further confirm the mechanisms underlying the potent anti-proliferative activities, effects of the three compounds on cellular markers were investigated. As expected, Western blot analysis after 24 h of exposure to various concentrations of the compounds indicated the depletion of the Hsp90 client proteins Akt, Erk, and phosphorylated Erk (p-Erk) and significant induction of Hsp70 in a dose-dependent manner. What's more, Hsp90 was slightly induced. The results confirmed that these compounds inhibit cell growth by an Hsp90-inhibition-dependent mechanism.

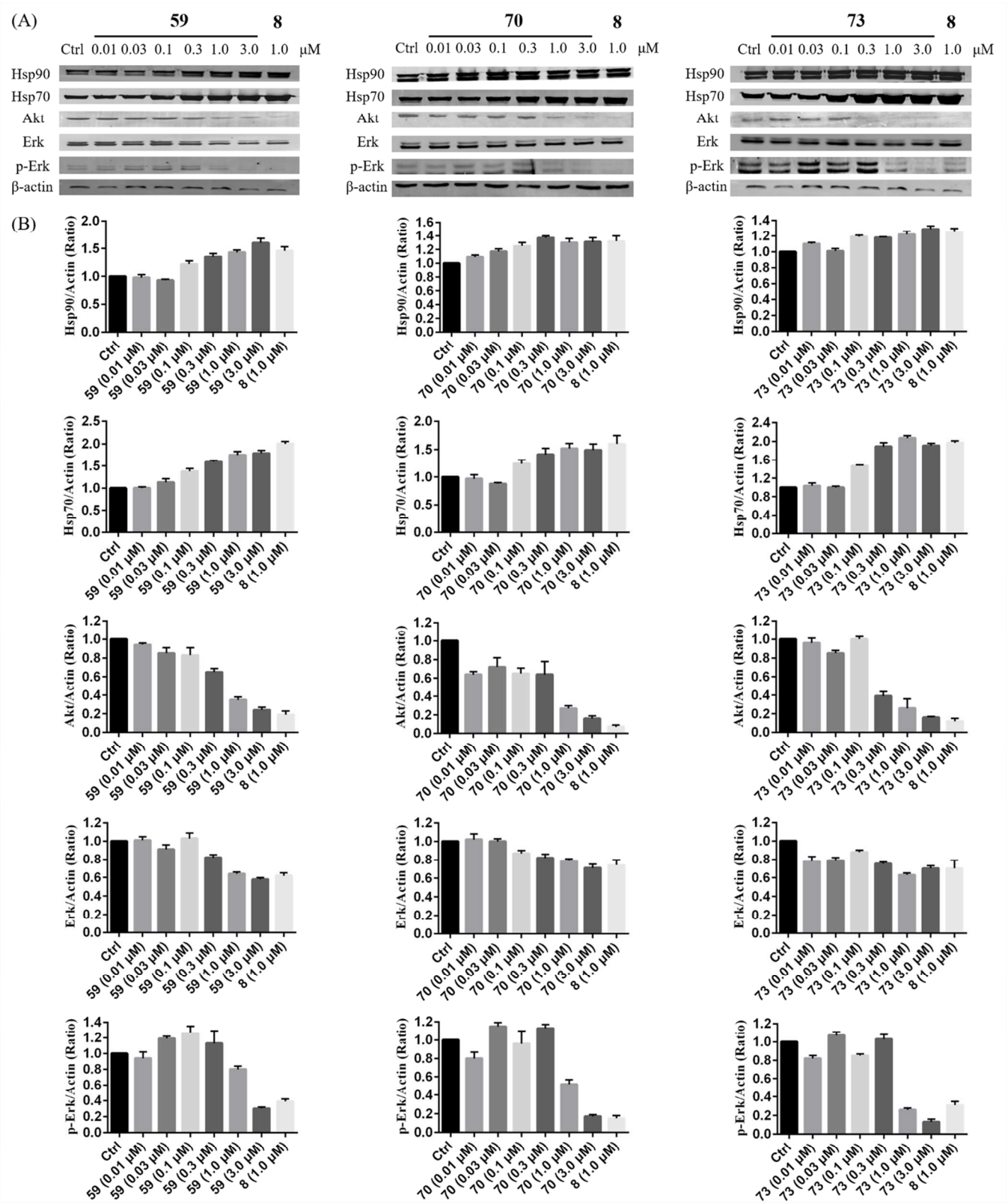

Figure 4. (A) Western blot analysis of the biomarker levels in HCT116 cells after incubation for 24 h with **59**, **70** and **73**. (B) Densitometry analysis of the protein levels are showed as normalized (to actin) ratios. Actin is used as the

control for protein loading. **8** is used as the reference compound.

In vitro metabolic stability, CYP450 inhibition, in vivo pharmacokinetics and tissue distribution

Preliminary ADME properties assessments of **59**, **70**, **73** were conducted to evaluate the potential for further development. The in vitro metabolic stability of the three compounds were assessed in human liver microsome. As shown in Table 7, compounds **59** and **73** possessed good human microsomal stability, especially **73**. By contrast, compound **70** showed poor human microsomal stability.

Table 7. In vitro metabolic stability in human liver microsome

Parameters	Compd		
	59	**70**	**73**
60 min remaining (%)	81.5	59.5	90.4
$t_{1/2}$ (min)	194	69	212
Clint (mL/kg)	4.88	13.74	4.45

Then compounds **59** and **73** were selected for further in vivo pharmacokinetics study in healthy rats. As shown in Figure 5, the two compounds showed low bioavailability after oral administration. For intravenous dosing, **59** and **73** exhibited acceptable half-lives (4.16 h and 3.95 h). In addition, **73** showed a higher exposure level than **59**. Both compounds showed high volumes of distribution (86.62 L/kg and 29.59 L/kg) after intravenous administration, indicating high penetration into tissues. Then compound **73**, which possessed higher exposure level, was selected for tissue distribution study in an HCT116 xenograft model. As shown in Figure 6, after intravenous administration of 60 mg/kg, **73** was rapidly cleared from blood, spleen and liver. In contrast, the compound showed higher concentration and longer retention in tumor, significant levels of compound were detected in tumors after 48h (>3 μM/L). This specific accumulation of **73** in tumors indicated the long action duration in xenograft models. Further CYP450 inhibition determination showed **73** had no serious inhibition on the five major isozymes (data shown in Table 8).

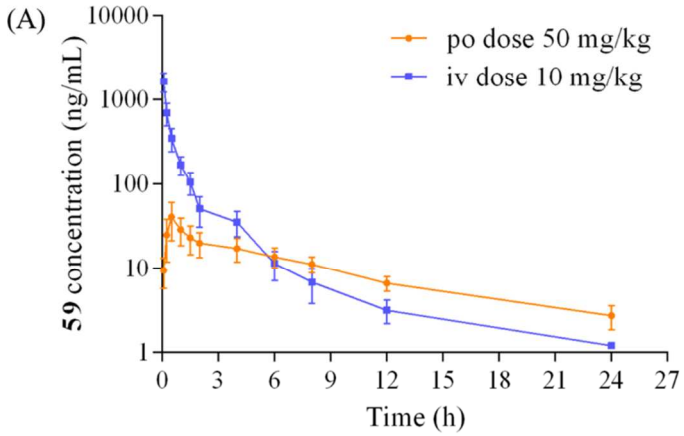

Parameters	59	
	p.o.	i.v.
Dose (mg/kg)	50	10
Cmax (μg/L)	40.69	/
Tmax (h)	0.5	/
$t_{1/2}$ (h)	7.40	4.16
CLz (L/h/kg)	198.95	14.12
Vz (L/kg)	2072.05	86.62
AUC_{0-t} (μg·h/L)	264.53	756.94
F (%)	7.0	/

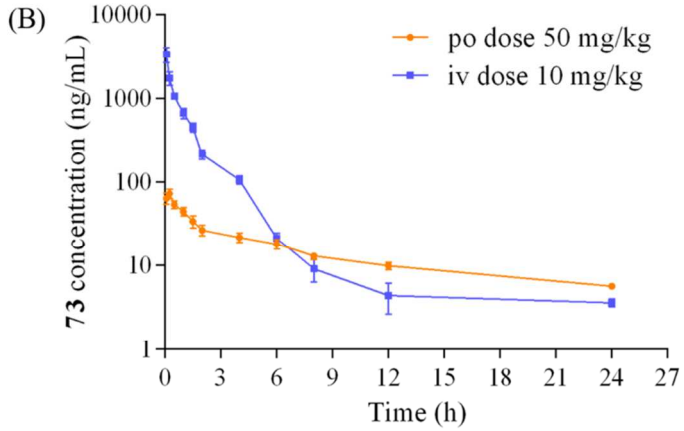

Parameters	73	
	p.o.	i.v.
Dose (mg/kg)	50	10
Cmax (μg/L)	72.60	/
Tmax (h)	0.5	/
$t_{1/2}$ (h)	9.40	3.95
CLz (L/h/kg)	123.87	5.25
Vz (L/kg)	1620.19	29.59
AUC_{0-t} (μg·h/L)	408.69	1932.03
F (%)	4.23	/

Figure 5. Pharmacokinetic analysis in healthy rats. (A) Plasma concentration vs. time profile and pharmacokinetic parameters of compound **59**. (B) Plasma concentration vs. time profile and pharmacokinetic parameters of compound **73**. The pharmacokinetic parameters are calculated using DAS2.0 software.

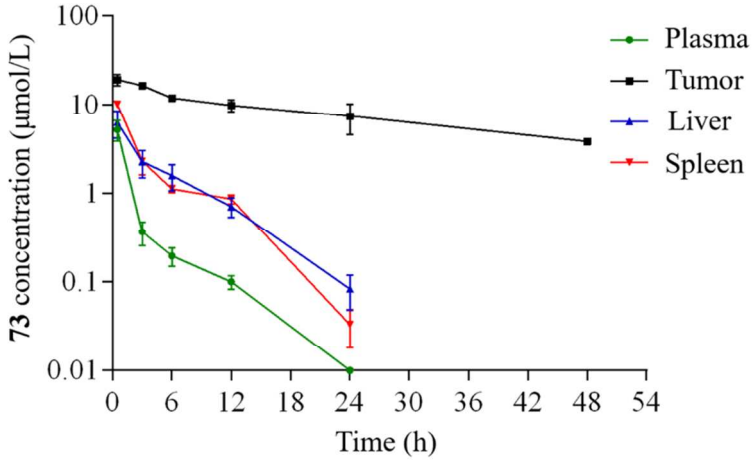

Figure 6. Tissue distribution of **73** in an HCT116 xenograft model. The plasma, tumors, livers, and spleens were collected at the indicated times after intravenous (iv) administration of 60 mg/kg **73**.

Table 8. CYP450 isozymes inhibition of **73**

Isozymes	% inhibition[a]	
	73	Positive controls[b]
CYP1A2	8	76
CYP2C9	36	82
CYP2C19	21	88
CYP2D6	48	89
CYP3A4	22	72

[a]Performed at 10 μM concentration. [b]α-naphthoflavone (CYP1A2), sulfaphenazole (CYP2C9), ticlopidine (CYP2C19), quinidine (CYP2D6), and ketoconazole (CYP3A4) are used as the positive control.

In vivo anti-tumor efficacy

The in vivo anti-tumor efficacy of compound **73** was evaluated in mice bearing HCT116 xenograft tumors. In this study, the hydrochloride salt of **73** was administered intraperitoneally (ip) at 40 and 60 mg/kg according q.o.d. for 16 days. **8** (60 mg/kg) was chosen as the reference compound. As shown in Figure 7A, compound **73** caused significant inhibition of tumor growth. The T/C values of the 40 mg/kg and 60 mg/kg doses were 45% and 23%, respectively. The 60 mg/kg dose showed equivalent tumor growth inhibition to that of the reference compound **8** (60 mg/kg). Compound **73** was well tolerated, as evidenced by the absence of serious weight loss (Figure 7B). Hematoxylin-eosin (H&E) staining (Figure 7C) revealed that tumor cells in the xenografts decreased significantly after treatment with compound **73**. The pharmacodynamic biomarker changes in tumor xenografts of compound **73** were assessed by Western blot 12 h after the final treatment. As shown in Figure 7D−E, compound **73** significantly upregulated Hsp90 and Hsp70 via a feedback response to Hsp90 inhibition and induced an obvious decrease of the client proteins Akt and Erk, confirming that its potent in vivo anti-tumor efficacy was Hsp90 dependent.

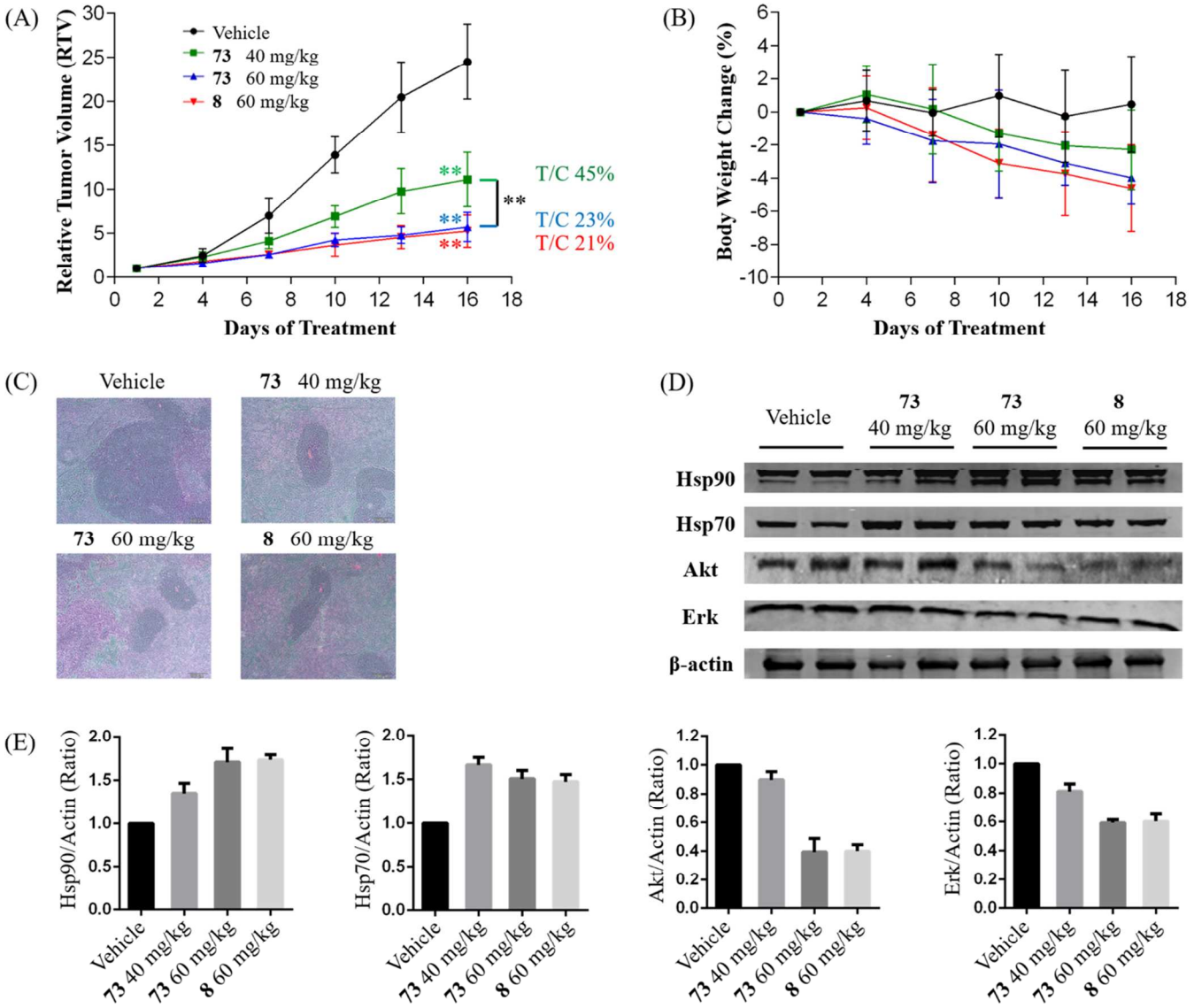

Figure 7. Anti-tumor efficacy of compound **73** in HCT116 human colon cancer xenografts. Compound **73** was intraperitoneally (ip) administrated according q.o.d. for 16 days once the mean tumor volume reached 100 mm^3. (A) Relative tumor volume (RTV) changes after treatment. Tumor diameters were measured every three days and used to calculate the tumor volumes. RTV = V_t/V_0, where V_t is the tumor volume measured at each time point, and V_0 is the tumor volume at the beginning of treatment. Bars represent SEM. ** $p < 0.01$, Student's t-test (n = 6). (B) Pharmacodynamic biomarker changes assessed by Western blot (12 h after final dose). (C) Representative H&E images of the sacrificed tumors. (D) Western blot analysis of the pharmacodynamic biomarker changes in tumor xenografts. Actin is used as the control for protein loading. (E) Densitometry analysis of the protein levels are showed as normalized (to actin) ratios.

Ocular toxicity evaluation

Visual disturbance is the most common adverse event of Hsp90 inhibitors in clinical trials. It was

reported that ocular toxicity is associated with the drug exposure level in retina. High retina exposed Hsp90 inhibitors would induce photoreceptor cell death and retinal damage. The inhibitors with lower retina/plasma exposure ratios and faster retinal elimination, including **6** and **11**, showed no ocular toxicity either in clinical trials or preclinical models, indicating the ocular toxicity was drug-related.[33, 39] In order to assess the safety profile, ocular toxicity of **73** was evaluated in a rat retinal damage model. **7** (NVP-AUY922) was chosen as the reference compound because visual disorders were observed both in clinical trials and the preclinical model.[36,39] Rats were intravenously treated with 2-day consecutive dosing of vehicle, **73** (20 mg/kg), or **7** (10 mg/kg), then retinas were harvested for further biological evaluation. Hsp70 upregulation is a surrogate marker for Hsp90 inhibition, so we detected the expression level of Hsp70 in retinal tissue by Western blot. As shown in Figure 8A−B, **73** treatment showed weak effect on Hsp70 expression while the reference compound **7** caused robust up-regulation of Hsp70. This indicated that **73** had minimal influence on retina. The Hsp70 up-regulation was also confirmed by immunohistochemistry assay (Figure 8C). At the same time, apoptotic induction effect on retinal cells was evaluated by TUNEL staining (Figure 8D). No obvious retina cell death was observed after treatment with **73**. In contrast, **7** treatment induced extensive retina cell death, which was consistent with the clinical visual disorders. Taken together, weak Hsp70 up-regulation and no retinal cell apoptotic induction indicated compound **73** exhibited no ocular toxicity.

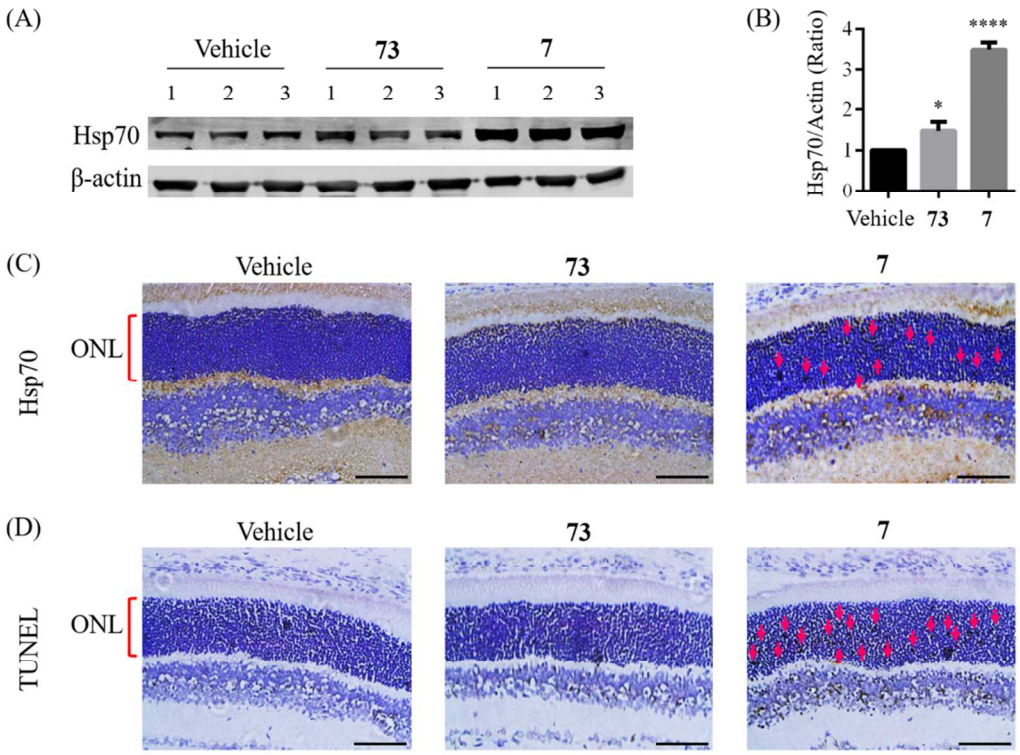

Figure 8. Ocular toxicity evaluation of compound **73** in a rat retinal damage model. SD rats (n = 3) were intravenously (iv) treated with 2 consecutive daily doses of vehicle, **73** (20 mg/kg) or **7** (NVP-AUY922, 10 mg/kg). The retina tissues were harvested 24 h after the last treatment. (A) Hsp70 regulation in retina tissues after treatment assessed by Western blot. Actin is used as the control for protein loading. (B) Densitometry graph of Hsp70 regulation. (C) Hsp70 immunohistochemistry in the retina after treatment. Scale bar, 50 μm. (D) Apoptosis induction in the retina after treatment evaluated by TUNEL staining. Scale bar, 50 μm.

CONCLUSION

The structure-activity relationships and structure-property relationships of novel Hsp90 inhibitors were extensively studied, focusing on the lead compound **15**. A series of derivatives were developed and exhibited improved Hsp90-inhibition and anti-proliferative activities. In addition, most of the synthetic compounds showed minimal to moderate Hsp90α selectivity versus Grp94, should be because of the conformation flexibility of the tetrahydropyrido[4,3-d]pyrimidine core. Compounds **59**, **70** and **73** were selected for further evaluation. Potent anti-proliferative activities of the three compounds against a panel of human cancer cell lines from diverse tissue origins indicated the broad-spectrum anti-cancer effects. Modulating the in vitro biomarkers in HCT116 cells resulted in significant degradation of the Hsp90 clients Akt, Erk and p-Erk associated with a dramatic induction of Hsp70, which is a commonly used biomarker for Hsp90 inhibition. In the ADME assessment, **59** and **73** showed good human microsomal

stability. After iv administration in healthy rats, both compounds showed acceptable half-lives. Considering the higher exposure level in blood, **73** was chosen for further in vivo study. In HCT116 xenografts, compound **73** showed significant tumor growth inhibition with no serious weight loss. Potent tumor accumulation of **73** was also observed. In a rat retina damage model, **73** showed no ocular toxicity, indicating its good safety profile. Overall, these results indicate that compound **73** is a promising candidate agent for the treatment of cancer.

EXPERIMENTAL SECTION

1. Biology.

1.1. FP competition assay.

FP competition assay was used to evaluate the binding affinities of the compounds to Hsp90α^N and Grp94^N. The compounds (in DMSO) were prepared into various concentration solutions by serial diluted in assay buffer (20 mM HEPES, PH 7.3, 50 mM KCl, 5 mM $MgCl_2$, 20 mM Na_2MoO_4, 0.01% NP40, 2 mM DTT, 0.1 mg/mL BGG). The fluorescent geldanamycin (GM-FITC) and purified Hsp90α^N or Grp94^N were diluted into the needed concentration in assay buffer. The experiments were conducted in 384 well black flat-bottomed polystyrene plates (Corning #3575). For each assay, equal volumes of the diluted compounds (20 μL), Hsp90α^N or Grp94^N (30 nM final) and GM-FITC solution (10 nM final) were added into the plate wells orderly and yielded a final volume of 60 μL. Plates were covered and rocked for 30 min at room temperature in the dark and then the FP values were detected using a SpectraMax multimode microplate reader (Molecular Devices) with excitation and emission wavelength at 485 and 535 nm, respectively. For each assay, the FP values of blank controls (GM-FITC only) were recorded as P_{min}, the FP values of negative controls (GM-FITC and protein) were recorded as P_{max} and the FP values of test wells (compounds, GM-FITC and protein) were recorded as P_{test}. The inhibition rate of the compounds at each concentration point was calculated using the equation as follows: inhibition rate (%) = $[1 - (P_{test} - P_{min}) / (P_{max} - P_{min})] \times 100\%$ and the IC_{50} values were calculated using Graphpad Prim 6.0 software.

1.2. In vitro anti-proliferative assay.

Anti-proliferative activities of the compounds against different cancer lines were determined using

MTT assay. Cells were seeded into 96-well plates at 5000 cells per well and incubated for 24 h. Then the cells were treated with either serial dilutions of the compounds or DMSO for 72 h. MTT solution (5 mg/mL) was added and the plates were incubated at the temperature of 37 ^{o}C for another 4 h. After removing the solution in the wells of the plates, 150 μL of DMSO was added to dissolve the MTT−formazan crystals. The absorbance values (OD value) were determined using the Elx800 absorbance microplate reader (BioTek, Vermont, USA) at 570 nm. Cell viability inhibition rates of the compounds at each concentration point were calculated using the equation as follows: inhibition rate (%) = $[1 - (OD_{test} - OD_{blank}) / (OD_{control} - OD_{blank})] \times 100\%$. The IC_{50} values were calculated using Graphpad Prim 6.0 software.

1.3. Western blot analysis.

Biomarker modulation was determined by Western blot. HCT116 cells seeded in petri dishes were treated with serially diluted compounds for 24 h. **8** (1 μM) was chosen as the reference compound. Then the cells were rinsed with PBS, trypsinized and lysed in lysis buffer (50 mM Tris-Cl, pH 7.5, 150 mM NaCl, 1 mM EDTA, 1% NP-40, 0.2 mM PMSF, 0.1 mM NaF and 1.0 mM DTT). The lysates were centrifuged at 13000 rpm for 10 min at 4 °C and the supernatants were collected. The protein concentration was determined using BCA assay (Thermo, Waltham, MA). Equal amounts of the total protein extracts were separated by SDS-PAGE and then transferred onto PVDF membranes (PerkinElmer, Northwalk, CT, USA). After blocking the nonspecific binding sites with 1% BSA for 1 h, membranes were incubated at 37 °C for 1 h and then at 4°C overnight with the following primary antibodies: Anti-Hsp90 (Cell Signaling Technology, Inc., USA), Anti-Hsp70 (Cell Signaling Technology, Inc., USA), Anti-Akt (Cell Signaling Technology, Inc., USA), Anti-Erk (Cell Signaling Technology, Inc., USA), Anti-Phospho Erk (Cell Signaling Technology, Inc., USA) and anti-actin (Proteintech Group, Inc., USA). Then the membranes were treated with a DyLight 800 labeled secondary antibody at 37 °C for 1 h and scanned using the Odyssey infrared imaging System (LI-COR, Lincoln, Nebraska, USA).

1.4. Human microsomal stability and CYP450 inhibition.

Compounds were pre-incubated with human microsome (0.5 mg/ml) at 1 μM for 5 min at 37 °C in phosphate buffer (100 mM, PH 7.4). Then 1 mM NADPH was added to initiate the reaction. After

incubation for different time (0 min, 15 min, 30 min, 60 min, 120 min) at 37 °C, cold acetonitrile was added to precipitate the protein. Then centrifuged and the supernatants were analyzed by LC−MS/MS.

The CYP450 inhibition activities of **73** on the five major isozymes (CYP1A2, CYP2C9, CYP2C19, CYP2D6, CYP3A4) were evaluated. The assay was conducted in phosphate buffer (100 mM, PH 7.4). For each assay, equal volumes (25 μL) of diluted microsome (0.2 mg/mL final), **73** or the positive control inhibitors (10 μM final, DMSO as the negative control), specific substrates of the isozymes (10 μM final, phenacetin, diclofenac, mephenytoin, dextromethorphan, and midazolam for CYP1A2, CYP2C9, CYP2C19, CYP2D6, and CYP3A4, respectively) were pre-incubated at 37 °C for 5 min. Then 25 μL NADPH (1 mM, final) was added to initiate the reaction. After 20 min incubation, 100 μL cold acetonitrile was added to terminate the reaction. The samples were centrifuged and supernatants were analyzed by LC−MS/MS to determine the metabolites. The inhibition rate was calculated using the following equation: inhibition rate (%) = [1− (Formation of the metabolite in the presence of tested compound)/ (Formation of the metabolite of negative control)] × 100%.

1.5. Pharmacokinetics.

The pharmacokinetic studies of the test compounds were conducted in rats (n = 6 per group). The rats were administered test compounds intravenously at 10 mg/kg or orally at 50 mg/kg. Blood samples (150 μL) were collected into heparinized Eppendorf tubes at predetermined time points (0, 0.083, 0.25, 0.5, 1, 1.5, 2, 4, 6, 8, 12, and 24 h) and centrifuged immediately at 4 °C and 8000 rpm for 5 min. The plasma samples were stored at −80 °C until analysis by LC−MS/MS.

1.6. Tissue distribution study.

Tissue distribution of **73** was assessed in an HCT116 xenograft model. When the average tumor volume reached approximately 500 mm^3, the mice were intravenously treated with **73** (60 mg/kg). The plasma, tumors, livers, and spleens were collected at the indicated times. Portion of the tumors, livers and spleens were weighed and homogenized. Acetonitrile was added into the samples to precipitate the protein and then centrifuged. The supernatants were analyzed by LC−MS/MS.

1.7. In vivo xenograft study.

The in vivo anti-tumor activity of compound **73** was evaluated in male nude mice. HCT116 cells (5

× 10^6) were injected subcutaneously in the right flank. When the average tumor volume reached approximately 100 mm^3, the mice were randomized into 4 cohorts and intraperitoneally treated according q.o.d. for 16 days. Tumor growth and body weight were monitored every three days. The tumor volume was calculated using the formula (smaller diameter)^2 × (larger diameter)/2, and the RTV was calculated according as RTV = V_t/V_0, where V_t is the tumor volume measured at each time point after treatment, and V_0 is the tumor volume at the beginning of treatment. The drug efficacy was assessed by calculating the T/C values on the final day of the study using the formula T/C = (mean $RTV_{Treated}$ / mean $RTV_{Control}$) ×100%.

Tumors were harvested 12 hours after the final treatment and immediately flash-frozen in liquid nitrogen. Half of the tumors were used for Western blot to analyze changes in the pharmacodynamic biomarkers after treatment. The tumors were homogenized, and the concentrations of the protein lysates were determined using a bicinchoninic acid (BCA) kit. Then, the protein lysates were analyzed by Western blot. The remaining tumors were embedded in paraffin for sectioning, and the sections were subjected to H&E staining analysis.

1.8. Ocular toxicity.

Ocular toxicity of **73** was assessed in a rat retinal damage model according to the reported methods.[39] SD rats (n = 3) were intravenously (iv) treated with 2 consecutive daily doses of vehicle, **73** (20 mg/kg) or **7** (NVP-AUY922, 10 mg/kg). Compounds were formulated in 10% DMSO/14% Cremophor RH40/76% D5W (5% dextrose in water). The retina tissues were harvested 24 h after the last treatment. Retina tissue from one eye of each rat was homogenized for western blot analysis. Retina tissue from another eye was sectioned for immunohistochemistry and TUNEL staining analysis.

2. Docking.

Compound **15** was imported to Discovery Studio (DS) 4.0 and the 3D conformation was generated by the "Prepare Ligands" protocol at pH 7.0. Then the compound was energy minimized in CHARMm force field for docking. The $Hsp90^N$-ligand complex (PDB code: 2XJX) downloaded from the Protein Data Bank was chosen for docking studies. The molecular docking was carried out using GOLD 5.1 software. The protein was prepared and the conserved water molecules HOH2039, HOH2084,

HOH2198 were kept for docking. Protein residues around the original ligand (radius 8.0 Å) that completely covered the ATP binding site were defined as the binding site. Docking studies were performed using the standard default settings with 100 GA runs of molecules. For each GA run, a maximum of 125,000 operations was performed. The annealing parameters were used as default. Cutoff values of 3.0 Å for hydrogen bonds and 4.0 Å for van der Waals interactions were set. Docking was terminated when the top ten solutions attained root-mean-square deviation (RMSD) values within 1.5 Å.

3. Crystallography.

Compound **50** was added to the purified Hsp90α N-terminal domain (20 mg/mL) in a 3:1 molar ratio, and the mixture was incubated for 1 h at 4 °C. After incubation, the mixture was centrifuged for 10 min, and the precipitate was removed. Crystallization was performed at 4 °C in a 24-well plate using the hanging drop vapor diffusion method. The cocrystals were grown in a reservoir solution consisting of 100-mM Tris-HCl, pH 8.5, 20% polyethylene glycol (PEG) 4000, and 200-mM $MgCl_2$.

The crystals were mounted and flash-frozen in liquid nitrogen for diffraction tests and data collection. All data sets were collected at 100 K on the BL17U1 beamline at the Shanghai Synchrotron Radiation Facility (SSRF, Shanghai, China) and were processed with the HKL2000 software package. The structures were solved by molecular replacement using the PHENIX software. The search model used for the crystal was the previously reported structure of $Hsp90\alpha^N$ (PDB code 3T0H). The structures were refined using PHENIX. With the aid of the program Coot, water and other molecules were fitted into the initial Fo-Fc map.

4. Physicochemical properties.

The partition coefficient (CLogP) values were calculated using ChemBioDraw software (CambridgeSoft). The distribution coefficients (Log $D_{7.4}$) and intrinsic aqueous solubility were determined on a Gemini Profiler instrument (pION) by the "gold standard" Avdeef-Bucher potentiometric titration method.[44] Permeability coefficients were determined via double-sink PAMPA on a PAMPA Explorer instrument (pION). The detailed experimental procedures have been reported previously.[46]

5. Chemistry.

General Methods. All solvents and reagents were obtained commercially. Solvents were dried according to standard procedures, air and moisture sensitive reactions were performed under nitrogen. Reactions were monitored by thin-layer chromatography (TLC) on 0.25 mm silica gel plates (GF254) and visualized under UV light. Melting points were determined with a Melt-Temp II apparatus. The ^{1}H NMR and ^{13}C NMR spectra were measured on a Bruker AV-300 instrument using deuterated solvents with tetramethylsilane (TMS) as internal standard. ESI-mass and high resolution mass spectra (HRMS) were recorded on a Water Q-Tof micro mass spectrometer. The purity (≥ 95%) of the compounds was verified by the HPLC study performed on Agilent C18 (4.6 mm × 150 mm, 3.5μm) column using a mixture of solvent methanol/water at a flow rate of 0.5 mL/min and monitoring by UV absorption at 254 nm.

The detailed synthesis procedures of the substituted benzoic acid intermediates **17a−c** were listed in the supporting information.

General procedure for the synthesis of 22a, 22b. The commercial **20a** or **20b** (40 mmol) was dissolved in N, N-dimethylformamide dimethyl acetal (55 mL), the mixture was refluxed for 1.5 h and concentrated. The residue was triturated with hexane, filtered and washed with hexane to give **21a** or **21b** without further purification. Then the intermediate was dissolved in EtOH (200 mL), acetamidine hydrochloride (22.7 g, 240 mmol) and Et_3N (33.3 mL, 240 mmol) were added and the mixture was refluxed for 42 h. The reaction mixture was filtered, and the insoluble material was extracted with $CHCl_3$ and washed with water. The organic layer was dried over anhydrous $MgSO_4$ and evaporated. The residue was purified by column chromatography (PE/EA, 30/70) to give a pale yellow powder. Then the solid was dissolved in TFA (40 mL) at 0 °C and stirred at room temperature for 1 h. After concentration, the residue was dissolved in 2-propanol and treated with concentrated HCl (7 mL). After removing the solvent, the resultant solid was triturated with EtOH, filtered, washed with EtOH and Et_2O to give intermediate **22a** or **22b**.

2-methyl-6,7-dihydro-5H-pyrrolo[3,4-d]pyrimidine hydrochloride (22a). White solid (4.5 g, 66%). mp 272−274 °C. ^{1}H NMR (300MHz, D_2O) δ 8.73−8.70 (m, 1H), 4.77−4.66 (m, 4H), 2.70 (s, 3H).

2-methyl-5,6,7,8-tetrahydropyrido[4,3-d]pyrimidine hydrochloride (22b). Pale yellow powder

(4.2 g, 57%). mp 279−281 °C. ^{1}H NMR (300MHz, D_2O) δ 8.25 (s, 1H), 4.41 (s, 2H), 3.62 (t, J = 6.0 Hz, 2H), 3.18 (t, J = 6.0 Hz, 2H), 2.73 (s, 3H).

General procedure for the synthesis of 24−28. A mixture of **17a** or **17b** or **17c** (1.00 mmol), EDCI (192 mg, 1.0 mmol), HOBt (135 mg, 1.0 mmol), Et_3N (416 μL, 3.0 mmol) and **22a** or **22b** (1.0 mmol) in DCM (10 mL) was stirred at room temperature for 24 h. The organic layer was washed successively with 2 M HCl solution and 2 M NaOH solution, then dried over anhydrous $MgSO_4$, filtered, concentrated and purified by normal phase column chromatography (PE/EA, 75/25) to afford intermediates **23a−e**. For **23a−c**, the solid was dissolved in DCM (10 mL) at 0°C and treated dropwise with BBr_3 in DCM (2 mL, 1 mol/L). After stirring for 3 h, the reaction was quenched by the addition of water and extracted with DCM. The organic phase was dried over anhydrous $MgSO_4$ and then evaporated in vacuo. The crude material was purified by normal phase column chromatography (EtOAc/MeOH, 90/10) to afford **24−26**. For **23d** and **23e**, the solid was dissolved in MeOH (10 mL) and conducted catalytic hydrogenation with 10% Pd/C (30 mg) at atmospheric pressure for 4 h. The mixture was filtered through celite and concentrated in vacuo. The residue was triturated with Et_2O, filtered and dried under vacuum to afford the target compounds **27** and **28**.

(5-chloro-2,4-dihydroxyphenyl)(2-methyl-5H-pyrrolo[3,4-d]pyrimidin-6(7H)-yl)methanone (24). White solid (195.6 mg, 64%). mp 252−253 °C. ^{1}H NMR (300 MHz, d_6-DMSO) δ 9.95 (brs, 1H), 9.57 (brs, 1H), 8.53 (s, 1H), 6.94 (s, 1H), 6.31 (s, 1H), 4.69 (s, 2H), 4.64 (s, 2H), 2.41 (s, 3H). HRMS (ESI): calcd for $C_{14}H_{13}ClN_3O_3$ $[M + H]^+$ 306.7164, found 306.7144. Purity: 98.27% by HPLC (MeOH/H_2O = 80:20).

(5-bromo-2,4-dihydroxyphenyl)(2-methyl-7,8-dihydropyrido[4,3-d]pyrimidin-6(5H)-yl)methanone (25). White solid (230 mg, 63%). mp 203−205 °C. ^{1}H NMR (300 MHz, d_6-DMSO) δ 8.52 (s, 1H), 6.91 (s, 1H), 6.40 (s, 1H), 4.65 (s, 2H), 3.71 (s, 2H), 2.87 (s, 2H), 2.55 (s, 3H). HRMS (ESI): calcd for $C_{15}H_{15}BrN_3O_3$ $[M + H]^+$ 365.1940, found 365.1952. Purity: 97.5% by HPLC (MeOH/H_2O = 80:20).

(5-bromo-2,4-dihydroxyphenyl)(2-methyl-5H-pyrrolo[3,4-d]pyrimidin-6(7H)-yl)methanone (26). White solid (233 mg, 67%). mp 272−273 °C. ^{1}H NMR (300 MHz, d_6-DMSO) δ 9.94 (brs, 1H), 9.58 (brs, 1H), 8.55 (s, 1H), 6.95 (s, 1H), 6.31 (s, 1H), 4.70 (s, 2H), 4.64 (s, 2H), 2.41 (s, 3H). HRMS (ESI): calcd

for $C_{14}H_{13}BrN_3O_3$ $[M + H]^+$ 351.1674, found 351.1691. Purity: 98.60% by HPLC (MeOH/H_2O = 80:20).

(2,4-dihydroxy-5-isopropylphenyl)(2-methyl-7,8-dihydropyrido[4,3-d]pyrimidin-6(5H)-yl)methanone (27). White solid (235 mg, 75%). mp 211−213 °C. ^{1}H NMR (300 MHz, d_6-DMSO) δ 9.52 (s, 1H), 9.49 (s, 1H), 8.49 (s, 1H), 6.87 (s, 1H), 6.36 (s, 1H), 4.61 (s, 2H), 3.68 (s, 2H), 3.10−3.00 (m, 1H), 2.83 (t, J = 5.6 Hz, 2H), 2.49 (s, 3H), 1.08 (d, J = 6.9 Hz, 6H). ^{13}C NMR (75 MHz, d_6-DMSO) δ 169.23, 165.33, 163.36, 157.39, 155.38, 153.64, 126.48, 125.88, 124.70, 113.67, 102.64, 31.75, 26.26, 25.64, 23.09. HRMS (ESI): calcd for $C_{18}H_{22}N_3O_3$ $[M + H]^+$ 328.3776, found 328.3781. Purity: 99.31% by HPLC (MeOH/H_2O = 80:20).

(2,4-dihydroxy-5-isopropylphenyl)(2-methyl-5H-pyrrolo[3,4-d]pyrimidin-6(7H)-yl)methanone (28). White solid (235 mg, 75%). mp 242−243 °C. ^{1}H NMR (300 MHz, d_6-DMSO) δ 9.94 (brs, 2H), 8.64 (s, 1H), 7.04 (s, 1H), 6.41 (s, 1H), 4.79 (s, 2H), 4.74 (s, 2H), 3.13−3.04 (m, 1H), 2.61 (s, 3H), 1.13(d, J = 6.9 Hz, 6H). HRMS (ESI): calcd for $C_{17}H_{20}N_3O_3$ $[M + H]^+$ 314.3511, found 314.3529. Purity: 97.40% by HPLC (MeOH/H_2O = 80:20).

6-benzyl-5,6,7,8-tetrahydropyrido[4,3-d]pyrimidine-2,4(1H,3H)-dione (30). The commercially available material **29** (10 g, 33.5 mmol) was dissolved in ethanol (150 mL), then urea (10 g, 167.0 mmol) and sodium methoxide (22.7 g, 118.0 mmol) were added and the mixture was refluxed for 24 h. After cooling to room temperature, the mixture was filtered and the filter cake were suspended in water. The pH value was adjusted to 6.0 with 6 M HCl solution. Stirring was further conducted at room temperature for 1 h and the suspension were filtered and dried in vacuo to afford intermediate **30** as a white solid (6.5 g, 75%). mp 293−295 °C. ^{1}H NMR (300 MHz, $CDCl_3$) δ 11.01 (s, 1H), 10.21 (s, 1H), 7.41−7.23 (m, 5H), 3.53 (s, 2H), 3.01 (s, 2H), 2.52−2.51 (m, 2H), 2.45−2.43 (m, 2H).

6-benzyl-2,4-dichloro-5,6,7,8-tetrahydropyrido[4,3-d]pyrimidine (31). Intermediate **30** (6 g, 23.1 mmol) was added to phosphoryl chloride (50 mL, 535.0 mmol) and the solution was refluxed for 3 h under nitrogen atmosphere. The remanent phosphoryl chloride was removed under reduced pressure, and the residue was poured into 200 mL ice water. 3 M NaOH solution was added to adjust the pH value to 10, and then the aqueous phase was extracted with DCM (3 × 100 mL). The combined organics were

dried over anhydrous $MgSO_4$ and concentrated to a tan oil. Then cold and stand the oil for a day to give **31** as a dark red solid (5.8 g, 85%). mp 273−275 °C. ^{1}H NMR (300 MHz, $CDCl_3$) δ 7.61−7.53 (m, 5H), 3.53 (s, 2H), 2.97 (s, 2H), 2.43−2.41 (m, 2H), 2.24−2.23 (m, 2H).

6-benzyl-2-chloro-5,6,7,8-tetrahydropyrido[4,3-d]pyrimidine (32). To a solution of **31** (5.5 g, 18.7 mmol) in ethanol (150 mL) was added zinc (9.8 g, 149.6 mmol) and ammonium hydroxide (13 mL, 93.8 mmol) and the reaction was refluxed for 12 h. After cooling to room temperature, the mixture was filtered through celite and washed with ethyl acetate. The filtrate was concentrated and redissolved into 100 mL water and 100 mL ethyl acetate. The layer of water was extracted with ethyl acetate (3 × 100 mL) and the combined organic phase was dried over anhydrous $MgSO_4$, then concentrated and purified by normal phase column chromatography (PE/EA,90/10) to afford **32** as a white solid (4.0 g, 82%). mp 253−254 °C. ^{1}H NMR (300 MHz, $CDCl_3$) δ 8.53 (s, 1H), 7.39−7.13 (m, 5H), 3.53 (s, 2H), 3.11 (s, 2H), 2.53−2.52 (m, 2H), 2.35−2.33 (m, 2H).

2-chloro-5,6,7,8-tetrahydropyrido[4,3-d]pyrimidine hydrochloride (33). Compound **32** (4.0 g, 15.4 mmol) was dissolved in 1,2-dichloroethane (45 mL), then triethylamine (2.4 mL, 15.4 mol) and 1-chloroethyl chloroformate (4.7 mL, 46.2 mol) were added and the mixture was refluxed for 10 h. Then the reaction mixture was cooled, washed with water and brine successively and dried over anhydrous $MgSO_4$. Then concentrated and the residue was dissolved in methanol (45 mL), the solution was refluxed for 1 h. After confirming the progress of the reaction by a thin-layer chromatography, it was concentrated to afford intermediate **33** (3.2 g, 95%). mp 142−144 °C ^{1}H NMR (300 MHz, d_6-DMSO) δ 9.9 (brs, 1H), 8.67 (s, 1H), 4.30 (s, 2H), 3.44 (t, J = 6.0 Hz, 2H), 3.11 (t, J = 6.0 Hz, 2H).

(2,4-bis(benzyloxy)-5-(prop-1-en-2-yl)phenyl)(2-chloro-7,8-dihydropyrido[4,3-d]pyrimidin-6(5H)-yl)methanone (34). A mixture of **17c** (6.6 g, 17.5 mmol), EDCI (3.4 g, 17.5 mmol), HOBt (2.4 g, 17.5 mmol), Et_3N (7.3 mL, 52.5 mmol) and **33** (3.0 g, 14.6 mmol) in DCM (100 mL) was stirred at room temperature for 24 h. After confirming the progress of the reaction by a thin-layer chromatography, the organic layer was washed successively with 2 M HCl solution and 2 M NaOH solution, then dried over anhydrous $MgSO_4$, concentrated and purified by normal phase column chromatography (PE/EA,80/20) to afford **34** as a white solid (6.4 g, 83%). mp 125−126 °C ^{1}H NMR (300 MHz, d_6-DMSO) δ 8.42 (s,

1H), 7.39−7.25 (m, 10H), 7.07−7.05 (m, 1H), 6.54 (s, 1H), 5.30 (s, 2H), 5.12 (s, 2H), 5.01 (s, 2H), 4.42 (s, 2H), 3.62 (t, J = 6.0 Hz, 2H), 2.88 (t, J = 6.0 Hz, 2H), 2.11 (s, 3H).

General procedure for the synthesis of 35−48. Intermediate **34** (300 mg, 0.57 mmol), different amines (2.85 mmol) and potassium carbonate (630 mg, 4.56 mmol) were stirred in dioxane (20 mL) at 85 °C for 24 h under atmosphere of nitrogen. The mixture was concentrated and redissolved into EtOAc (20 mL), then washed with water and brine. The organic phase was dried over anhydrous $MgSO_4$, concentrated and purified by normal phase column chromatography (PE/EA, 50/50) to afford a white solid. The white product was dissolved in MeOH (10 mL), treated with 10% Pd/C (30 mg) and subjected to hydrogenation at atmospheric pressure for 4 h. The mixture was filtered through celite and concentrated in vacuo. The residue was triturated with Et_2O, filtered and then dried under vacuum to afford the target compounds **35**−**48**.

(2,4-dihydroxy-5-isopropylphenyl)(2-(methylamino)-7,8-dihydropyrido[4,3-d]pyrimidin-6(5H)-yl)methanone (35). White solid (32 mg, 16%). mp 141−143 °C. ^{1}H NMR (300 MHz, d_6-DMSO) δ 9.55 (s, 2H), 8.10 (s, 1H), 6.87 (s, 1H), 6.37 (s, 1H), 4.45 (s, 2H), 3.63 (s, 2H), 3.08−3.04 (m, 1H), 2.75 (s, 3H), 2.67 (s, 2H), 1.10 (d, J = 5.9 Hz, 6H). ^{13}C NMR (75 MHz, d_6-DMSO) δ 168.95, 163.74, 162.05, 156.86, 156.16, 153.29, 126.39, 125.92, 115.20, 114.17, 102.61, 31.94, 28.37, 26.27, 23.08. HRMS (ESI): calcd for $C_{18}H_{23}N_4O_3$ $[M + H]^+$ 343.1765, found 343.1771. Purity: 97.04% by HPLC ($MeOH/H_2O$ = 80:20).

(2,4-dihydroxy-5-isopropylphenyl)(2-(ethylamino)-7,8-dihydropyrido[4,3-d]pyrimidin-6(5H)-yl)methanone (36). White solid (28 mg, 14%). mp 129−131 °C. ^{1}H NMR (300 MHz, d_6-DMSO) δ 9.55−9.54 (m, 2H), 8.09 (s, 1H), 6.95 (s, 1H), 6.86 (s, 1H), 6.36 (s, 1H), 4.44 (s, 2H), 3.62 (s, 2H), 3.24 (t, J = 5.7 Hz, 2H), 3.10−3.00 (m, 1H), 2.67 (s, 2H), 1.10−1.05 (m, 9H). HRMS (ESI): calcd for $C_{19}H_{25}N_4O_3$ $[M + H]^+$ 357.1921, found 357.1921. Purity: 95.20% by HPLC ($MeOH/H_2O$ = 80:20).

(2,4-dihydroxy-5-isopropylphenyl)(2-(propylamino)-7,8-dihydropyrido[4,3-d]pyrimidin-6(5H)-yl)methanone (37). White solid (42 mg, 20%). mp 143−145 °C. ^{1}H NMR (300 MHz, d_6-DMSO) δ 9.53 (s, 2H), 8.08 (s, 1H), 6.98 (s, 1H), 6.86 (s, 1H), 6.37 (s, 1H), 4.44 (s, 2H), 3.62 (s, 2H), 3.18−3.16 (m, 2H), 3.08−3.04 (m, 1H), 2.66 (s, 2H), 1.53−1.46 (m, 2H), 1.10 (d, J = 6.8 Hz, 6H), 0.86 (t, J = 7.3 Hz,

3H). HRMS (ESI): calcd for $C_{20}H_{27}N_4O_3$ $[M + H]^+$ 371.2078, found 371.2085. Purity: 95.80% by HPLC (MeOH/H_2O = 80:20).

(2,4-dihydroxy-5-isopropylphenyl)(2-(isopropylamino)-7,8-dihydropyrido[4,3-d]pyrimidin-6(5H)-yl)methanone (38). White solid (23 mg, 11%). mp 130−132 °C. ^{1}H NMR (300 MHz, d_6-DMSO) δ 9.56−9.55 (m, 2H), 8.10 (s, 1H), 6.89 (s, 1H), 6.83−6.80 (m, 1H), 6.39 (s, 1H), 4.47 (s, 2H), 4.05−3.95 (m, 1H), 3.65 (s, 2H), 3.10−3.06 (m, 1H), 2.68−2.66 (m, 2H), 1.13−1.11 (m, 12H). HRMS (ESI): calcd for $C_{20}H_{27}N_4O_3$ $[M + H]^+$ 371.2078, found 371.2079. Purity: 95.54% by HPLC (MeOH/H_2O = 80:20).

(2,4-dihydroxy-5-isopropylphenyl)(2-(dimethylamino)-7,8-dihydropyrido[4,3-d]pyrimidin-6(5H)-yl)methanone (39). White solid (143 mg, 70%). mp 136−138 °C. ^{1}H NMR (300 MHz, d_6-DMSO) δ 9.45−9.43 (m, 2H), 8.08 (s, 1H), 6.77 (s, 1H), 6.28 (s, 1H), 4.38 (s, 2H), 3.54 (s, 2H), 2.98 (s, 6H), 2.96−2.90 (m, 1H), 2.63−2.61 (m, 2H), 1.00 (d, J = 6.8 Hz, 6H). ^{13}C NMR (75 MHz, d_6-DMSO) δ 168.94, 163.66, 161.26, 156.85, 156.00, 153.26, 126.35, 125.90, 114.71, 114.21, 102.63, 37.12, 32.18, 26.27, 23.10. HRMS (ESI): calcd for $C_{19}H_{25}N_4O_3$ $[M + H]^+$ 357.1921, found 357.1929. Purity: 96.03% by HPLC (MeOH/H_2O = 80:20).

(2-(diethylamino)-7,8-dihydropyrido[4,3-d]pyrimidin-6(5H)-yl)(2,4-dihydroxy-5-isopropylphenyl)methanone (40). White solid (158 mg, 72%). mp 197−198 °C. ^{1}H NMR (300 MHz, $CDCl_3$) δ 10.17 (s, 1H), 8.07 (s, 1H), 7.16 (s, 1H), 6.40 (s, 1H), 5.95 (s, 1H), 4.66 (s, 2H), 3.93 (t, J = 5.7 Hz, 2H), 3.63 (q, J = 6.8 Hz, 4H), 3.23−3.14 (m, 1H), 2.95 (t, J = 5.7 Hz, 2H), 1.26−1.17 (m, 12H). HRMS (ESI): calcd for $C_{21}H_{29}N_4O_3$ $[M + H]^+$ 385.4720, found 385.4742. Purity: 98.86% by HPLC (MeOH/H_2O = 80:20).

(2,4-dihydroxy-5-isopropylphenyl)(2-(dipropylamino)-7,8-dihydropyrido[4,3-d]pyrimidin-6(5H)-yl)methanone (41). White solid (183 mg, 78%). mp 212−214 °C. ^{1}H NMR (300 MHz, d_6-DMSO) δ 9.52−9.50 (m, 2H), 8.14 (s, 1H), 6.87 (s, 1H), 6.37 (s, 1H), 4.46 (s, 2H), 3.63 (s, 2H), 3.57−3.44 (m, 4H), 3.11−3.02 (m, 1H), 2.68 (t, J = 5.7 Hz, 2H), 1.54 (q, J = 7.4 Hz, 4H), 1.10 (d, J = 6.9 Hz, 6H), 0.87−0.82 (m, 6H). HRMS (ESI): calcd for $C_{23}H_{33}N_4O_3$ $[M + H]^+$ 413.5252, found 413.5267. Purity: 97.60% by HPLC (MeOH/H_2O = 80:20).

(2-(dibutylamino)-7,8-dihydropyrido[4,3-d]pyrimidin-6(5H)-yl)(2,4-dihydroxy-5-isopropylphenyl)methanone (42). White solid (178 mg, 71%). mp 185-187 °C. ^{1}H NMR (300 MHz, d_6-DMSO) δ

9.52−9.51 (m, 2H), 8.14 (s, 1H), 6.87 (s, 1H), 6.37 (s, 1H), 4.46 (s, 2H), 3.63 (s, 2H), 3.49 (t, J = 7.3 Hz, 4H), 3.11−3.02 (m, 1H), 2.70−2.66 (m, 2H), 1.56−1.46 (m, 4H), 1.33−1.21 (m, 4H), 1.10 (d, J = 6.9 Hz, 6H), 0.90 (t, J = 7.4 Hz, 6H). HRMS (ESI): calcd for $C_{25}H_{37}N_4O_3$ $[M + H]^+$ 441.5783, found 441.5798. Purity: 99.45% by HPLC (MeOH/H_2O = 80:20).

(2,4-dihydroxy-5-isopropylphenyl)(2-(pyrrolidin-1-yl)-7,8-dihydropyrido[4,3-d]pyrimidin-6(5H)-yl)methanone(43). White solid (159 mg, 73%). mp 202−204 °C. ^{1}H NMR (300 MHz, $CDCl_3$) δ 10.07 (s, 1H), 8.07 (s, 1H), 7.13 (s, 1H), 6.41 (s, 2H), 4.65 (s, 2H), 3.91 (t, J = 5.7 Hz, 2H), 3.60 (s, 4H), 3.22−3.13 (m, 1H), 2.98 (t, J = 5.7 Hz, 2H), 2.00 (s, 4H), 1.22 (d, J = 6.9 Hz, 6H). HRMS (ESI): calcd for $C_{21}H_{27}N_4O_3$ $[M + H]^+$ 383.4561, found 383.4580. Purity: 96.89% by HPLC (MeOH/H_2O = 80:20).

(2,4-dihydroxy-5-isopropylphenyl)(2-(piperidin-1-yl)-7,8-dihydropyrido[4,3-d]pyrimidin-6(5H)-yl)methanone (44). White solid (169 mg, 75%). mp 204−205 °C. ^{1}H NMR (300 MHz, d_6-DMSO) δ 9.53 (s, 2H), 8.16 (s, 1H), 6.86 (s, 1H), 6.37 (s, 1H), 4.46 (s, 2H), 3.69 (brs, 6H), 3.10−3.02 (m, 1H), 2.68 (s, 2H), 1.60 (s, 2H), 1.48−1.47 (m, 4H), 1.10−1.09 (m, 6H). HRMS (ESI): calcd for $C_{22}H_{29}N_4O_3$ $[M + H]^+$ 397.4827, found 397.4843. Purity: 95.14% by HPLC (MeOH/H_2O = 80:20).

(2,4-dihydroxy-5-isopropylphenyl)(2-morpholino-7,8-dihydropyrido[4,3-d]pyrimidin-6(5H)-yl) methanone (45). White solid (159 mg, 70%). mp 217−219 °C. ^{1}H NMR (300 MHz, $CDCl_3$) δ 10.11 (s, 1H), 8.10 (s, 1H), 7.14 (s, 1H), 6.39 (s, 1H), 5.49 (s, 1H), 4.67 (s, 2H), 3.93 (t, J = 5.7 Hz, 2H), 3.80−3.78 (m, 8H), 3.22−3.12 (m, 1H), 2.96 (t, J = 5.7 Hz, 2H), 1.23 (d, J = 6.9 Hz, 6H). ^{13}C NMR (75 MHz, d_6-DMSO) δ 169.24, 164.01, 160.65, 157.50, 156.17, 153.84, 126.33, 125.81, 116.28, 113.66, 102.74, 66.44, 44.48, 32.17, 26.27, 23.13. HRMS (ESI): calcd for $C_{21}H_{27}N_4O_4$ $[M + H]^+$ 399.4555, found 399.4576. Purity: 96.53% by HPLC (MeOH/H_2O = 80:20).

(2,4-dihydroxy-5-isopropylphenyl)(2-(4-methylpiperazin-1-yl)-7,8-dihydropyrido[4,3-d]pyrimidin-6(5H)-yl)methanone (46). White solid (160 mg, 68%). mp 201−202 °C. ^{1}H NMR (300 MHz, d_6-DMSO) δ 9.55 (s, 2H), 8.19 (s, 1H), 6.87 (s, 1H), 6.37 (s, 1H), 4.47 (s, 2H), 3.67 (brs, 6H), 3.08−3.04 (m, 1H), 2.70 (s, 2H), 2.31 (s, 4H), 2.18 (s, 3H), 1.10 (d, J = 6.9 Hz, 6H). ^{13}C NMR (75 MHz, d_6-DMSO) δ 169.00, 163.88, 160.60, 156.95, 153.31, 126.36, 125.90, 115.76, 114.10, 102.65, 54.85, 46.31, 43.82, 32.17, 26.28, 23.09. HRMS (ESI): calcd for $C_{22}H_{30}N_5O_3$ $[M + H]^+$ 412.4974, found 412.4950. Purity:

98.66% by HPLC (MeOH/H_2O = 80:20).

(2,4-dihydroxy-5-isopropylphenyl)(2-(4-ethylpiperazin-1-yl)-7,8-dihydropyrido[4,3-d]pyrimidin-6(5H)-yl)methanone (47). White solid (187 mg, 77%). mp 194−195 °C. ^{1}H NMR (300 MHz, d_6-DMSO) δ 9.54−9.53 (m, 2H), 8.19 (s, 1H), 6.87 (s, 1H), 6.37 (s, 1H), 4.48 (s, 2H), 3.67 (brs, 6H), 3.09−3.02 (m, 1H), 2.70 (s, 2H), 2.37−2.33 (m, 6H), 1.10 (d, J = 6.7 Hz, 6H), 1.02 (t, J = 6.9 Hz, 3H). HRMS (ESI): calcd for $C_{23}H_{32}N_5O_3$ $[M + H]^+$ 426.5239, found 426.5253. Purity: 98.38% by HPLC (MeOH/H_2O = 80:20).

1-(4-(6-(2,4-dihydroxy-5-isopropylbenzoyl)-5,6,7,8-tetrahydropyrido[4,3-d]pyrimidin-2-yl)piperazin-1-yl)ethanone (48). White solid (178 mg, 71%). mp 284−285 °C. ^{1}H NMR (300 MHz, d_6-DMSO) δ 9.50−9.48 (m, 2H), 8.21 (s, 1H), 6.86 (s, 1H), 6.36 (s, 1H), 4.48 (s, 2H), 3.63 (s, 10H), 3.10−3.01 (m, 1H), 2.71 (t, J = 5.7 Hz, 2H), 1.22 (s, 3H), 1.09 (d, J = 6.9 Hz, 6H). HRMS (ESI): calcd for $C_{23}H_{30}N_5O_4$ $[M + H]^+$ 440.5075, found 440.5090. Purity: 99.04% by HPLC (MeOH/H_2O = 80:20).

General procedure for the synthesis of 49−65. Intermediate **34** (300 mg, 0.57 mmol) and different alcohols (1.71 mmol) were dissolved in THF (5 mL), NaH (68 mg, 2.85 mmol) was added into the mixture slowly. The mixture was stirred at room temperature for 10 h. After confirming the progress of the reaction by a thin-layer chromatography, the reaction was quenched with water (20 mL). Then EtOAc (20 mL) was added and the organic layer was washed with water and brine, dried over anhydrous $MgSO_4$, and then concentrated in vacuo. Purification by silica gel chromatography (PE/EA, 80/20) to afford a white solid. The white product was dissolved in MeOH (10 mL), treated with 10% Pd/C (30 mg), then subjected to hydrogenation at atmospheric pressure for 4 h. The mixture was filtered through celite and washed with MeOH. The filtrate was concentrated and the residue was triturated with Et_2O, filtered and then dried under vacuum to give the target compounds **49**−**65**.

(2,4-dihydroxy-5-isopropylphenyl)(2-methoxy-7,8-dihydropyrido[4,3-d]pyrimidin-6(5H)-yl)methanone (49). White solid (166 mg, 85%). mp 203−205 °C.^{1}H NMR (300 MHz, d_6-DMSO) δ 9.57 (s, 1H),9.54 (s, 1H), 8.44 (s, 1H), 6.88 (s, 1H), 6.38 (s, 1H), 4.59 (s, 2H), 3.87 (s, 3H), 3.68 (s, 2H), 3.10−3.01 (m, 1H), 2.83 (t, J = 5.7 Hz, 2H), 1.09 (d, J = 6.9 Hz, 6H). HRMS (ESI): calcd for $C_{18}H_{22}N_3O_4$ $[M + H]^+$ 344.1605, found 344.1600. Purity: 98.63% by HPLC (MeOH/H_2O = 80:20).

(2,4-dihydroxy-5-isopropylphenyl)(2-ethoxy-7,8-dihydropyrido[4,3-d]pyrimidin-6(5H)-yl)methanone (50). White solid (175 mg, 86%). mp 282−283 °C. ^{1}H NMR (300 MHz, d_6-DMSO) δ 9.97 (brs, 2H), 8.40 (s, 1H), 6.84 (s, 1H), 6.40 (s, 1H), 4.56 (s, 2H), 4.27 (q, J = 7.0 Hz, 2H), 3.65 (s, 2H), 3.08−2.99 (m, 1H), 2.79 (t, J = 5.6 Hz, 2H), 1.28 (t, J = 7.0 Hz, 3H), 1.07 (d, J = 6.9 Hz, 6H). ^{13}C NMR (75 MHz, d_6-DMSO) δ 168.99, 165.65, 163.26, 157.31, 157.18, 153.44, 126.02, 125.39, 120.84, 113.27, 102.48, 62.61, 59.91, 31.67, 25.94, 22.78, 20.88, 14.45. HRMS (ESI): calcd for $C_{19}H_{24}N_3O_4$ $[M + H]^+$ 358.4036, found 358.4052. Purity: 98.37% by HPLC (MeOH/H_2O = 80:20).

(2,4-dihydroxy-5-isopropylphenyl)(2-propoxy-7,8-dihydropyrido[4,3-d]pyrimidin-6(5H)-yl)methanone (51). White solid (108 mg, 51%). mp 165−167 °C. ^{1}H NMR (300 MHz, d_6-DMSO) δ 9.56 (s, 1H), 9.53 (s, 1H), 8.41 (s, 1H), 6.87 (s, 1H), 6.36 (s, 1H), 4.57 (s, 2H), 4.19 (t, J = 6.6 Hz, 2H), 3.66 (brs, 2H), 3.09−3.00 (m, 1H), 2.80 (t, J = 5.7 Hz, 2H), 1.76−1.64 (m, 2H), 1.08 (d, J = 6.9 Hz, 6H), 0.93 (t, J = 7.3 Hz, 3H). ^{13}C NMR (75 MHz, d_6-DMSO) δ 169.01, 165.94, 163.76, 157.60, 156.97, 153.25, 126.50, 125.98, 121.14, 114.08, 102.60, 68.84, 60.21, 31.98, 26.28, 23.06, 22.16, 21.19, 10.78. HRMS (ESI): calcd for $C_{20}H_{26}N_3O_4$ $[M + H]^+$ 372.1918, found 372.1920. Purity: 96.29% by HPLC (MeOH/H_2O = 80:20).

(2,4-dihydroxy-5-isopropylphenyl)(2-isopropoxy-7,8-dihydropyrido[4,3-d]pyrimidin-6(5H)-yl)methanone (52). White solid (115 mg, 55%). mp 212−213 °C. ^{1}H NMR (300 MHz, d_6-DMSO) δ 9.54 (s, 1H), 9.52 (s, 1H), 8.40 (s, 1H), 6.88 (s, 1H), 6.38 (s, 1H), 5.20−5.12 (m, 1H), 4.58 (s, 2H), 3.68 (s, 2H), 3.11−3.02 (m, 1H), 2.80 (t, J = 5.6 Hz, 2H), 1.28 (d, J = 6.2 Hz, 6H), 1.10 (d, J = 6.9 Hz, 6H). HRMS (ESI): calcd for $C_{20}H_{26}N_3O_4$ $[M + H]^+$ 372.1918, found 372.1913. Purity: 98.22% by HPLC (MeOH/H_2O = 80:20).

(2-butoxy-7,8-dihydropyrido[4,3-d]pyrimidin-6(5H)-yl)(2,4-dihydroxy-5-isopropylphenyl)methanone (53). White solid (136 mg, 62%). mp 183−185 °C. ^{1}H NMR (300 MHz, d_6-DMSO) δ 9.56 (s, 1H), 9.53 (s, 1H), 8.40 (s, 1H), 6.87 (s, 1H), 6.36 (s, 1H), 4.57 (s, 2H), 4.23 (t, J = 6.5 Hz, 2H), 3.66 (s, 2H), 3.08−2.99 (m, 1H), 2.81 (t, J = 5.1 Hz, 2H), 1.71−1.61 (m, 2H), 1.08 (d, J = 6.9 Hz, 6H), 0.89 (t, J = 7.3 Hz, 3H). HRMS (ESI): calcd for $C_{21}H_{28}N_3O_4$ $[M + H]^+$ 386.2074, found 386.2075. Purity: 95.45% by HPLC (MeOH/H_2O = 80:20).

(2,4-dihydroxy-5-isopropylphenyl)(2-isobutoxy-7,8-dihydropyrido[4,3-d]pyrimidin-6(5H)-yl)methanone (54). White solid (147 mg, 67%). mp 251−252 °C. ^{1}H NMR (300 MHz, d_6-DMSO) δ 9.56 (s, 1H), 9.53 (s, 1H), 8.40 (s, 1H), 6.87 (s, 1H), 6.36 (s, 1H), 4.57 (s, 2H), 4.01 (d, J = 6.6 Hz, 2H), 3.66 (s, 2H), 3.08−2.99 (m, 1H), 2.80 (t, J = 5.5 Hz, 2H), 2.07−1.93 (m, 1H), 1.08 (d, J = 6.9 Hz, 6H), 0.93 (d, J = 6.7 Hz, 6H). HRMS (ESI): calcd for $C_{21}H_{28}N_3O_4$ $[M + H]^+$ 386.2074, found 386.2075. Purity: 96.64% by HPLC (MeOH/H_2O = 80:20).

(2-(cyclopentyloxy)-7,8-dihydropyrido[4,3-d]pyrimidin-6(5H)-yl)(2,4-dihydroxy-5-isopropylphenyl)methanone (55). White solid (80 mg, 35%). mp 249−251 °C. ^{1}H NMR (300 MHz, d_6-DMSO) δ 9.55 (s, 1H), 9.53 (s, 1H), 8.39 (s, 1H), 6.87 (s, 1H), 6.36 (s, 1H), 5.29 (t, J = 5.9 Hz, 1H), 4.56 (s, 2H), 3.65 (s, 2H), 3.08−2.99 (m, 1H), 2.79 (t, J = 5.7 Hz, 2H), 1.93−1.87 (m, 2H), 1.69−1.56 (m, 6H), 1.08 (d, J = 6.9 Hz, 6H). HRMS (ESI): calcd for $C_{22}H_{28}N_3O_4$ $[M + H]^+$ 398.2074, found 398.2084. Purity: 97.80% by HPLC (MeOH/H_2O = 80:20).

(2-(cyclohexyloxy)-7,8-dihydropyrido[4,3-d]pyrimidin-6(5H)-yl)(2,4-dihydroxy-5-isopropylphenyl)methanone (56). White solid (96 mg, 41%). mp 185−186 °C.^{1}H NMR (300 MHz, d_6-DMSO) δ 9.55 (s, 1H), 9.53 (s, 1H), 8.39 (s, 1H), 6.87 (s, 1H), 6.36 (s, 1H), 4.92−4.87 (m, 1H), 4.55 (s, 2H), 3.65 (s, 2H), 3.09−3.00 (m, 1H), 2.78 (t, J = 4.9 Hz, 2H), 1.88−1.85 (m, 2H), 1.70−1.69 (m, 2H), 1.50−1.22 (m, 6H), 1.08 (d, J = 6.9 Hz, 6H). HRMS (ESI): calcd for $C_{23}H_{30}N_3O_4$ $[M + H]^+$ 412.2231, found 412.2235. Purity: 96.27% by HPLC (MeOH/H_2O = 80:20).

(2,4-dihydroxy-5-isopropylphenyl)(2-((tetrahydro-2H-pyran-4-yl)oxy)-7,8-dihydropyrido[4,3-d]pyrimidin-6(5H)-yl)methanone (57). White solid (111 mg, 47%). mp 265−266 °C. ^{1}H NMR (300 MHz, d_6-DMSO) δ 9.57 (s, 1H), 9.55 (s, 1H), 8.43 (s, 1H), 6.88 (s, 1H), 6.37 (s, 1H), 5.13−5.07 (m, 1H), 4.58 (s, 2H), 3.85−3.81 (m, 2H), 3.67 (s, 2H), 3.52−3.45 (m, 2H), 3.10−3.01 (m, 1H), 2.81 (t, J = 5.5 Hz, 2H), 2.00−1.97 (m, 2H), 1.67−1.60 (m, 2H), 1.19 (d, J = 6.9 Hz, 6H). HRMS (ESI): calcd for $C_{22}H_{28}N_3O_5$ $[M + H]^+$ 414.2023, found 414.2032. Purity: 95.09% by HPLC (MeOH/H_2O = 80:20).

(2,4-dihydroxy-5-isopropylphenyl)(2-((1-methylpiperidin-4-yl)oxy)-7,8-dihydropyrido[4,3-d]pyrimidin-6(5H)-yl)methanone (58). White solid (112 mg, 46%). mp 210−212 °C. ^{1}H NMR (300 MHz, d_6-DMSO) δ 9.56 (s, 1H), 9.53 (s, 1H), 8.40 (s, 1H), 6.86 (s, 1H), 6.35 (s, 1H), 4.98−4.89 (m, 1H), 4.56

(s, 2H), 3.65 (s, 2H), 3.09−3.00 (m, 1H), 2.78 (t, J = 5.7Hz, 2H), 2.61−2.58 (m, 2H), 2.17 (s, 5H), 1.97−1.91 (m, 2H), 1.67−1.64 (m, 2H), 1.08 (d, J = 6.9 Hz, 6H). HRMS (ESI): calcd for $C_{23}H_{31}N_4O_4$ [M + H]$^+$ 427.2348, found 427.2350. Purity: 96.60% by HPLC (MeOH/H_2O = 80:20).

(2,4-dihydroxy-5-isopropylphenyl)(2-(2-methoxyethoxy)-7,8-dihydropyrido[4,3-d]pyrimidin-6(5H)-yl)methanone (59). White solid (109 mg, 49%). mp 156−157 °C. ^{1}H NMR (300 MHz, d_6-DMSO) δ 9.58 (s, 1H), 9.55 (s, 1H), 8.44 (s, 1H), 6.89 (s, 1H), 6.37 (s, 1H), 4.59 (s, 2H), 4.37 (t, J = 4.4 Hz, 2H), 3.65−3.62 (m, 4H), 3.28 (s, 3H), 3.11−3.02 (m, 1H), 2.82 (t, J = 5.6 Hz, 2H), 1.10 (d, J = 6.9 Hz, 6H). ^{13}C NMR (75 MHz, d_6-DMSO) δ 169.01, 166.02, 163.57, 157.67, 156.96, 153.24, 126.50, 126.00, 121.37, 114.03, 102.61, 70.48, 66.27, 60.21, 58.54, 31.97, 26.28, 23.07, 21.20. HRMS (ESI): calcd for $C_{20}H_{26}N_3O_5$ [M + H]$^+$ 388.1867, found 388.1867. Purity: 96.61% by HPLC (MeOH/H_2O = 80:20).

(2,4-dihydroxy-5-isopropylphenyl)(2-(2-(dimethylamino)ethoxy)-7,8-dihydropyrido[4,3-d]pyrimidin-6(5H)-yl)methanone (60). White solid (117 mg, 51%). mp 135−136 °C. ^{1}H NMR (300 MHz, d_6-DMSO) δ 9.58 (s, 1H), 9.55 (s, 1H), 8.43 (s, 1H), 6.88 (s, 1H), 6.38 (s, 1H), 4.59 (s, 2H), 4.35 (t, J = 5.7 Hz, 2H), 3.68 (s, 2H), 3.11−3.02 (m, 1H), 2.82 (t, J = 5.5 Hz, 2H), 2.63 (t, J = 5.6 Hz, 2H), 2.21 (s, 6H), 1.10 (d, J = 6.9 Hz, 6H). HRMS (ESI): calcd for $C_{21}H_{29}N_4O_4$ [M + H]$^+$ 401.2183, found 401.2182. Purity: 98.57% by HPLC (MeOH/H_2O = 80:20, with 1‰ Et_3N).

(2-(2-(diethylamino)ethoxy)-7,8-dihydropyrido[4,3-d]pyrimidin-6(5H)-yl)(2,4-dihydroxy-5-isopropylphenyl)methanone (61). White solid (77 mg, 32%). mp 181−183 °C. ^{1}H NMR (300 MHz, d_6-DMSO) δ 9.58 (s, 1H), 9.55 (s, 1H), 8.43 (s, 1H), 6.88 (s, 1H), 6.38 (s, 1H), 4.58 (s, 2H), 4.29 (t, J = 6.2 Hz, 2H), 3.68 (s, 2H), 3.11−3.02 (m, 1H), 2.81 (t, J = 5.1 Hz, 2H), 2.73 (t, J = 6.5 Hz, 2H), 2.50 (s, 4H), 1.10 (d, J = 6.9 Hz, 6H), 0.95 (t, J = 7.1 Hz, 6H). HRMS (ESI): calcd for $C_{23}H_{33}N_4O_4$ [M + H]$^+$ 429.2496, found 429.2494. Purity: 97.00% by HPLC (MeOH/H_2O = 80:20, with 1‰ Et_3N).

(2,4-dihydroxy-5-isopropylphenyl)(2-(3-(dimethylamino)propoxy)-7,8-dihydropyrido[4,3-d]pyrimidin-6(5H)-yl)methanone (62). White solid (60 mg, 25%). mp 116−118 °C. ^{1}H NMR (300 MHz, d_6-DMSO) δ 9.59 (s, 1H), 9.56 (s, 1H), 8.43 (s, 1H), 6.88 (s, 1H), 6.38 (s, 1H), 4.59 (s, 2H), 4.27 (t, J = 6.4 Hz, 2H), 3.67 (s, 2H), 3.10−3.01 (m, 1H), 2.82 (t, J = 5.5 Hz, 2H), 2.42 (t, J = 7.0 Hz, 2H), 2.20 (s, 6H), 1.90−1.81 (m, 2H), 1.09 (d, J = 6.9 Hz, 6H). HRMS (ESI): calcd for $C_{22}H_{31}N_4O_4$ [M + H]$^+$

415.2340, found 415.2340. Purity: 97.13% by HPLC (MeOH/H_2O = 80:20, with 1‰ Et_3N).

(2,4-dihydroxy-5-isopropylphenyl)(2-(2-(pyrrolidin-1-yl)ethoxy)-7,8-dihydropyrido[4,3-d]pyrimidin-6(5H)-yl)methanone (63). White solid (120 mg, 49%). mp 163−165 °C. ^{1}H NMR (300 MHz, d_6-DMSO) δ 9.58 (s, 1H), 9.55 (s, 1H), 8.44 (s, 1H), 6.88 (s, 1H), 6.39 (s, 1H), 4.60 (s, 2H), 4.41 (t, J = 5.5 Hz, 2H), 3.68 (s, 2H), 3.11−3.02 (m, 1H), 2.95 (s, 2H), 2.82 (t, J = 5.6 Hz, 2H), 2.69 (s, 4H), 1.73 (s, 4H), 1.10 (d, J = 6.9 Hz，6H). HRMS (ESI): calcd for $C_{23}H_{31}N_4O_4$ $[M + H]^+$ 427.2340, found 427.2339. Purity: 95.02% by HPLC (MeOH/H_2O = 80:20, with 1‰ Et_3N).

(2,4-dihydroxy-5-isopropylphenyl)(2-(2-(piperidin-1-yl)ethoxy)-7,8-dihydropyrido[4,3-d]pyrimidin-6(5H)-yl)methanone (64). White solid (105 mg, 42%). mp 127−128 °C. ^{1}H NMR (300 MHz, d_6-DMSO) δ 9.58 (s, 1H), 9.55 (s, 1H), 8.43 (s, 1H), 6.88 (s, 1H), 6.38 (s, 1H), 4.59 (s, 2H), 4.35 (t, J = 5.7 Hz, 2H), 3.67 (s, 2H), 3.11−3.02 (m, 1H), 2.81 (t, J = 5.4 Hz, 2H), 2.64 (s, 2H), 2.42 (s, 4H), 1.47−1.46 (m, 4H), 1.37−1.35 (m, 2H), 1.10 (d, J = 6.9 Hz, 6H). HRMS (ESI): calcd for $C_{24}H_{33}N_4O_4$ $[M + H]^+$ 441.2496, found 441.2498. Purity: 95.15% by HPLC (MeOH/H_2O = 80:20, with 1‰ Et_3N).

(2,4-dihydroxy-5-isopropylphenyl)(2-(2-morpholinoethoxy)-7,8-dihydropyrido[4,3-d]pyrimidin-6(5H)-yl)methanone (65). White solid (116 mg, 46%). mp 188−189 °C. ^{1}H NMR (300 MHz, d_6-DMSO) δ 9.57 (s, 1H), 9.55 (s, 1H), 8.43 (s, 1H), 6.88 (s, 1H), 6.38 (s, 1H), 4.59 (s, 2H), 4.37 (t, J = 5.7 Hz, 2H), 3.67 (s, 2H), 3.55 (t, J = 4.6 Hz, 4H), 3.11−3.02 (m, 1H), 2.81 (t, J = 5.6 Hz, 2H), 2.65 (t, J = 5.6 Hz, 2H), 2.44 (t, J = 4.2 Hz, 4H), 1.10 (d, J = 6.9 Hz, 6H). ^{13}C NMR (75 MHz, d_6-DMSO) δ 169.01, 165.98, 163.58, 157.63, 156.97, 153.25, 126.50, 125.98, 121.29, 114.02, 102.60, 66.62, 64.49, 61.15, 58.72, 57.19, 54.19, 54.01, 31.98, 26.28, 23.07, 21.74. HRMS (ESI): calcd for $C_{23}H_{31}N_4O_5$ $[M + H]^+$ 443.2289, found 443.2290. Purity: 96.95% by HPLC (MeOH/H_2O = 80:20).

General procedure for the synthesis of 66a−d. Intermediate **31** (500 mg, 1.69 mmol) and different alcohols (8.45 mmol) were dissolved in THF (15 mL), NaH (203 mg, 5.07 mmol) was added into the mixture very slowly. The mixture was stirred under a condition of room temperature for 0.5 h. After confirming the progress of the reaction by a thin-layer chromatography, the reaction was quenched with water (20 mL). Then EtOAc (20 mL) was added and the organic layer was washed with water and brine, dried over anhydrous $MgSO_4$, and concentrated in vacuo and afforded light yellow solids. Then the solid

was dissolved in THF (15 mL), 2-methoxyethanol (631 μL, 8.0 mmol) was added and NaH (192 mg, 4.80 mmol) was added into the mixture very slowly. After refluxing for 1 h, the mixture was dealed with just like the last step and yielded **66a−d** without purification.

6-benzyl-4-methoxy-2-(2-methoxyethoxy)-5,6,7,8-tetrahydropyrido[4,3-d]pyrimidine (66a). Light yellow oil (315 mg, 59%). ^{1}H NMR (300 MHz, $CDCl_3$) δ 7.40−7.29 (m, 5H), 4.48 (t, *J* = 5.1 Hz, 2H), 3.94 (s, 3H), 3.76 (t, *J* = 5.0 Hz, 2H), 3.72 (s, 2H), 3.45 (s, 2H), 3.39 (s, 3H), 2.81−2.74(m, 4H).

6-benzyl-4-ethoxy-2-(2-methoxyethoxy)-5,6,7,8-tetrahydropyrido[4,3-d]pyrimidine (66b). Light yellow oil (368 mg, 66%). ^{1}H NMR (300 MHz, $CDCl_3$) δ 7.41−7.27 (m, 5H), 4.46 (t, *J* = 4.9 Hz, 2H), 4.42 (q, *J* = 4.6 Hz, 2H), 3.75 (t, *J* = 5.1 Hz, 2H), 3.72 (s, 2H), 3.47 (s, 2H), 3.40 (s, 3H), 2.79−2.71 (m, 4H).

6-benzyl-2-(2-methoxyethoxy)-4-propoxy-5,6,7,8-tetrahydropyrido[4,3-d]pyrimidine (66c). Light yellow oil (390 mg, 67%). ^{1}H NMR (300 MHz, $CDCl_3$) δ 7.41−7.29 (m, 5H), 4.46 (t, *J* = 4.9 Hz, 2H), 4.31 (t, *J* = 6.7 Hz, 2H), 3.75 (t, *J* = 5.0 Hz, 2H), 3.73 (s, 2H), 3.49 (s, 2H), 3.43 (s, 3H), 2.79−2.71 (m, 4H), 1.82−1.70 (m, 2H), 0.98 (t, *J* = 7.4 Hz, 2H).

6-benzyl-4-isopropoxy-2-(2-methoxyethoxy)-5,6,7,8-tetrahydropyrido[4,3-d]pyrimidine (66d). Light yellow oil (402 mg, 69%). ^{1}H NMR (300 MHz, $CDCl_3$) δ 7.40−7.29 (m, 5H), 5.44−5.39 (m, 1H), 4.45 (t, *J* = 4.9 Hz, 2H), 3.75 (t, *J* = 5.1 Hz, 2H), 3.73 (s, 2H), 3.48 (s, 2H), 3.43 (s, 3H), 2.78−2.71 (m, 4H), 1.32 (d, *J* = 6.2 Hz, 6H).

General procedure for the synthesis of 66e−k. Intermediate **31** (500 mg, 1.69 mmol) and different amines (8.45 mmol) were dissolved in THF (15 mL), DIPEA (2.35 mL, 13.5 mmol) was added and the mixture was refluxed for 24 h. After confirming the progress of the reaction by a thin-layer chromatography, the solvent was concentrated and the residue was dissolved in the mixture of EtOAc (20 mL) and H_2O (20 mL). The organic layer was washed with water and brine, dried over anhydrous $MgSO_4$, and then concentrated in vacuo. The following procedures were conducted similar with **66a−d**.

6-benzyl-2-(2-methoxyethoxy)-N-methyl-5,6,7,8-tetrahydropyrido[4,3-d]pyrimidin-4-amine (66e). Colorless oil (270 mg, 49%). ^{1}H NMR (300 MHz, $CDCl_3$) δ 7.36−7.23 (m, 5H), 4.39 (t, *J* = 4.9 Hz, 2H), 4.15 (s, 1H), 3.71−3.66 (m, 4H), 3.35 (s, 3H), 3.17 (s, 2H), 2.86 (s, 3H), 2.76−2.64 (m, 4H).

6-benzyl-N-ethyl-2-(2-methoxyethoxy)-5,6,7,8-tetrahydropyrido[4,3-d]pyrimidin-4-amine (66f). Colorless oil (340 mg, 59%). ^{1}H NMR (300 MHz, $CDCl_3$) δ 7.36−7.23 (m, 5H), 4.39 (t, *J* = 5.0 Hz, 2H), 4.16 (t, *J* = 5.5 Hz, 1H), 3.71−3.68 (m, 4H), 3.37 (s, 3H), 3.17 (s, 2H), 2.73−2.71 (m, 4H), 1.15 (t, *J* = 7.2 Hz, 2H).

6-benzyl-2-(2-methoxyethoxy)-N-propyl-5,6,7,8-tetrahydropyrido[4,3-d]pyrimidin-4-amine (66g). Colorless oil (390 mg, 65%). ^{1}H NMR (300 MHz, $CDCl_3$) δ 7.37−7.27 (m, 5H), 4.43 (t, *J* = 4.7 Hz, 2H), 4.26 (s, 1H), 3.75−3.74 (m, 4H), 3.46−3.41 (m, 5H), 3.23 (s, 2H), 2.75 (s, 4H), 1.63−1.56 (m, 2H), 0.93 (t, *J* = 7.3 Hz, 2H).

6-benzyl-N-isopropyl-2-(2-methoxyethoxy)-5,6,7,8-tetrahydropyrido[4,3-d]pyrimidin-4-amine (66h). Colorless oil (368 mg, 61%). ^{1}H NMR (300 MHz, $CDCl_3$) δ 7.36−7.25 (m, 5H), 4.38 (t, *J* = 5.1 Hz, 2H), 4.36−4.29 (m, 1H), 3.96 (d, *J* = 9.8 Hz, 1H), 3.71−3.68 (m, 4H), 3.37 (s, 3H), 3.18 (s, 2H), 2.68 (s, 4H), 1.16 (d, *J* = 6.5 Hz, 2H).

6-benzyl-N-cyclopropyl-2-(2-methoxyethoxy)-5,6,7,8-tetrahydropyrido[4,3-d]pyrimidin-4-amine (66i). Colorless oil (330 mg, 55%). ^{1}H NMR (300 MHz, $CDCl_3$) δ 7.28−7.26 (m, 5H), 4.38 (t, *J* = 5.1 Hz, 2H), 3.68−3.62 (m, 4H), 3.33 (s, 3H), 3.09 (s, 2H), 2.79−2.70 (m, 1H)2.66 (s, 4H), 0.73−0.70 (m, 2H), 0.42−0.40 (m, 2H).

6-benzyl-2-(2-methoxyethoxy)-N,N-dimethyl-5,6,7,8-tetrahydropyrido[4,3-d]pyrimidin-4-amine (66j). Colorless oil (400 mg, 69%). ^{1}H NMR (300 MHz, $CDCl_3$) δ 7.35−7.27 (m, 5H), 4.43 (t, *J* = 4.6 Hz, 2H), 3.73 (t, *J* = 4.4 Hz, 2H), 3.69 (s, 2H), 3.48 (s, 2H), 3.41 (s, 3H), 2.97 (s, 6H), 2.81−2.75 (m, 4H).

6-benzyl-N,N-diethyl-2-(2-methoxyethoxy)-5,6,7,8-tetrahydropyrido[4,3-d]pyrimidin-4-amine (66k). Colorless oil (280 mg, 45%). ^{1}H NMR (300 MHz, $CDCl_3$) δ 7.35−7.29 (m, 5H), 4.40 (t, *J* = 4.9 Hz, 2H), 3.73 (t, *J* = 4.9 Hz, 2H), 3.69 (s, 2H), 3.41 (s, 3H), 3.39 (s, 2H), 3.38−3.30 (m, 4H), 2.83−2.77 (m, 4H), 1.08(t, *J* = 6.9 Hz, 6H).

General procedure for the synthesis of 68−78. The intermediate **66a−k** (1.0 mmol) was dissolved in MeOH (10 mL), treated with $Pd(OH)_2$ (30 mg) and then subjected to hydrogenation at atmospheric pressure for 6 h. The mixture was filtered through celite and washed with MeOH. Then concentrated in

vacuo to afford the amine intermediates as light yellow oil. A mixture of the amine intermediates, intermediate **17c** (374 mg, 1.0 mmol), EDCI (192 mg, 1.0 mmol), HOBt (135 mg, 1.0 mmol), Et_3N (416 μL, 3.0 mmol) in DCM (10 mL) was stirred at room temperature for 24 h. The organic layer was washed successively with 2 M HCl solution and 2 M NaOH solution, then dried over anhydrous $MgSO_4$, filtered, concentrated in vacuo to afford a white solid. The solid was dissolved in MeOH (10 mL) and hydrogenated for 4 h in the presence of 10% Pd/C (30 mg). The mixture was filtered through celite and washed with MeOH. Then concentrated in vacuo and afforded the target compounds **68**−**78**.

(2,4-dihydroxy-5-isopropylphenyl)(4-methoxy-2-(2-methoxyethoxy)-7,8-dihydropyrido[4,3-d]pyrimidin-6(5H)-yl)methanone (68). White solid (90 mg, 22%). mp 107-108 °C. ^{1}H NMR (300 MHz, d_6-DMSO) δ 9.50 (s, 1H), 9.48 (s, 1H), 6.82 (s, 1H), 6.31 (s, 1H), 4.32−4.29 (m, 4H), 3.85 (s, 3H), 3.59−3.56 (m, 4H), 3.23 (s, 3H), 3.05−2.96 (m, 1H), 2.67 (t, J = 5.3 Hz, 2H), 1.04 (d, J = 6.9 Hz, 6H). ^{13}C NMR (75 MHz, d_6-DMSO) δ 168.47, 167.16, 164.03, 162.39, 156.47, 152.76, 126.06, 125.49, 113.51, 106.74, 102.09, 69.95, 65.72, 57.99, 53.87, 31.15, 25.77, 22.55. HRMS (ESI): calcd for $C_{21}H_{28}N_3O_6$ $[M + H]^+$ 418.1973, found 418.1966. Purity: 96.67% by HPLC (MeOH/H_2O = 80:20).

(2,4-dihydroxy-5-isopropylphenyl)(4-ethoxy-2-(2-methoxyethoxy)-7,8-dihydropyrido[4,3-d]pyrimidin-6(5H)-yl)methanone (69). White solid (121 mg, 28%). mp 117−118 °C. ^{1}H NMR (300 MHz, d_6-DMSO) δ 9.51 (s, 1H), 9.50 (s, 1H), 6.83 (s, 1H), 6.31 (s, 1H), 4.36−4.28 (m, 6H), 3.59−3.56 (m, 4H), 3.23 (s, 3H), 3.06−2.97 (m, 1H), 2.66 (t, J = 4.9 Hz, 2H), 1.25 (t, J = 7.0 Hz, 3H), 1.04 (d, J = 6.9 Hz, 6H). HRMS (ESI): calcd for $C_{22}H_{30}N_3O_6$ $[M + H]^+$ 432.2129, found 432.2114. Purity: 96.89% by HPLC (MeOH/H_2O = 80:20).

(2,4-dihydroxy-5-isopropylphenyl)(2-(2-methoxyethoxy)-4-propoxy-7,8-dihydropyrido[4,3-d]pyrimidin-6(5H)-yl)methanone (70). White solid (86 mg, 19%). mp 118−120 °C. ^{1}H NMR (300 MHz, d_6-DMSO) δ 9.55−9.54 (m, 2H), 6.87 (s, 1H), 6.35 (s, 1H), 4.38 (s, 2H), 4.33 (s, 2H), 4.26 (t, J = 6.1 Hz, 2H), 3.61 (s, 4H), 3.27 (s, 3H), 3.07−3.03 (m, 1H), 2.71 (s, 2H), 1.70−1.67 (m, 2H), 1.08 (d, J = 6.6 Hz, 6H), 0.90 (s, 3H). ^{13}C NMR (75 MHz, d_6-DMSO) δ 168.64, 166.85, 164.07, 162.37, 156.52, 153.03, 125.96, 125.46, 113.24, 106.71, 102.10, 69.95, 67.73, 65.69, 57.98, 31.17, 25.76, 22.53, 21.53, 10.11. HRMS (ESI): calcd for $C_{23}H_{32}N_3O_6$ $[M + H]^+$ 446.2286, found 446.2270. Purity: 97.00% by HPLC

(MeOH/H_2O = 80:20).

(2,4-dihydroxy-5-isopropylphenyl)(4-isopropoxy-2-(2-methoxyethoxy)-7,8-dihydropyrido[4,3-d]pyrimidin-6(5H)-yl)methanone (71). White solid (120 mg, 27%). mp 109−111 °C. ^{1}H NMR (300 MHz, d_6-DMSO) δ 9.55 (s, 2H), 6.87 (s, 1H), 6.35 (s, 1H), 5.30−5.26 (m, 1H), 4.35−4.33(m, 4H), 3.61 (s, 4H), 3.27 (s, 3H), 3.08−3.03 (m, 1H), 2.70 (s, 2H), 1.28 (d, J = 5.7 Hz, 6H), 1.09 (d, J = 6.5 Hz, 6H). HRMS (ESI): calcd for $C_{23}H_{32}N_3O_6$ $[M + H]^+$ 446.2286, found 446.2277. Purity: 96.80% by HPLC (MeOH/H_2O = 80:20).

(2,4-dihydroxy-5-isopropylphenyl)(2-(2-methoxyethoxy)-4-(methylamino)-7,8-dihydropyrido[4,3-d]pyrimidin-6(5H)-yl)methanone (72). White solid (200 mg, 48%). mp 218−221 °C. ^{1}H NMR (300 MHz, d_6-DMSO) δ 9.51 (s, 2H), 6.96 (s, 1H), 6.85 (s, 1H), 6.36 (s, 1H), 4.27 (s, 4H), 3.58 (s, 4H), 3.27 (s, 3H), 3.08−3.04 (m, 1H), 2.80 (s, 3H), 2.56 (s, 2H), 1.09 (d, J = 6.6 Hz, 6H). HRMS (ESI): calcd for $C_{21}H_{29}N_4O_5$ $[M + H]^+$ 417.2132, found 417.2128. Purity: 95.74% by HPLC (MeOH/H_2O = 80:20).

(2,4-dihydroxy-5-isopropylphenyl)(4-(ethylamino)-2-(2-methoxyethoxy)-7,8-dihydropyrido[4,3-d]pyrimidin-6(5H)-yl)methanone (73). White solid (181 mg, 42%). mp 120−121 °C. ^{1}H NMR (300 MHz, $CDCl_3$) δ 10.02 (s, 1H), 8.13 (s, 1H), 7.16 (s, 1H), 6.87 (s, 1H), 5.09 (s, 1H), 4.53 (t, J = 4.0 Hz, 2H), 4.46 (s, 2H), 3.86 (t, J = 4.0 Hz, 2H), 3.73 (s, 2H), 3.50 (t, J = 7.0 Hz, 2H), 3.47 (s, 3H), 3.22−3.14 (m, 1H), 2.96 (s, 2H), 1.24−1.19 (m, 9H). ^{13}C NMR (75 MHz, d_6-DMSO) δ 168.65, 160.01, 156.65, 156.35, 152.66, 149.46, 125.97, 125.53, 113.16, 104.79, 102.36, 69.23, 67.91, 58.05, 36.46, 26.43, 25.81, 22.55, 13.80. HRMS (ESI): calcd for $C_{22}H_{31}N_4O_5$ $[M + H]^+$ 431.2289, found 431.2289. Purity: 98.83% by HPLC (MeOH/H_2O = 80:20).

(2,4-dihydroxy-5-isopropylphenyl)(2-(2-methoxyethoxy)-4-(propylamino)-7,8-dihydropyrido[4,3-d]pyrimidin-6(5H)-yl)methanone (74). White solid (200 mg, 45%). mp 98−101 °C. ^{1}H NMR (300 MHz, d_6-DMSO) δ 9.52 (s, 1H), 9.49 (s, 1H), 7.01 (s, 1H), 6.84 (s, 1H), 6.36 (s, 1H), 4.28−4.26 (m, 4H), 3.58 (s, 4H), 3.26 (s, 5H), 3.08−3.03 (m, 1H), 2.55 (s, 2H), 1.55−1.52 (m, 2H), 1.09 (d, J = 6.2 Hz, 6H), 0.86 (t, J = 6.5 Hz, 3H). HRMS (ESI): calcd for $C_{23}H_{33}N_4O_5$ $[M + H]^+$ 445.2445, found 445.2437. Purity: 98.08% by HPLC (MeOH/H_2O = 80:20).

(2,4-dihydroxy-5-isopropylphenyl)(4-(isopropylamino)-2-(2-methoxyethoxy)-7,8-dihydropyrido[

4,3-d]pyrimidin-6(5H)-yl)methanone (75). White solid (124 mg, 28%). mp 131−134 °C. ^{1}H NMR (300 MHz, d_6-DMSO) δ 9.54 (s, 1H), 9.51 (s, 1H), 6.84 (s, 1H), 6.67−6.65 (m, 1H), 6.37 (s, 1H), 4.31 (s, 2H), 4.26 (t, J = 4.3 Hz, 2H), 3.58 (t, J = 4.9 Hz, 2H), 3.52 (s, 2H), 3.27 (s, 3H), 3.13−3.02 (m, 1H), 2.55 (s, 2H), 1.16 (d, J = 6.5 Hz, 6H), 1.09 (d, J = 6.9 Hz, 6H). HRMS (ESI): calcd for $C_{23}H_{33}N_4O_5$ $[M + H]^+$ 445.2445, found 445.2445. Purity: 96.77% by HPLC (MeOH/H_2O = 80:20).

(4-(cyclopropylamino)-2-(2-methoxyethoxy)-7,8-dihydropyrido[4,3-d]pyrimidin-6(5H)-yl)(2,4-dihydroxy-5-isopropylphenyl)methanone (76). White solid (208 mg, 47%). mp 196−198 °C. ^{1}H NMR (300 MHz, d_6-DMSO) δ 9.50 (s, 2H), 7.07 (s, 1H), 6.83 (s, 1H), 6.36 (s, 1H), 4.30−4.27 (m, 4H), 3.60 (t, J = 4.9 Hz, 2H), 3.53 (s, 2H), 3.27 (s, 3H), 3.10−3.01 (m, 1H), 2.81−2.76 (m, 1H), 2.57 (s, 2H), 1.09 (d, J = 6.9 Hz, 6H), 0.71−0.65 (m, 2H), 0.54−0.53 (m, 2H). ^{13}C NMR (75 MHz, d_6-DMSO) δ 168.98, 163.06, 162.14, 160.39, 156.78, 153.25, 126.23, 125.86, 114.22, 104.18, 102.64, 70.75, 65.37, 65.24, 58.46, 32.05, 26.30, 24.39, 23.07, 22.61, 6.66. HRMS (ESI): calcd for $C_{23}H_{31}N_4O_5$ $[M + H]^+$ 443.2289, found 443.2285. Purity: 98.22% by HPLC (MeOH/H_2O = 80:20). Purity: 95.70% by HPLC (MeOH/H_2O = 80:20).

(2,4-dihydroxy-5-isopropylphenyl)(4-(dimethylamino)-2-(2-methoxyethoxy)-7,8-dihydropyrido[4,3-d]pyrimidin-6(5H)-yl)methanone (77). White solid (168 mg, 39%). mp 188−190 °C. ^{1}H NMR (300 MHz, d_6-DMSO) δ 9.56 (s, 1H), 9.54 (s, 1H), 6.82 (s, 1H), 6.35 (s, 1H), 4.57 (s, 2H), 4.28 (s, 2H), 3.60−3.59 (m, 4H), 3.26 (s, 3H), 3.07−3.02 (m, 1H), 2.96 (s, 6H), 2.68 (s, 2H), 1.07 (d, J = 6.7 Hz, 6H). ^{13}C NMR (75 MHz, d_6-DMSO) δ 168.54, 165.10, 163.95, 162.30, 156.95, 153.56, 126.30, 125.90, 113.64, 107.19, 102.66, 70.66, 65.44, 60.21, 58.48, 40.56, 32.40, 26.23, 23.04, 21.19. HRMS (ESI): calcd for $C_{22}H_{31}N_4O_5$ $[M + H]^+$ 431.2289, found 431.2281. Purity: 97.66% by HPLC (MeOH/H_2O = 80:20).

(4-(diethylamino)-2-(2-methoxyethoxy)-7,8-dihydropyrido[4,3-d]pyrimidin-6(5H)-yl)(2,4-dihydroxy-5-isopropylphenyl)methanone (78). White solid (150 mg, 33%). mp 181−183 °C. ^{1}H NMR (300 MHz, $CDCl_3$) δ 10.02 (s, 1H), 7.77 (s, 1H), 7.09 (s, 1H), 6.60 (s, 1H), 4.66 (s, 2H), 4.46 (t, J = 5.0 Hz, 2H), 4.44−3.77 (m, 4H), 3.51−3.46 (m, 4H), 3.44 (s, 3H), 3.21−3.11 (m, 1H), 3.00 (t, J = 5.9 Hz, 2H), 1.26−1.20 (m, 6H), 1.18 (d, J = 6.9 Hz, 6H). HRMS (ESI): calcd for $C_{24}H_{35}N_4O_5$ $[M + H]^+$ 459.2602,

found 459.2599. Purity: 97.30% by HPLC (MeOH/H_2O = 80:20).

ASSOCIATED CONTENT

Supporting Information

Permeability data of compounds **27** and **28** (Table S1); The crystallography statistics of the Hsp90α^N-**50** complex (Table S2); Detailed procedures for the synthesis of the intermediates **17a**−**c**; ^{1}H, ^{13}C NMR of the compounds **24**−**28**, **35**−**65**, **68**−**78**.

PDB ID Codes

The crystal complex of Hsp90α^N with compound **50** can be accessed using PDB code: 5GGZ. Authors will release the atomic coordinates and experimental data upon article publication.

AUTHOR INFORMATION

Corresponding Authors

* Dr. Xiao-li Xu, Tel/Fax: +86 025 83271216. E-mail address: xuxiao_li@126.com

* Prof. Qi-Dong You, Tel/Fax: +86 025 83271351. E-mail address: youqidong@gmail.com

Notes

The authors declare no competing financial interest.

ACKNOWLEDGMENTS

This work was supported by the project 81230078, 81573346 and 81502990 of National Natural Science Foundation of China; BK20150691 of Natural Science Foundation of Jiangsu Province of China; 2013ZX09402102-001-005 and 2014ZX09507002-005-015 of the National Major Science and Technology Project of China (Innovation and Development of New Drugs); 20130096110002 of Specialized Research Fund for the Doctoral Program of Higher Education; A Project Funded by the Priority Academic Program Development of Jiangsu Higher Education Institutions; 2015ZD009 of key program of China Pharmaceutical University; SKLNMZZCX201611 of program of State Key Laboratory of Natural Medicines, China Pharmaceutical University.

ABBREVIATIONS USED

Hsp90, Heat-shock protein 90; Grp94, glucose regulated protein 94; SAR, structure-activity relationship; 17-AAG, 17-allylamino-17-desmethoxygeldanamycin; FP, fluorescence polarization; Hsp70, Heat-shock protein 70; Akt, protein kinase B; Erk, Extracellular signal-regulated protein kinase; p-Erk, phosphorylated Erk; AUC, area under the drug concentration-time curve; q.o.d, dosing every other day; RTV, relative tumor volume; TFA, trifluoroacetic acid; T/C, relative tumor growth rate; BGG, bovine gamma-globulin; D5W, 5% dextrose in water; EDCI, 1-ethyl-3-(3-dimethylaminopropyl)carboiimide; HOBt, hydroxybenzotriazole; ACE-Cl, 1-chloroethyl chloroformate; MTT, 3-(4,5)-dimethylthiahiazo (-z-y1)-3,5-di- phenytetrazoliumromide

REFERENCES

(1) Janin, Y. L. ATPase inhibitors of heat-shock protein 90, second season. *Drug Discovery Today* **2010**, *15*, 342−353.

(2) Porter, J. R.; Fritz, C. C.; Depew, K. M. Discovery and development of Hsp90 inhibitors: a promising pathway for cancer therapy. *Curr. Opin. Chem. Biol.* **2010**, *14*, 412−420.

(3) Taldone, T.; Sun, W.; Chiosis, G. Discovery and development of heat shock protein 90 inhibitors. *Bioorg. Med. Chem.* **2009**, *17*, 2225−2235.

(4) Biamonte, M. A.; Van de Water, R.; Arndt, J. W.; Scannevin, R. H.; Perret, D.; Lee, W.-C. Heat Shock Protein 90: Inhibitors in Clinical Trials. *J. Med. Chem.* **2010**, *53*, 3−17.

(5) Wang, M.; Shen, A.; Zhang, C.; Song, Z.; Ai, J.; Liu, H.; Sun, L.; Ding, J.; Geng, M.; Zhang, A. Development of Heat Shock Protein (Hsp90) Inhibitors To Combat Resistance to Tyrosine Kinase Inhibitors through Hsp90-Kinase Interactions. *J. Med. Chem.* **2016**, *59*, 5563−5586.

(6) Pearl, L. H.; Prodromou, C. Structure and mechanism of the Hsp90 molecular chaperone machinery. *Annu. Rev. Biochem.* **2006**, *75*, 271−294.

(7) Chiosis, G.; Vilenchik, M.; Kim, J.; Solit, D. Hsp90: the vulnerable chaperone. *Drug Discovery Today* **2004**, *9*, 881−888.

(8) Jhaveri, K.; Modi, S. Ganetespib: research and clinical development. *Onco Targets Ther.* **2015**, *8*, 1849−1858.

(9) Bhat, R.; Tummalapalli, S. R.; Rotella, D. P. Progress in the discovery and development of heat shock protein 90

(Hsp90) inhibitors. *J. Med. Chem.* **2014**, *57*, 8718−8728.

(10) Taddei, M.; Ferrini, S.; Giannotti, L.; Corsi, M.; Manetti, F.; Giannini, G.; Vesci, L.; Milazzo, F. M.; Alloatti, D.; Guglielmi, M. B.; Castorina, M.; Cervoni, M. L.; Barbarino, M.; Fodera, R.; Carollo, V.; Pisano, C.; Armaroli, S.; Cabri, W. Synthesis and evaluation of new Hsp90 inhibitors based on a 1,4,5-trisubstituted 1,2,3-triazole scaffold. *J. Med. Chem.* **2014**, *57*, 2258−2274.

(11)Chen, D.; Shen, A.; Li, J.; Shi, F.; Chen, W.; Ren, J.; Liu, H.; Xu, Y.; Wang, X.; Yang, X.; Sun, Y.; Yang, M.; He, J.; Wang, Y.; Zhang, L.; Huang, M.; Geng, M.; Xiong, B.; Shen, J. Discovery of potent N-(isoxazol-5-yl)amides as HSP90 inhibitors. *Eur. J. Med. Chem.* **2014**, *87*, 765−781.

(12) Egorin, M. J.; Rosen, D. M.; Wolff, J. H.; Callery, P. S.; Musser, S. M.; Eiseman, J. L. Metabolism of 17-(allylamino)-17-demethoxygeldanamycin (NSC 330507) by murine and human hepatic preparations. *Cancer Res.* **1998**, *58*, 2385−2396.

(13) Ge, J.; Normant, E.; Porter, J. R.; Ali, J. A.; Dembski, M. S.; Gao, Y.; Georges, A. T.; Grenier, L.; Pak, R. H.; Patterson, J.; Sydor, J. R.; Tibbitts, T. T.; Tong, J. K.; Adams, J.; Palombella, V. J. Design, synthesis, and biological evaluation of hydroquinone derivatives of 17-amino-17-demethoxygeldanamycin as potent, water-soluble inhibitors of Hsp90. *J. Med. Chem.* **2006**, *49*, 4606−4615.

(14) Modi, S.; Stopeck, A. T.; Gordon, M. S.; Mendelson, D.; Solit, D. B.; Bagatell, R.; Ma, W.; Wheler, J.; Rosen, N.; Norton, L.; Cropp, G. F.; Johnson, R. G.; Hannah, A. L.; Hudis, C. A. Combination of trastuzumab and tanespimycin (17-AAG, KOS-953) is safe and active in trastuzumab-refractory HER-2 overexpressing breast cancer: a phase I dose-escalation study. *J. Clin. Oncol.* **2007**, *25*, 5410−5417.

(15) Wagner, A. J.; Chugh, R.; Rosen, L. S.; Morgan, J. A.; George, S.; Gordon, M.; Dunbar, J.; Normant, E.; Grayzel, D.; Demetri, G. D. A phase I study of the HSP90 inhibitor retaspimycin hydrochloride (IPI-504) in patients with gastrointestinal stromal tumors or soft-tissue sarcomas. *Clin. Cancer Res.* **2013**, *19*, 6020−6029.

(16) Jhaveri, K.; Taldone, T.; Modi, S.; Chiosis, G. Advances in the clinical development of heat shock protein 90 (Hsp90) inhibitors in cancers. *Biochim. Biophys. Acta* **2012**, *1823*, 742−755.

(17) Garcia-Carbonero, R.; Carnero, A.; Paz-Ares, L. Inhibition of HSP90 molecular chaperones: moving into the clinic. *Lancet Oncol.* **2013**, *14*, E358−E369.

(18)Kasibhatla, S. R.; Hong, K.; Biamonte, M. A.; Busch, D. J.; Karjian, P. L.; Sensintaffar, J. L.; Kamal, A.; Lough, R.

E.; Brekken, J.; Lundgren, K.; Grecko, R.; Timony, G. A.; Ran, Y.; Mansfield, R.; Fritz, L. C.; Ulm, E.; Burrows, F. J.; Boehm, M. F. Rationally Designed High-Affinity 2-Amino-6-halopurine Heat Shock Protein 90 Inhibitors That Exhibit Potent Antitumor Activity. *J. Med. Chem.* **2007**, *50*, 2767−2778.

(19)He, H.; Zatorska, D.; Kim, J.; Aguirre, J.; Llauger, L.; She, Y.; Wu, N.; Immormino, R. M.; Gewirth, D. T.; Chiosis, G. Identification of Potent Water Soluble Purine-Scaffold Inhibitors of the Heat Shock Protein 90. *J. Med. Chem.* **2006**, *49*, 381−390.

(20) Kim, S. H.; Bajji, A.; Tangallapally, R.; Markovitz, B.; Trovato, R.; Shenderovich, M.; Baichwal, V.; Bartel, P.; Cimbora, D.; McKinnon, R.; Robinson, R.; Papac, D.; Wettstein, D.; Carlson, R.; Yager, K. M. Discovery of (2S)-1-[4-(2-{6-amino-8-[(6-bromo-1,3-benzodioxol-5-yl)sulfanyl]-9H-purin-9-yl}ethyl)piperidin-1-yl]-2-hydroxyprop an-1-one (MPC-3100), a purine-based Hsp90 inhibitor. *J. Med. Chem.* **2012**, *55*, 7480−7501.

(21) Lin, T. Y.; Bear, M.; Du, Z.; Foley, K. P.; Ying, W.; Barsoum, J.; London, C. The novel HSP90 inhibitor STA-9090 exhibits activity against Kit-dependent and -independent malignant mast cell tumors. *Exp. Hematol.* **2008**, *36*, 1266−1277.

(22) Brough, P. A.; Aherne, W.; Barril, X.; Borgognoni, J.; Boxall, K.; Cansfield, J. E.; Cheung, K. M.; Collins, I.; Davies, N. G.; Drysdale, M. J.; Dymock, B.; Eccles, S. A.; Finch, H.; Fink, A.; Hayes, A.; Howes, R.; Hubbard, R. E.; James, K.; Jordan, A. M.; Lockie, A.; Martins, V.; Massey, A.; Matthews, T. P.; McDonald, E.; Northfield, C. J.; Pearl, L. H.; Prodromou, C.; Ray, S.; Raynaud, F. I.; Roughley, S. D.; Sharp, S. Y.; Surgenor, A.; Walmsley, D. L.; Webb, P.; Wood, M.; Workman, P.; Wright, L. 4,5-diarylisoxazole Hsp90 chaperone inhibitors: potential therapeutic agents for the treatment of cancer. *J. Med. Chem.* **2008**, *51*, 196−218.

(23) Woodhead, A. J.; Angove, H.; Carr, M. G.; Chessari, G.; Congreve, M.; Coyle, J. E.; Cosme, J.; Graham, B.; Day, P. J.; Downham, R.; Fazal, L.; Feltell, R.; Figueroa, E.; Frederickson, M.; Lewis, J.; McMenamin, R.; Murray, C. W.; O'Brien, M. A.; Parra, L.; Patel, S.; Phillips, T.; Rees, D. C.; Rich, S.; Smith, D. M.; Trewartha, G.; Vinkovic, M.; Williams, B.; Woolford, A. J. Discovery of (2,4-dihydroxy-5-isopropylphenyl)-[5-(4-methylpiperazin-1-ylmethyl)-1,3-dihydrois oindol-2-yl]methanone (AT13387), a novel inhibitor of the molecular chaperone Hsp90 by fragment based drug design. *J. Med. Chem.* **2010**, *53*, 5956−5969.

(24) Huang, K. H.; Veal, J. M.; Fadden, R. P.; Rice, J. W.; Eaves, J.; Strachan, J. P.; Barabasz, A. F.; Foley, B. E.; Barta,

T. E.; Ma, W.; Silinski, M. A.; Hu, M.; Partridge, J. M.; Scott, A.; DuBois, L. G.; Freed, T.; Steed, P. M.; Ommen, A. J.; Smith, E. D.; Hughes, P. F.; Woodward, A. R.; Hanson, G. J.; McCall, W. S.; Markworth, C. J.; Hinkley, L.; Jenks, M.; Geng, L.; Lewis, M.; Otto, J.; Pronk, B.; Verleysen, K.; Hall, S. E. Discovery of novel 2-aminobenzamide inhibitors of heat shock protein 90 as potent, selective and orally active antitumor agents. *J. Med. Chem.* **2009**, *52*, 4288−4305.

(25) McBride, C. M.; Levine, B.; Xia, Y.; Bellamacina, C.; Machajewski, T.; Gao, Z.; Renhowe, P.; Antonios-McCrea, W.; Barsanti, P.; Brinner, K.; Costales, A.; Doughan, B.; Lin, X.; Louie, A.; McKenna, M.; Mendenhall, K.; Poon, D.; Rico, A.; Wang, M.; Williams, T. E.; Abrams, T.; Fong, S.; Hendrickson, T.; Lei, D.; Lin, J.; Menezes, D.; Pryer, N.; Taverna, P.; Xu, Y.; Zhou, Y.; Shafer, C. M. Design, structure-activity relationship, and in vivo characterization of the development candidate NVP-HSP990. *J. Med. Chem.* **2014**, *57*, 9124−9129.

(26) Modi, S.; Stopeck, A.; Linden, H.; Solit, D.; Chandarlapaty, S.; Rosen, N.; D'Andrea, G.; Dickler, M.; Moynahan, M. E.; Sugarman, S.; Ma, W.; Patil, S.; Norton, L.; Hannah, A. L.; Hudis, C. HSP90 inhibition is effective in breast cancer: a phase II trial of tanespimycin (17-AAG) plus trastuzumab in patients with HER2-positive metastatic breast cancer progressing on trastuzumab. *Clin. Cancer Res.* **2011**, *17*, 5132−5139.

(27) Richardson, P. G.; Chanan-Khan, A. A.; Lonial, S.; Krishnan, A. Y.; Carroll, M. P.; Alsina, M.; Albitar, M.; Berman, D.; Messina, M.; Anderson, K. C. Tanespimycin and bortezomib combination treatment in patients with relapsed or relapsed and refractory multiple myeloma: results of a phase 1/2 study. *Br. J. Haematol.* **2011**, *153*, 729−740.

(28) Keer, H. S., T.; Courtin, A.; Hearn, K.; Lyons, J.; Wallis, N.; Oganesian, A.; Azab, M. Combination of HSP90 inhibitor onalespib with crizotinib to treat or delay resistance in NSCLC: Preclinical and clinical investigations, 13th Int Symp Target Anticancer Ther, Paris, March 2−4, **2015**, Abst O3.6.

(29) Shi, J.; Van de Water, R.; Hong, K.; Lamer, R. B.; Weichert, K. W.; Sandoval, C. M.; Kasibhatla, S. R.; Boehm, M. F.; Chao, J.; Lundgren, K.; Timple, N.; Lough, R.; Ibanez, G.; Boykin, C.; Burrows, F. J.; Kehry, M. R.; Yun, T. J.; Harning, E. K.; Ambrose, C.; Thompson, J.; Bixler, S. A.; Dunah, A.; Snodgrass-Belt, P.; Arndt, J.; Enyedy, I. J.; Li, P.; Hong, V. S.; McKenzie, A.; Biamonte, M. A. EC144 is a potent inhibitor of the heat shock protein 90. *J. Med. Chem.* **2012**, *55*, 7786−7795.

(30) Samuni, Y.; Ishii, H.; Hyodo, F.; Samuni, U.; Krishna, M. C.; Goldstein, S.; Mitchell, J. B. Reactive oxygen species mediate hepatotoxicity induced by the Hsp90 inhibitor geldanamycin and its analogs. *Free Radic. Biol. Med.*

2010, *48*, 1559−1563.

(31) Gewirth, D. T. Paralog Specific Hsp90 Inhibitors - A Brief History and a Bright Future. *Curr. Top. Med. Chem.* **2016**, *16*, 2779−2791.

(32) Patel, H. J.; Patel, P. D.; Ochiana, S. O.; Yan, P.; Sun, W.; Patel, M. R.; Shah, S. K.; Tramentozzi, E.; Brooks, J.; Bolaender, A.; Shrestha, L.; Stephani, R.; Finotti, P.; Leifer, C.; Li, Z.; Gewirth, D. T.; Taldone, T.; Chiosis, G. Structure-activity relationship in a purine-scaffold compound series with selectivity for the endoplasmic reticulum Hsp90 paralog Grp94. *J. Med. Chem.* **2015**, *58*, 3922−3943.

(33) Ohkubo, S.; Kodama, Y.; Muraoka, H.; Hitotsumachi, H.; Yoshimura, C.; Kitade, M.; Hashimoto, A.; Ito, K.; Gomori, A.; Takahashi, K.; Shibata, Y.; Kanoh, A.; Yonekura, K. TAS-116, a Highly Selective Inhibitor of Heat Shock Protein 90alpha and beta, Demonstrates Potent Antitumor Activity and Minimal Ocular Toxicity in Preclinical Models. *Mol. Cancer Ther.* **2015**, *14*, 14−22.

(34) Patel, P. D.; Yan, P.; Seidler, P. M.; Patel, H. J.; Sun, W.; Yang, C.; Que, N. S.; Taldone, T.; Finotti, P.; Stephani, R. A.; Gewirth, D. T.; Chiosis, G. Paralog-selective Hsp90 inhibitors define tumor-specific regulation of HER2. *Nat. Chem. Biol.* **2013**, *9*, 677−684.

(35) Crowley, V. M.; Khandelwal, A.; Mishra, S.; Stothert, A. R.; Huard, D. J.; Zhao, J.; Muth, A.; Duerfeldt, A. S.; Kizziah, J. L.; Lieberman, R. L.; Dickey, C. A.; Blagg, B. S. Development of Glucose Regulated Protein 94-Selective Inhibitors Based on the BnIm and Radamide Scaffold. *J. Med. Chem.* **2016**, *59*, 3471−3488.

(36) Sessa, C.; Shapiro, G. I.; Bhalla, K. N.; Britten, C.; Jacks, K. S.; Mita, M.; Papadimitrakopoulou, V.; Pluard, T.; Samuel, T. A.; Akimov, M.; Quadt, C.; Fernandez-Ibarra, C.; Lu, H.; Bailey, S.; Chica, S.; Banerji, U. First-in-human phase I dose-escalation study of the HSP90 inhibitor AUY922 in patients with advanced solid tumors. *Clin. Cancer Res.* **2013**, *19*, 3671−3680.

(37) Shapiro, G. I.; Kwak, E.; Dezube, B. J.; Yule, M.; Ayrton, J.; Lyons, J.; Mahadevan, D. First-in-Human Phase I Dose Escalation Study of a Second-Generation Non-Ansamycin HSP90 Inhibitor, AT13387, in Patients with Advanced Solid Tumors. *Clin. Cancer Res.* **2015**, *21*, 87−97.

(38) Infante, J. R.; Weiss, G. J.; Jones, S.; Tibes, R.; Bauer, T. M.; Bendell, J. C.; Hinson, J. M.; Von Hoff, D. D.; Burris, H. A.; Orlemans, E. O.; Ramanathan, R. K. Phase I dose-escalation studies of SNX-5422, an orally bioavailable heat shock protein 90 inhibitor, in patients with refractory solid tumours. *Eur. J. Cancer* **2014**, *50*, 2897−2904.

(39) Zhou, D.; Liu, Y.; Ye, J.; Ying, W.; Ogawa, L. S.; Inoue, T.; Tatsuta, N.; Wada, Y.; Koya, K.; Huang, Q.; Bates, R. C.; Sonderfan, A. J. A rat retinal damage model predicts for potential clinical visual disturbances induced by Hsp90 inhibitors. *Toxicol. Appl. Pharmacol.* **2013**, *273*, 401−409.

(40) Sun, H. P.; Jia, J. M.; Jiang, F.; Xu, X. L.; Liu, F.; Guo, X. K.; Cherfaoui, B.; Huang, H. Z.; Pan, Y.; You, Q. D. Identification and optimization of novel Hsp90 inhibitors with tetrahydropyrido[4,3-d]pyrimidines core through shape-based screening. *Eur. J. Med. Chem.* **2014**, *79*, 399−412.

(41) Chessari, G. C., M.; Figueroa, E.; Frederickson, M.;Murray, C. W.; Woolford, A. J.; Carr, M. G.; O'Brien, M. A.;Woodhead, A. J. Preparation of benzamides as Hsp90 inhibitors. WO 2006/109075, **2006**.

(42) Jez, J. M.; Chen, J. C.; Rastelli, G.; Stroud, R. M.; Santi, D. V. Crystal structure and molecular modeling of 17-DMAG in complex with human Hsp90. *Chem. Biol.* **2003**, *10*, 361−368.

(43) Ernst, J. T.; Liu, M.; Zuccola, H.; Neubert, T.; Beaumont, K.; Turnbull, A.; Kallel, A.; Vought, B.; Stamos, D. Correlation between chemotype-dependent binding conformations of HSP90alpha/beta and isoform selectivity-Implications for the structure-based design of HSP90alpha/beta selective inhibitors for treating neurodegenerative diseases. *Bioorg. Med. Chem. Lett.* **2014**, *24*, 204−208.

(44) Avdeef, A.; Tsinman, O. Miniaturized rotating disk intrinsic dissolution rate measurement: effects of buffer capacity in comparisons to traditional wood's apparatus. *Pharm. Res.* **2008**, *25*, 2613−2627.

(45) Lipinski, C. A.; Lombardo, F.; Dominy, B. W.; Feeney, P. J. Experimental and computational approaches to estimate solubility and permeability in drug discovery and development settings. *Adv. Drug Deliv. Rev.* **1997**, *23*, 3−25.

(46) Zhang, X.; Li, X.; Sun, H.; Wang, X.; Zhao, L.; Gao, Y.; Liu, X.; Zhang, S.; Wang, Y.; Yang, Y.; Zeng, S.; Guo, Q.; You, Q. Garcinia xanthones as orally active antitumor agents. *J. Med. Chem.* **2013**, *56*, 276−292.

Table of Contents Graphic

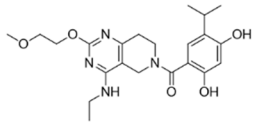

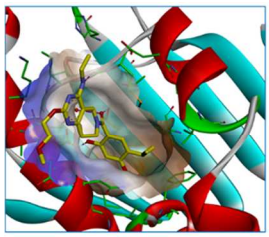

Conformation A

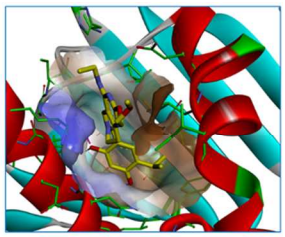

Conformation B

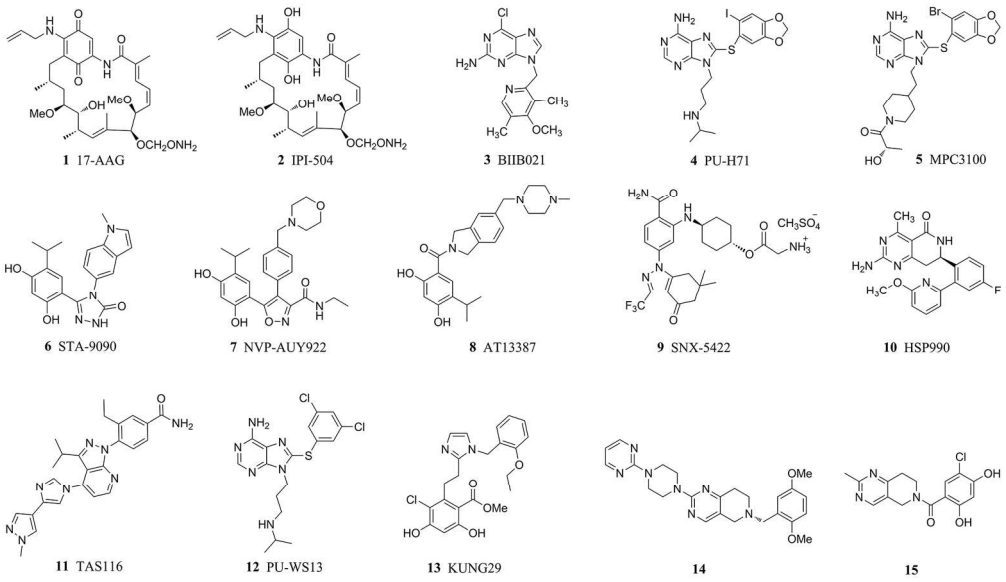

Figure 1. Some representative Hsp90 inhibitors and compounds 14 and 15

177x102mm (300 x 300 DPI)

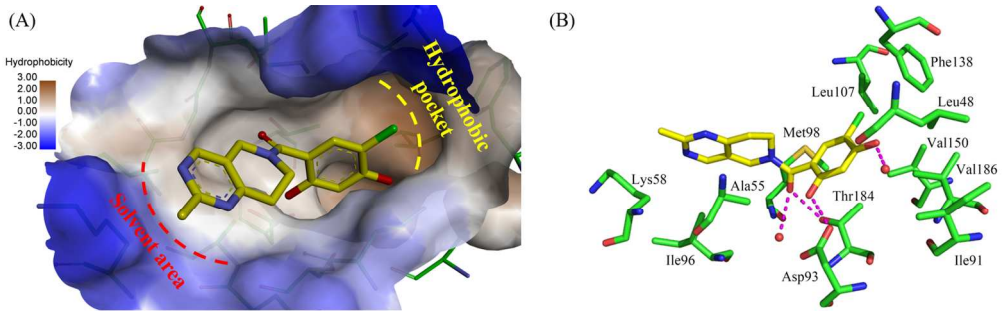

Figure 2. Docking analysis of the binding mode between Hsp90 and compound 15 (protein structure from PDB 2XJX).23 (A) Compound 15 inserts into the active site of Hsp90 with a surface colored in terms of the hydrophobic state. (B) The detailed interaction between Hsp90 and compound 15. The carbon atoms of compound 15 and the residues in the Hsp90's active site are shown in yellow and green, respectively. Conserved water molecules are presented as red spheres, and hydrogen bonds are indicated by magenta dashed lines.

177x54mm (300 x 300 DPI)

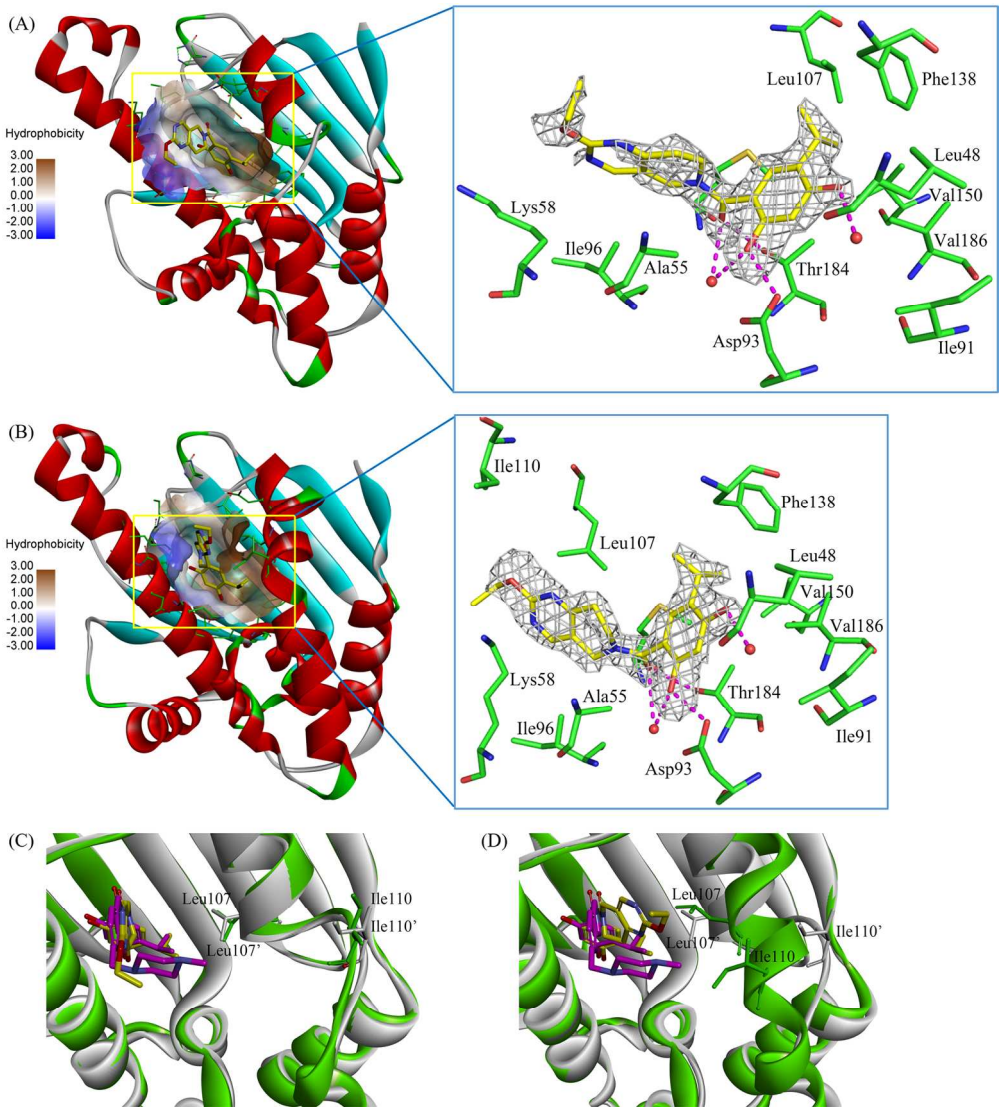

Figure 3. X-ray structure of compound 50 bound to the active site of Hsp90 (PDB: 5GGZ). (A) Compound 50 adopts conformation A to bind with the open-loop conformation of Hsp90. (B) Compound 50 adopts conformation B to bind with the extended α-helix conformation of Hsp90. The active site of Hsp90 is surfaced according to the hydrophobic state, and detailed interaction is shown. The carbon atoms of compound 50 and the residues in the active site of Hsp90 are yellow and green, respectively. Conserved water molecules are shown as red spheres, and hydrogen bonds are indicated by magenta dashed lines. The omit Fo – Fc electron density for 50 is shown at the 3.0 σ contour level. (C) Overlaps of Hsp90-50 complex and Hsp90-8 complex when 50 adopts conformation A. (D) Overlaps of Hsp90-50 complex and Hsp90-8 complex when 50 adopts conformation B. The protein in Hsp90-50 complex and Hsp90-8 complex are colored as green and grey, respectively. Compound 50 is colored yellow and compound 8 is colored magenta.

177x195mm (300 x 300 DPI)

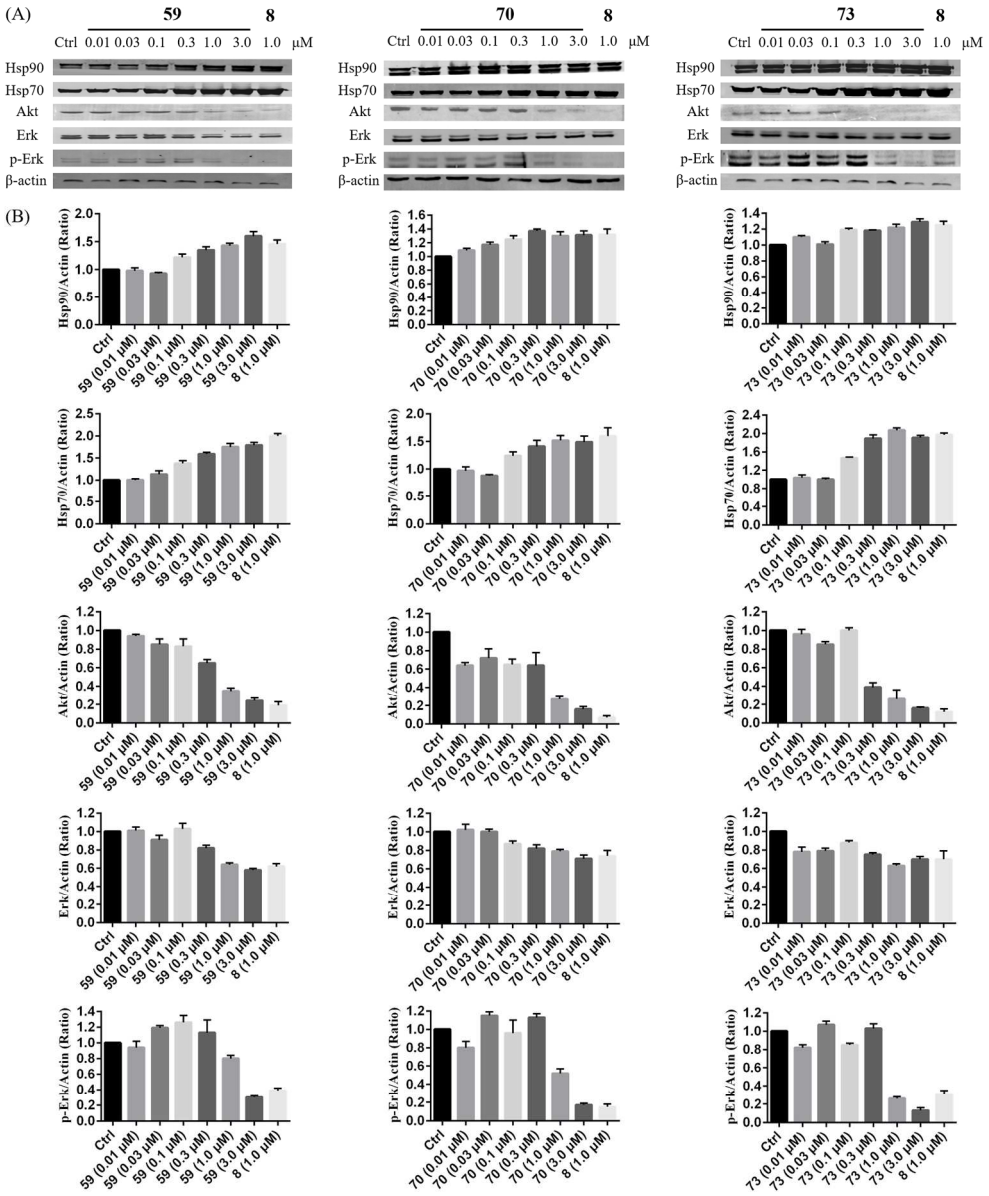

Figure 4. (A) Western blot analysis of the biomarker levels in HCT116 cells after incubation for 24 h with 59, 70 and 73. (B) Densitometry analysis of the protein levels are showed as normalized (to actin) ratios. Actin is used as the control for protein loading. 8 is used as the reference compound.

177x212mm (300 x 300 DPI)

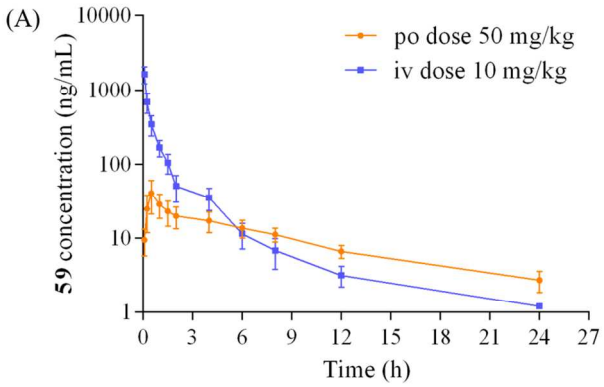

Parameters	59	
	p.o.	i.v.
Dose (mg/kg)	50	10
Cmax (μg/L)	40.69	/
Tmax (h)	0.5	/
$t_{1/2}$ (h)	7.40	4.16
CLz (L/h/kg)	198.95	14.12
Vz (L/kg)	2072.05	86.62
AUC_{0-t} (μg·h/L)	264.53	756.94
F (%)	7.0	/

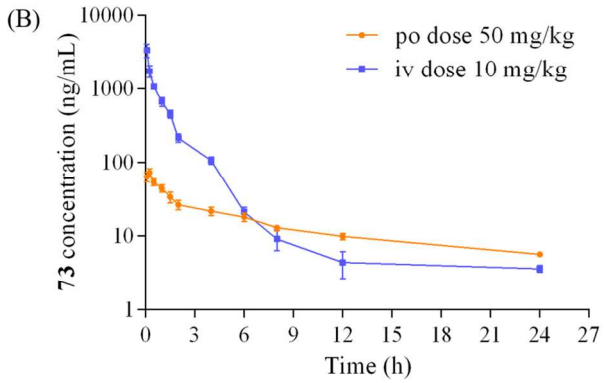

Parameters	73	
	p.o.	i.v.
Dose (mg/kg)	50	10
Cmax (μg/L)	72.60	/
Tmax (h)	0.5	/
$t_{1/2}$ (h)	9.40	3.95
CLz (L/h/kg)	123.87	5.25
Vz (L/kg)	1620.19	29.59
AUC_{0-t} (μg·h/L)	408.69	1932.03
F (%)	4.23	/

Figure 5. Pharmacokinetic analysis in healthy rats. (A) Plasma concentration vs. time profile and pharmacokinetic parameters of compound 59. (B) Plasma concentration vs. time profile and pharmacokinetic parameters of compound 73. The pharmacokinetic parameters are calculated using DAS2.0 software.

150x124mm (300 x 300 DPI)

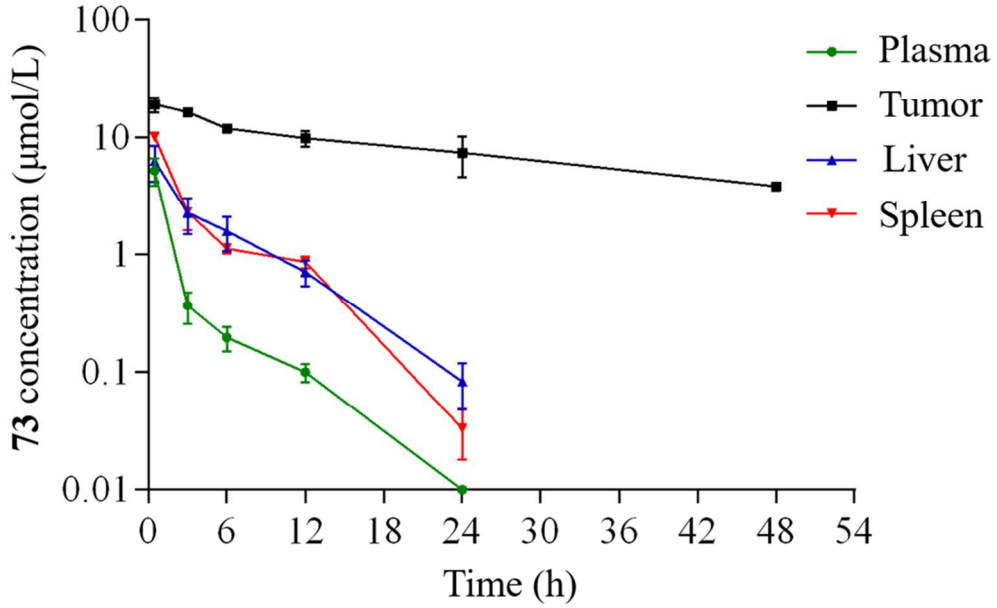

Figure 6. Tissue distribution of 73 in an HCT116 xenograft model. The plasma, tumors, livers, and spleens were collected at the indicated times after intravenous (iv) administration of 60 mg/kg 73.

99x61mm (300 x 300 DPI)

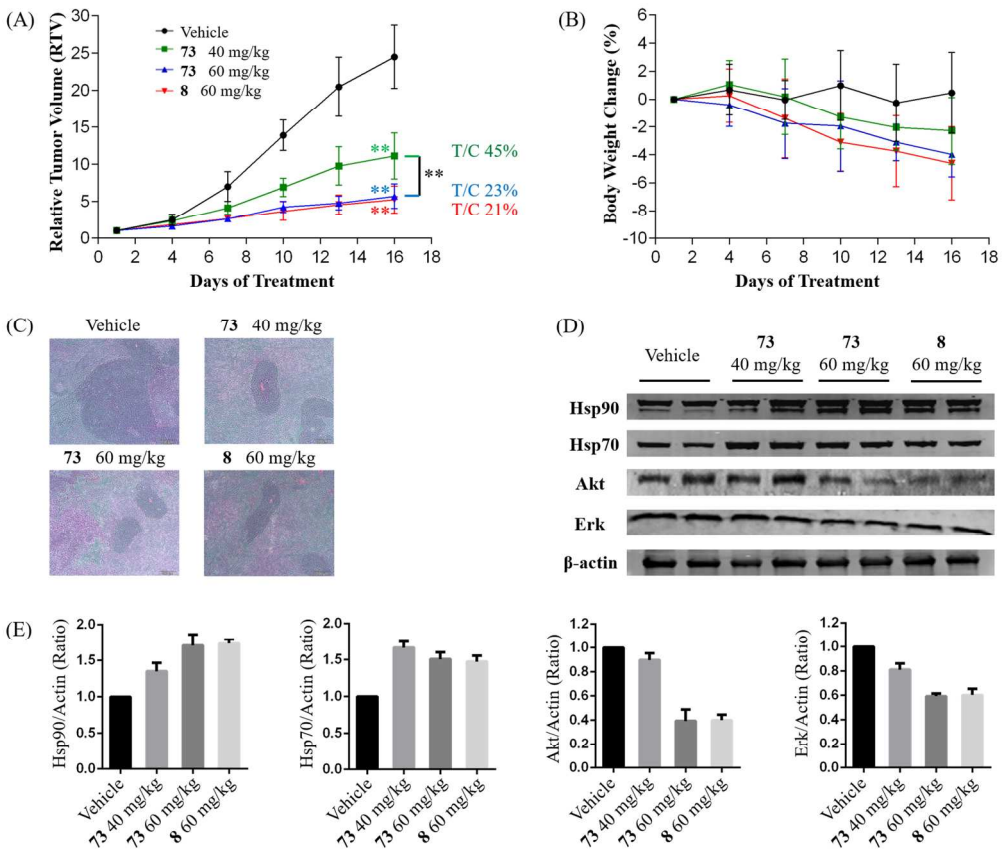

Figure 7. Anti-tumor efficacy of compound 73 in HCT116 human colon cancer xenografts. Compound 73 was intraperitoneally (ip) administrated according q.o.d. for 16 days once the mean tumor volume reached 100 mm3. (A) Relative tumor volume (RTV) changes after treatment. Tumor diameters were measured every three days and used to calculate the tumor volumes. RTV = Vt/V0, where Vt is the tumor volume measured at each time point, and V0 is the tumor volume at the beginning of treatment. Bars represent SEM. ** $p < 0.01$, Student's t-test (n = 6). (B) Pharmacodynamic biomarker changes assessed by Western blot (12 h after final dose). (C) Representative H&E images of the sacrificed tumors. (D) Western blot analysis of the pharmacodynamic biomarker changes in tumor xenografts. Actin is used as the control for protein loading. (E) Densitometry analysis of the protein levels are showed as normalized (to actin) ratios.

177x150mm (300 x 300 DPI)

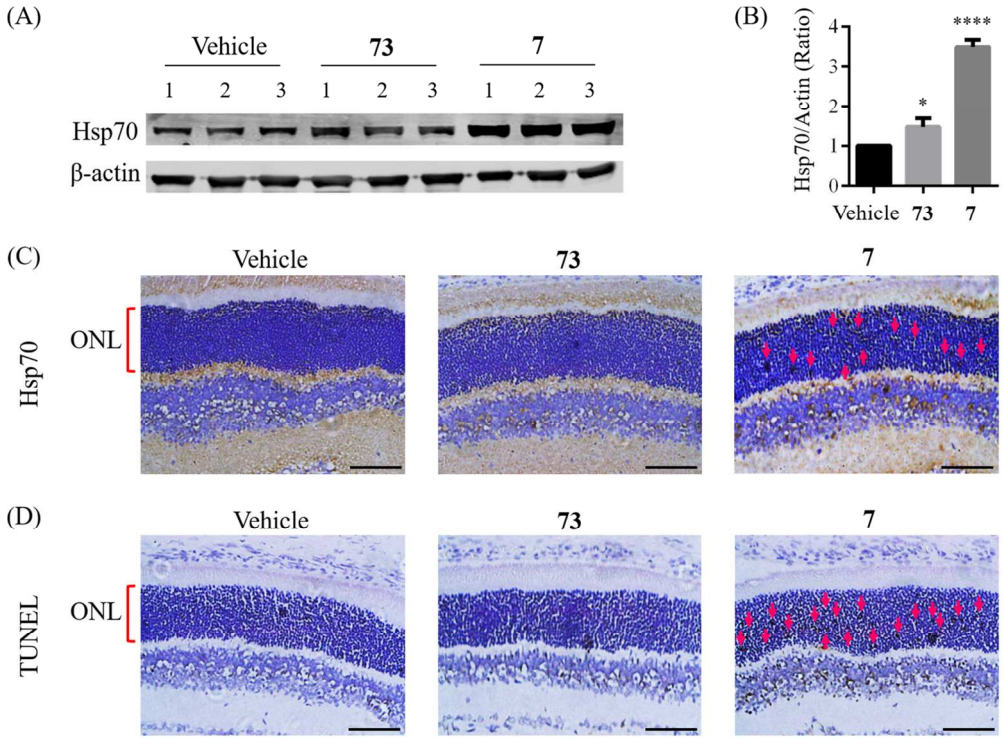

Figure 8. Ocular toxicity evaluation of compound 73 in a rat retinal damage model. SD rats (n = 3) were intravenously (iv) treated with 2 consecutive daily doses of vehicle, 73 (20 mg/kg) or 7 (NVP-AUY922, 10 mg/kg). The retina tissues were harvested 24 h after the last treatment. (A) Hsp70 regulation in retina tissues after treatment assessed by Western blot. Actin is used as the control for protein loading. (B) Densitometry graph of Hsp70 regulation. (C) Hsp70 immunohistochemistry in the retina after treatment. Scale bar, 50 μm. (D) Apoptosis induction in the retina after treatment evaluated by TUNEL staining. Scale bar, 50 μm.

134x98mm (300 x 300 DPI)

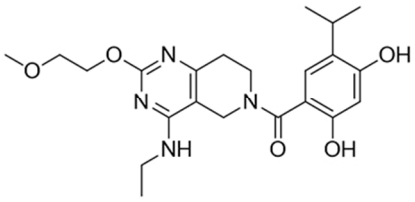

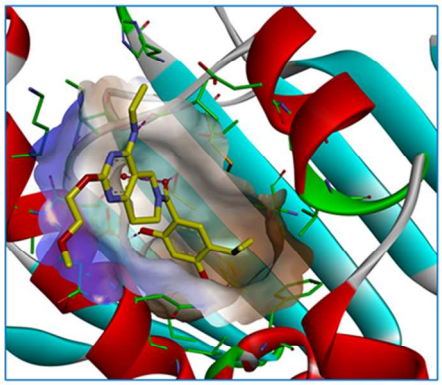

Conformation A

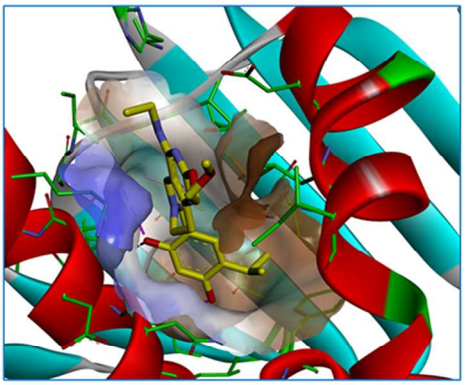

Conformation B

Table of Contents Graphic

79x52mm (300 x 300 DPI)